1970

Identification of single cells by flourescent and darkfield optical techniques

John Allan Steinkamp
Iowa State University

IDENTIFICATION OF SINGLE CELLS BY FLUORESCENT AND DARKFIELD OPTICAL TECHNIQUES

by

John Allan Steinkamp

A Dissertation Submitted to the
Graduate Faculty in Partial Fulfillment of
The Requirements for the Degree of
DOCTOR OF PHILOSOPHY

Major Subject: Electrical Engineering

Approved:

Signature was redacted for privacy.

In Charge of Major Work

Signature was redacted for privacy.

Head of Major Department

Signature was redacted for privacy.

Dean of Graduate College

Iowa State University
Ames, Iowa

1970

TABLE OF CONTENTS

INTRODUCTION

In many morphological and histological studies it is of significant interest to accurately determine such parameters as overall cell size, nucleus size or DNA content, or the ratio between these two parameters. Fluorescent techniques (microfluorometry) offer a method for investigating normal and pathological cells, along with other subcellular components or characteristics of the cell. Darkfield or light scatter techniques present a nondestructive method for estimating overall cell size (cross sectional area or volume).

This work is primarily concerned with the development of a method for identification of various types of biological cells in aqueous suspension according to their fluorescence and darkfield (light scatter) optical properties. The method described in this dissertation is capable of identifying and measuring large numbers of fluorescing (nucleated) and non-fluorescing (non-nucleated) cells within certain size limitations. A rapid and statistically significant method is presented for determination of the frequency distribution histograms (size distributions) of cell fluorescence, light scatter, and the simultaneous ratio of these two optical parameters. Computer programs were used to obtain the distributions for the various types of cells from data recorded on magnetic tape. This method is an alternative approach to the more complex automatic scanning methods and the time

consuming manual methods of the microscopists.

Various types of biological cells, ranging from large pollen grains to small bacteria, were selected for evaluation of the method and overall system performance. Cells were tagged with the fluorescent dye acridine orange, placed in dilute aqueous suspension, and allowed to flow through a rapid opto-photoelectric measurement system. Acridine orange was chosen as the basic fluorochrome in this study because of its ease of staining and specific affinity for the nucleic acids (DNA and RNA) present in the cell. Measurement of tagged cells is based on the assumption that the light emitted by the fluorescing nucleus is proportional to its projected cross sectional area and light scattered by the cell is proportional to total cross sectional area. The measurement of non-fluorescing cells is based only on the assumption that light scattered from the cell is proportional to the total projected cross sectional area.

Although fluorescence and darkfield (light scatter) microscopial techniques are a little over 60 and 120 years old, respectively, the quantitative information accumulated from their application to medicine and biology is still relatively meager. Both fluorescence and darkfield light scatter techniques have not been used quantitatively to any large extent. Difficulties in working with complex physical equipment have limited progress in these areas.

Automatic cellular analysis had its beginning in the early 1930's. A brightfield photometric method was reported in 1934 (59) for individually counting microscopic cells in a fluid suspension, by forcing the cell suspension through a fine capillary tube located on a microscope stage. Due to difficulties of cell clumping, focusing of cells in the capillary tube, and lack of sufficient sensitivity in the measurement system, the experiment was not successful. A few years later, Lagercrantz (51) attempted to count human erythrocytes photoelectrically by the capillary tube method using darkfield illumination. This method failed because of light reflection by the capillary tube into the microscope objective lens causing loss of dark background and thus creating a low signal-to-noise ratio in the opto-photoelectric measurement system. During the capillary tube experiments, Lagercrantz made an interesting observation. When a dilute suspension of cells was placed on a microscope slide or in a counting chamber, which was then moved with respect to the microscope objective, distinct light signals from individual cells were obtained. This was the initiation of the scanning method for counting and sizing individual cells. Since Lagercrantz's initial discovery, numerous automatic scanning techniques have evolved (60). Frommer (28, 29) capitalized on Lagercrantz's observation by designing a direct-reading blood-count meter based on the darkfield photoelectric detection scheme. Cells flow

through a 60 μ deep by 1 cm wide darkfield illuminated zone which is monitored by a photomultiplier tube.

A high speed automatic cell counter and size analyzer was reported in 1956 by Coulter (19). This type of cell analyzer measures particles suspended in an electrolyte by means of the change in electrical resistance as they pass through a small orifice. The Coulter automatic cell analyzer has been used extensively for volume determinations of cells ranging from bacteria (49) to various larger cell types (88).

The use of ultraviolet light energy coupled with fluorescent dyes for automatic cell counting and sizing purposes had its beginning in the early 1950's with the development of a scanning apparatus for the differential detection of cancer cells in preparations of exfoliated cells on microscope slides (55, 56). This method was based on the selective staining of cell nuclei with a fluorescent dye. Nuclei emitting more than a certain amount of light (threshold) were counted by a photomultiplier tube and an associated electronic system. Mansberg and Kusnetz (53) have recently reported a micro-fluorometric scanner capable of detecting and counting fluorescein isothiocyanate-tagged Escherichia coli bacteria. This experimental microscanner employed brightfield ultraviolet illumination and liquid dye immersion filtering. Careful selection was made in matching the light source and filter spectral characteristics to improve system sensitivity.

Lack of adequate excitation sources, sensitive photomultiplier tubes, and methods for generating a single cell flow stream have slowed the development of a rapid flow-through fluorometric micromeasurement technique. Van Dilla et al. (93) have recently reported a high speed (10^4-10^5 cells/min) narrow flow-through (50 μ effective diameter) system for quantitative determination of cell fluorescence. This method employs a blue laser (argon-ion) for excitation, coupled with right angle darkfield illumination. Feulgen-DNA distributions in populations of tissue culture cell and human leucocytes were obtained. Their results compare well with results of other independent methods. Steinkamp (82), in 1967, developed a slightly different type of fluorescence measurement apparatus capable of detecting and measuring fluorescing cells stained with the basic fluorochrome acridine orange. Although this device was capable of measuring small cells in aqueous suspension, difficulties were encountered in generating a narrow cell flow stream. Only a small portion of a 75 μ deep x 5000 μ wide cell flow channel was monitored by an opto-photoelectric measurement system.

Light scattering techniques employing various forms of darkfield illumination have successfully been used for size determination of small particles ranging from dust particles to blood cells (68). Light scattering in itself represents another means for obtaining information on the physical

properties and behavior of matter. "Turbidimetry" was employed in the 1930's and 1940's (12, 13) as an early automatic method of counting cells in aqueous suspension. The method consisted of using a photoelectric device to measure light transmission through a suspension of cells. Meyer-Arendt (58) successfully measured the diameter of leukemic cells using light diffraction as a means of size determination. Studies were made on blood samples from patients with lymphatic leukemia and from healthy individuals. He found this method of size determination to be in close agreement with measurements made with a microscope eyepiece micrometer. Kurozumi and Shibata (50) have investigated the possibility of using the positions of diffraction maxima and minima for the determination of cellular dimensions of yeast, chorella, chloraplasts, and human erythrocytes. Their maximum error was estimated to be about 13 per cent. Recently, light scattering methods have gained popularity as a method for rapid quantitative cell size determinations. Mullaney et al. (62) have investigated small angle scattering (diffraction) between 0.5° and 2.0° from individual particles 5 to 20 μ diameter, ranging from plastic monospheres to mammalian cells. They determined that small angle light scattering is nearly proportional to volume and insensitive to refractive index. Their volume distributions were well within agreement with other independent methods.

Techniques capable of automatically measuring two or more optical parameters of a cell simultaneously have not been reported until recently. Kamentsky et al. (45) reported a new device in 1965 capable of measuring and displaying multiple spectrophotometric properties of biological cells at rates of 500 cells per second. Photometric measurements of human cells from different parts within the body were made at 253.7 mμ (UV absorption) and 410.0 mμ (light scatter) wavelength excitation to estimate the DNA per unit volume of individual cell populations. Cells were individually measured while passing through a 100 μ wide x 100 μ deep channel cut into a quartz microscope slide. Wheeless et al. (101) in 1968 described a relatively slow complex computer controlled multiparameter cyto-fluorescence scanning system capable of measuring green fluorescence (530 mμ wavelength) of the cell nucleus (DNA), red fluorescence (650 mμ wavelength) of the RNA in the cytoplasm, and light scatter from individual cells. This system is being used to study secondary fluorescence of stained cells using fluorochromes and techniques selective to RNA and DNA. Van Dilla et al. (94) briefly discuss the possibility of multiparameter optical spectral analysis (fluorescence) using more than one photomultiplier tube with appropriate filtration coupled with small-angle light scatter.

One of the more crucial areas of importance in the automatic cell identification and measurement system is the

development of a reliable method for generating a very narrow (50-100 μ wide) cell flow stream. Various flow stream schemes have been previously reported. Coulter's (19) high speed cell counter/analyzer uses a cylindrical aperture for volume determinations of microscopic particles. Frommer's (28) device statistically determines cell counts by light scatter from a small portion of a parallel plate flow chamber. Kamentsky's et al. (45) multiparameter measurement system individually counts and sizes cells while flowing through a narrow channel cut into a quartz microscope slide. More recently, Van Dilla et al. (94) described a liquid sheath-flow chamber capable of creating a cylindrical 50 μ diameter flow stream.

Automatic sorting of biological cells according to some measurable physical parameter has gained success only in this decade. Fulwyler et al. (30, 31), in 1965, was first to report a rapid electronic separation method of biological cells according to volume. Cell volume is measured using a Coulter aperture, and the cells then isolated into droplets of the medium which are electrically charged according to sensed volume. The charged droplets then enter an electrostatic field and are deflected into collection vessels. Hulett et al. (41) have recently reported (1969) a cell sorting scheme employing Fulwyler's charged droplet technique for separating fluorescein diacetate (FDA) tagged mammalian cells. The flow stream from the nozzle is darkfield illuminated from a mercury arc and the

fluorescing cells measured with a microscope and photomultiplier tube. After the cells are sensed, they are deflected according to Fulwyler's method. Kamentsky and Melamed (44) have reported a spectrophotometric cell sorter capable of sorting cells according to UV absorption and light scatter of the cell. This device is an outgrowth of an earlier spectrophotometer (45). It employs a special crossed flow channel for pulsing a fluid pulse across the channel to remove a cell from the flow stream after it has been sensed.

CELL IDENTIFICATION SYSTEM CONSIDERATIONS

Various cellular parameters such as volume, nucleus size, cytoplasm size, total DNA and RNA content, antibodies, etc., are often of interest and are required to be measured. The measurement process can be manual or automatic. Manual techniques are usually slow and cumbersome. Automatic techniques are not only rapid, but produce statistically significant results when properly employed. In measuring large numbers of cells, some sort of flow-through or scanning device is used.

Normally, automatic techniques measure some quantity of the cell which is proportional to the parameter being investigated. For example, by proper interpretation of UV absorption (65) or fluorescence (Feulgen technique (76)) the DNA content of a cell nucleus can be determined within 5-10 per cent. Resistivity measurements employing the Coulter detector have been used extensively to measure cell volume.

In this study both the fluorescence and light scattering of single cells in aqueous suspension were measured simultaneously. The fluorescent dye (acridine orange) employed in this work is highly specific to staining the nucleic acids and nucleoproteins (73). DNA and nucleoproteins, normally found in the cell nucleus, fluoresce green-yellow, whereas RNA, located outside the nucleus fluoresces red-orange.

In order for cells to be measured in this type of system, they must flow through a detection or identification chamber.

Interaction of the incident (UV) light and cells flowing through the system occurs within the chamber. As each cell comes in contact with the incident radiation, it simultaneously fluoresces and light is scattered from it. An optical system projects individual cell images onto the photocathodes of the fluorescence and darkfield photomultiplier tubes. Rectangular aperture masks were placed ahead of the photocathodes to limit the flow channel observation zone.

A fluorescing cell behaves optically as a self-luminous body; it emits light in all directions. Depending upon its numerical aperture, the optical system captures part of this emitted light and transfers it to the fluorescence photomultiplier tube (10). The radiant energy flux (F) emitted per unit time is directly proportional to the radiant energy absorbed (W) per unit time multiplied by the quantum yield Φ and is given by

$$F = K_f W \Phi \qquad (1)$$

where K_f is the proportionality constant and the unit of energy is lumens or watts. The radiant energy absorbed per unit time W can also be expressed as

$$W = E\ A \qquad (2)$$

where E is the incident illuminance per unit time and A is the cross sectional area of the cell nucleus. It has previously been demonstrated that the fluorescent light energy flux given

off by the nucleus fluorescent-tagged (acridine orange) cell is proportional to its projected area (82). Certain factors such as dye concentration, pH, temperature, viscosity, saturation, etc., which affect quantum yield, are discussed in Appendix A.

Incident UV light energy scattered by a cell at any distant point has the character of a spherical wave, in which energy flows outward from the cell. The direction of scattering, i.e., the direction from the cell to this point, is characterized by the angle θ which it makes with the direction of propagation of the incident light. The overall intensity coefficient $I(\theta,d)$ of light scattered at a given angle θ from the direction of incident wave propagation given by Hodkinson and Greenleaves (40) is defined as the light flux per unit solid-angle scattered in the direction θ divided by the flux geometrically incident on the cell. It is calculated as though it arose separately from diffraction, external reflection, and refraction (Appendix A).

The intensity of the scattered incident light energy in lumens per unit solid angle is given by

$$I = K_s EAI(\theta,d) \qquad (3)$$

where E is the illuminance of the source of incident light, A is the cell cross sectional area, $I(\theta,d)$ is the scattered intensity coefficient, and K_s is a constant of proportionality. The collection angle or numerical aperture of the optical

system for measuring scattered light is thus important. For small angle scattering intensity is nearly proportional to cell volume and insensitive to cell refractive index (62). In the case of large angle scattering, which is of interest in the study, the scattered intensity is nearly proportional to cell cross sectional area, but dependent upon the refractive index of the cell (63).

The instantaneous signal amplitude is a direct function of the cellular area (circle) as it is intercepted by the photomultiplier tube mask aperture borders (82). The complex signal waveform can be very closely approximated by a triangular wave, in which the peak signal amplitude is a function of the fluorescence and light scatter intensities and is proportional to the cellular area of interest (πr^2). This is assuming uniform staining characteristics in the case of fluorescence and invariant refractive index for light scatter.

Before describing the measurement system employed in this study, there are numerous important design criteria that should be discussed concerning the development of the fluorescence/darkfield (light scatter) measurement system. The measurement system is composed basically of three subsystems: (1) Excitation system, (2) detection chamber, and (3) measurement system.

Excitation System

The choice of the type of blue-ultraviolet excitation light source is of crucial importance in the fluorescence-darkfield micro-measurement system and is primarily influenced by the necessity of satisfactory fluorescence. It is important that the excitation light energy be in the proper spectral excitation range of the fluorochrome, since the radiant light energy emitted is proportional to the radiant light energy absorbed. For example, the acridine and xanthene fluorochrome families are characterized by high absorption in the 400-500 mμ wavelength region. Monochromatic excitation sources are extremely valuable when the absorption and emission spectral bands are situated in close proximity. Size and homogeneity of the excitation source is also important. Usually, the larger the excitation source, the lower its brightness. Not only should the source be large enough to cover the cell flow stream, but also be homogenous across it.

Laser light sources represent the theoretical optimum with respect to energy output and partial or complete monochromasy of emitted radiation. A continuous wave (cw) laser operating with a power output in the milliwatt range can provide a spot irradiance of at least 1000 times greater than the mercury arc lamp (53).

Until recently, the most intense sources of irradiation available for use has been the compact high pressure arc lamps.

and carbon arc. Various types of compact arcs, along with their characteristics are listed in Mansberg and Kusnetz (53) and Rigler (73). Xenon high pressure arc lamps produce a continuous band of radiation from the UV to IR region of the spectrum with a large amount of infrared radiation. By adding mercury to xenon, this type of lamp has the combined xenon/ mercury spectrum. The mercury high pressure arc lamp has a strong blue, violet, and ultraviolet output spectrum. Low voltage, high amperage tungsten quartz iodide lamps can also be used as excitation sources. Their main disadvantage is the high infrared output. The blue-ultraviolet energy is not great, but the continuous spectrum increases the output in this region.

A spherical or parabolic aluminum coated reflector placed directly behind the excitation light source at a distance of one focal length will increase the lumen output up to as much as 50 per cent (81).

The lamp condenser lens system serves to form a collimated beam of light energy from the excitation source. Spherical and chromatic aberrations are the chief lens distortions in this part of the system (81). Chromatic effects can be held to a tolerable level without achromatizing, whereas, spherical aberration can be controlled by splitting the condenser into two or three lens elements of approximately equal power. An aspherical lens can be used as one of the lens elements to

further reduce spherical aberration. The numerical or angular aperture of the lamp condenser determines the intensity of irradiation (71).

When an excitation source having a strong infrared output is employed, a heat filter should be placed in front of the lamp condenser to remove the unwanted infrared radiation. Infrared radiation greater than 1000 mμ wavelength can permanently damage the exciter filter. This type of filter should be able to freely pass wavelengths greater than 350 mμ wavelength and block infrared greater than 1000 mμ wavelength.

An ultraviolet transmitting filter (exciter filter) must be used between the excitation source and the detection chamber in order to pass the blue-ultraviolet excitation energy and absorb any unwanted excitation in the non-absorbing spectral region of the fluorochrome. The exciter filter is normally placed in front of the lamp condenser, protected by the heat filter from damaging infrared irradiation. Careful selection of the exciter filter is important in connection with image brightness and is essential if good contrast is to be obtained. In selecting an exciter filter, careful attention should be paid to the absorption region of the fluorochrome being used and the spectral characteristics of the excitation source. The filter thickness when using darkfield illumination need be only about one-half as thick as when brightfield illumination is employed. The transmission characteristics for

various types of exciter filters are given in Richards (72) and Sani et al. (77).

The optical element following the exciter filter is the detection chamber condenser lens system. The detection chamber condenser functions to condense the collimated blue-ultraviolet excitation light energy into an intense spot of irradiation across the cell flow stream in the detection chamber. A microscope condenser is normally employed to perform this function, although a number of different methods may be used, each having its advantages and disadvantages. Brightfield refracting condensers offer the advantage of transmitting the largest amount of the source excitation light. The two lens element Abbe condenser is by far the most extensively used brightfield microscope condenser, but does have considerable chromatic and spherical aberration. One of the main disadvantages of brightfield condensers is the bright background, even with a good exciter filter. It is also difficult to measure light scatter using this type of a condenser.

Darkfield condensers transmit about one-half as much excitation light as brightfield condensers but offer greater image-background contrast. By working with less heavy excitation filtration to improve contrast, some excitation energy gain can be achieved. High contrast achieved by the darkfield system is due to practically none of the exciting light entering the lens system used to measure cell fluorescence, with

exception the amount that is scattered by a cell. Not only can fluorescence be effectively measured, but light scatter can readily be determined using this type of condenser. A darkfield condenser has the property of illuminating the cell flow stream at the apex of a partially hollow cone. The inner aperture of this hollow cone was chosen to be about nine-tenths the numerical or angular aperture of the cell measurement lens system (6).

The most frequently used darkfield condensers are the reflecting types, such as the cardioid and less popular parabolic type. A bright-field condenser such as an Abbe type can be used for darkfield work by placing a circular disc in front of the back lens of the condenser.

Another type of condensing system now being used for quantitative microfluorometry is the vertical illuminator. In this system the exciting light enters from the side and is reflected downward by either an aluminumized or dichrotic mirror toward the built-in objective lens of the illuminator. The images formed are of high contrast and brilliance with a favorable signal-to-noise ratio. Light scatter measurements may be possible to achieve with type of condenser system.

If oil immersion ($n = 1.515$) is used between the detection chamber condenser and the front glass of the chamber an increase in excitation brightness is achieved (10). Caution is required to eliminate air bubble formation. Low viscosity

oils are employed for this purpose. Non-fluorescent immersion oil is required to reduce autofluorescence.

Detection Chamber

The detection chamber is another crucial part of the cell identification system. Interaction of the incident excitation light energy and cell flowing through the system occur within the chamber. The cell flow path (channel) cross section must be large enough to permit reasonable flow, but small enough to permit sufficient optical contrast in the measurement process. Excessive depth creates contrast problems with undissolved dye and focusing difficulties of the optical system (excitation and measurement). Cell concentration in the diluent must be low enough so that the probability of coincidence within the field of view of the chamber is negligible (82). Other important considerations are laminar flow and the velocity profile of the channel. If the cell concentration is too large and/or clumping of cells occur, the channel may become plugged. Air bubble formation within the chamber can not only alter the cell flow stream, but can appear as false (darkfield) signals.

When darkfield illumination is to be employed, the glass thickness between the front of the condenser and cell flow stream should be chosen to give maximum irradiation of the flow stream. The glass thickness plus one-half the cell flow stream thickness should be equal to the working distance of

the condenser. Glass thicknesses between 1.15 and 1.25 mm are usually employed (6). The type of glass used to construct the chamber should be one which has good transmission properties above 350 mμ wavelength and as free as possible from autofluorescence, since autofluorescence reduces image brightness (optical contrast) in microfluorometry. Scratches and pits in the glass scatter the excitation light, thus lowering the darkfield image contrast.

The glass slide thickness on the measurement side of the chamber is also important. If a commercial microscope objective lens system is used for cell measurement it will have a working distance, which is the distance from the specimen (cell) to the front lens of objective, as specified in air or oil immersion. The thickness of the glass plus one-half the thickness of the cell flow stream should not exceed this distance.

The depth of the flow channel determines how the cells are dispersed. If the channel is too deep, then the cells are dispersed such that a large percentage will be out of focus of the optical measuring system. Excessive depth also creates optical contrast problems with unbound dissolved dye and cell suspension media (blood plasma). Also, when the flow stream reaches a certain critical depth, turbulence will occur as determined by the Reynolds number (84).

Laminar flow of the cell flow stream is an important condition in the detection chamber, so as not to destroy the velocity profile of the cell stream. The critical (lower) Reynolds number for laminar flow in tubes (pipes) is about 2000, whereas, for laminar flow between parallel plates, which is of interest in work, it is approximately 1000 (96). Thus, by knowing the Reynolds number, the type of fluid, and the flow channel dimensions, the critical flow velocity for which turbulence will occur, can be determined.

The velocity profile (distribution) in the flow chamber is also of importance, as this will determine, to a certain extent, the central location of the cells as they traverse the chamber. For steady laminar flow through a circular tube and between infinite parallel plates the velocity distribution is parabolic (36).

Measurement System

The fluorescence/darkfield optical lens system functions to project the channel image, i.e., cells flowing through it, onto the photocathodes of the fluorescence and darkfield photomultiplier tubes. Selection of the lens system for measurement of fluorescence and light scatter depends upon a number of important factors. Normally the decisive criterion in microfluorometry is the image brightness of the fluorescing cell. Since cell fluorescence is emitted in all directions,

the intensity of the fluorescent light as collected by a lens system (microscope objective) increases as the square of the numerical or angular aperture (6, 71). For example, a 20X objective (N.A. 0.5) increases the signal by a factor of 4 over a 10X objective (N.A. 0.25). In fluorescence and darkfield work it should also be remembered that the numerical aperture of the objective lens should be slightly less than that of the darkfield region of the detection chamber excitation condenser.

In the measurement of light scatter from a cell it is important that none of the direct excitation light enter the objective. Since light scatter is not emitted in all directions, but is dependent upon the diffraction, refraction, and reflection, the degree of the angular measurement is important (Appendix A).

Since cellular fluorescence and light scatter are emitted within rather narrow spectral regions, i.e., nearly monochromatic, there is no need for full chromatic correction of the lens system over the entire spectral range. Achromatic lens systems do not contain fluorite, so that the danger of excessive autofluorescence of the objective is eliminated. Simple lens systems may be employed, with some reduction in numerical aperture. Apochromatic lens systems, containing fluorite, can be used with the darkfield condenser.

In order to focus the entire depth of the flow channel onto the photomultiplier measurement tubes, a low to medium

power objective should be used. As a general rule, the higher the magnification (numerical aperture), the smaller the depth of focus. This problem can be eased some, since cells tend to congregate near the center of the channel, where the velocity is the greatest (velocity profile).

A magnifier lens may be used in conjunction with an objective to increase the cell image size at the photocathodes of the photomultiplier tubes, thus increasing photomultiplier masks sizes. Although the image brightness is decreased by this additional stage of magnification, the only amount of light energy loss occurs due to absorption and reflection of this lens.

The primary function of the optical system is to gather as much of fluorescent and scattered light energy as possible and transfer it to the fluorescence and darkfield photomultiplier tubes for quantitative measurement. Not only does the optical system transmit fluorescence and scattered light from a cell, but a certain amount of background fluorescence and unwanted stray excitation light is also transmitted, which greatly affects image contrast. Background fluorescence which is caused by a number of factors is difficult to reduce, especially if its emission overlaps that of the fluorescing cell. Also, light scattered by the cell must not reach the fluorescence photomultiplier tube.

To reduce unwanted scattered and stray excitation light in the fluorescence measurement system, an ultraviolet absorbing filter (barrier or suppression filter) is placed between the optical system and the image formed of the photocathode of the fluorescence photomultiplier tube. This filter functions to absorb unwanted excitation light energy and pass fluorescence emitted by the cell. A wide range of barrier filters are available for fluorescence work (72, 77). These usually have a high transmission percentage and sharp cut-offs. Transmission wavelengths vary from 350 mμ wavelength to well within the infrared region of the spectrum.

In order to verify that a particular combination of excitation and suppression filters are not passing the excitation light, it is only necessary to monitor the fluorescence photomultiplier tube output, while large (5-25 μ dia.) nonfluorescent latex particles are flowing through the chamber. This is a modification of the cross-filter method given in Price and Schwartz (71).

Barrier filters in general have the property of considerable autofluorescence. In order to partially alleviate this problem, the barrier filter is usually placed out of focus between the objective lens and fluorescence photomultiplier tube.

If it is desired also to simultaneously measure the excitation light energy scattered by a cell, then the darkfield photomultiplier tube need not have a barrier filter placed in

front of it. The darkfield photomultiplier tube will not only measure light scattered by the cell (82), but also cell fluorescence which is about 100 times smaller than the scatter measurement. If a beam splitter is placed between the magnifier lens of the optical system and the barrier filter located in front of the fluorescence photomultiplier tube, the light signal from an individual cell can be split into its fluorescence and darkfield components.

The majority of exciter filters transmit some residual red light above 650 mμ wavelength, which further reduces the optical contrast. If a photomultiplier tube having an extended red sensitive photocathode such as the S-20 or S-25, is used, it may be necessary to filter out this red component. The red background can be effectively suppressed at the photomultiplier tube rather than at the source of excitation. Barrier filters of this type are available (53) which have excellent transmission from the 300-350 mμ to 625-725 mμ wavelength regions.

A mask having a rectangular aperture is placed directly in front of each of the photocathodes of photomultiplier tubes to limit the observation zone of the projected cell flow channel. The mask aperture sizes depend upon the size of the observation zone to be monitored and the total optical system magnification from the cell channel to the photocathodes of photomultiplier tubes. Zone height should be at least equal the largest nuclear and overall cell dimension for

the fluorescence and darkfield measurement channels, respectively. Zone width is a function of optical contrast and the percentage of cells flowing through the chamber that are to be measured without error (82).

Selection of the proper photomultiplier tube for both the fluorescence and darkfield measurement channels is important. The measurement of low light levels necessitate the use of photomultiplier tubes in a system of this type. In selecting a photomultiplier tube there are a number of important factors to be considered. The overall performance depends upon the photocathode sensitivity (S) - μamps per lumen, which is dependent upon the photocathode material and the incident irradiation wavelength. By choosing a photocathode with a high sensitivity at the wavelength of interest, a higher signal-to-noise ratio can be obtained.

Current amplification is extremely sensitive to variations in applied voltage. For example, a 1 per cent change in the overall voltage on a ten stage photomultiplier tube will result in a 7 per cent change in output level. The dynamic change in gain as a function of the change in overall voltage is given as (24)

$$\frac{dG}{G} = 0.7n \frac{dV}{V} , \qquad (4)$$

where G is the current gain, V is the overall voltage, and n is the total number of stages of amplification (dynodes). The expression for photomultiplier tube gain as a function of

voltage can be determined by the integration of Equation 4 and is given by

$$\log_{10} \frac{V}{V_1} = \frac{1}{0.7n} \log_{10} \frac{G}{G_1} \qquad (5)$$

The smallest fluorescent-tagged cell that can be measured will be dependent upon the intensity of the fluorescence emission and loss of optical contrast caused by autofluorescence of optics and glass filters, fluorescence of unbound dye in the flow stream, detection chamber autofluorescence and reflections, and the close proximity of excitation and emission spectra (wavelengths) of fluorochromes. The fluorescence signal is normally of much lower magnitude than the darkfield signal, and is thus the limiting factor in overall system performance.

Electrical noise due to loss of optical contrast appears to be the main source of noise in this type of measurement system and is due to many complex factors. This type of noise not only increases the d-c background level of the photomultiplier tube output, but also produces random fluctuations in the photomultiplier tube photocathode incident light flux, i.e., quantum noise. These random fluctuations are a consequence of the corpuscular nature of light and dependent upon fluctuations in the UV light source, i.e., quantum noise. Shot noise can also result from this type of noise. Shot noise is another form of electrical noise which arises from

random fluctuations in the photomultiplier tube photocathode electron current. This type of noise is proportional to the square root of the cathode current multiplied by the system bandwidth (24).

In the practical situation, the electrical noise level cannot be completely suppressed without some sacrifice in the signal level. Shot noise, which is random in nature can be reduced by either lowering the system bandwidth (Δf) or the photocathode illumination (I_c). The portion of the electrical noise which is a function of incident photon flux and correlated to UV light source fluctuations can be reduced by a 180^{o} feedback scheme with respect to the photomultiplier tube signal. By varying the conditions of excitation, optical filtering, choice of UV light source, optics, etc., a wide range of signal and noise levels can be obtained.

The cell stream flow rate through the chamber, coupled with cell size, imposes limitations on the system bandwidth in the low S/N ratio measurement situation. Slowing down of the flow rate in the detection chamber has the effect of widening the signal duration of a cell passing through the chamber. By widening the time duration of the signal, the system bandwidth can be lowered, thus raising the signal-to-noise ratio. The peak signal amplitude, assuming no dye saturation (fading), remains unchanged.

The system bandwidth and filtering characteristics are of importance in the fluorescence/darkfield measurement system, since the peak signal-to-noise ratio is decisive in determining the error in the measurement process. It is possible, although not necessary, to choose a filter transfer function to maximize the signal-to-noise ratio, i.e., a matched filter (34), for a given signal shape. In actual practice the exact shape of the matched filter is of secondary importance, the proper filter bandwidth being the crucial quantity. Calculations of the output signal-to-noise ratio for a single RC network (low pass), a Gaussian filter, and an ideal rectangular low pass filter indicate that there is one db or less difference in the signal-to-noise ratio between these filters and the matched filter, i.e., if the bandwidth is chosen properly (79). For example, the optimum bandwidth for maximizing the peak signal-to-noise ratio is in the order of 1/T for a rectangular pulse of pulsewidth T passing through a rectangular low pass filter (78). Other signal shapes give essentially the same result. System bandwidth thus plays an important role in maximizing signal detectability in the presence of noise. The shape of the filter also plays an important role, but not as decisively.

INSTRUMENTATION

All optical components of the measurement system were mounted on a 48 inch optical bench and completely enclosed in an aluminum housing (inside blackened with flat black paint), as illustrated in Figure 1.

An Illumination Industries[1] Type III-110 100 watt high intensity mercury arc lamp was chosen for the excitation source of blue-ultraviolet light because of its high brilliance (140,000 cd/cm^2). This type of lamp normally operates at 20 volts @ 5 amps d-c. Characterized by a brilliant small diameter arc (0.3 mm) with an extremely high current density, the lamp operates at 40 atmospheres pressure. The arc lamp electrodes are enclosed in a quartz glass bulb which transmitts all radiation, as illustrated by the relative amplitude emission spectrum in Figure 2. Average rated lumen output is 2,200 lumens, with a life (average) of 100 hours. Total radiant power at 435.8 mμ wavelength was calculated to be about 2.5 watts (91). This corresponds to an output of 25.5 lumens (9).

The major difficulty of the short arc lamp was its extremely small arc. Since the focal length of the detection chamber condenser (≈5 cm) was shorter than the focal length of the lamp condenser (26.3 cm), the image size of the mercury

---

[1] Illumination Industries, Sunnyvale, California.

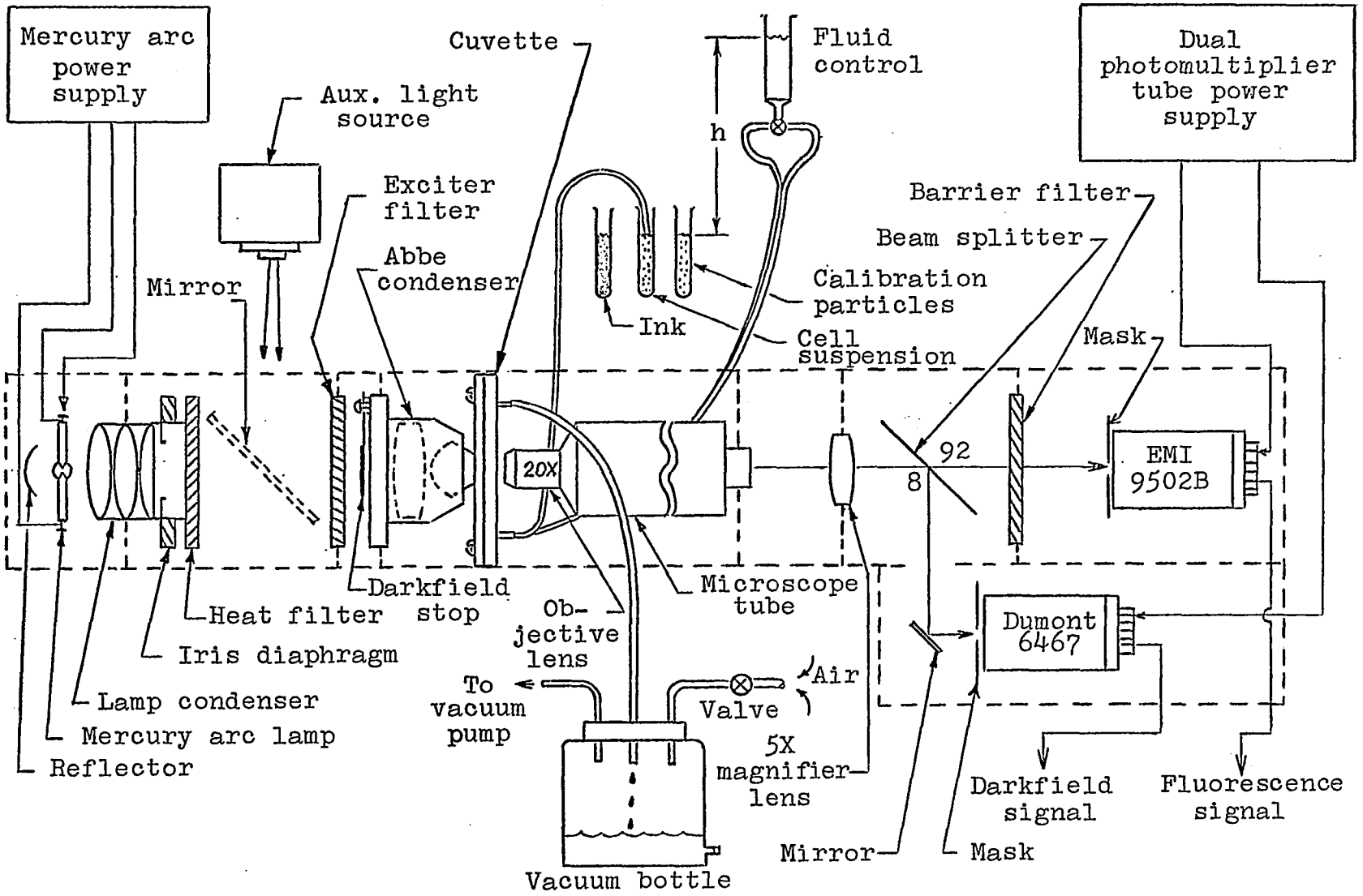

Figure 1. Detailed diagram of fluorescence/darkfield optical measurement system

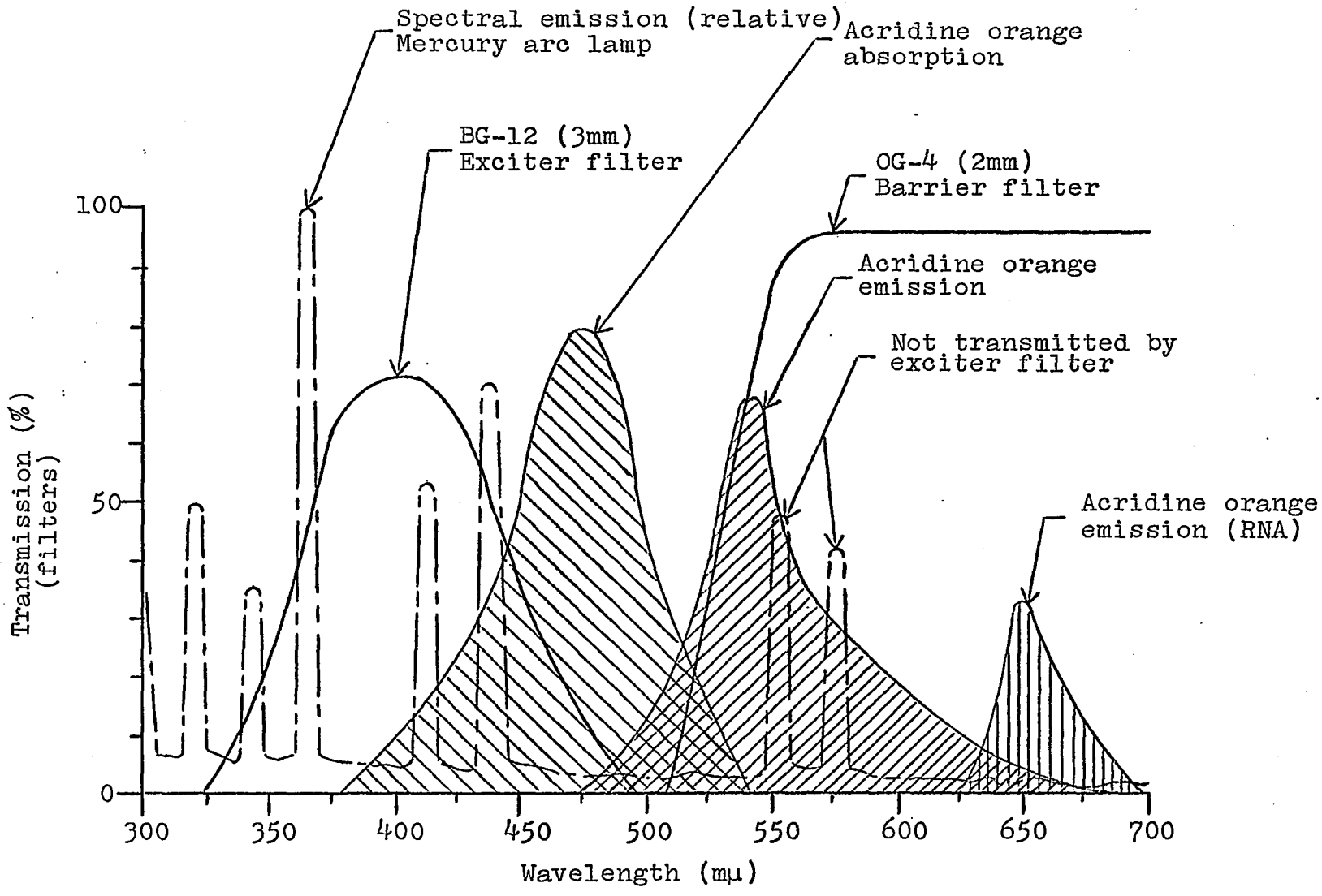

Figure 2. Characteristics of the mercury excitation source, filters, and absorption and emission of acridine orange

arc across the cell flow stream was further reduced in size (60μ).

Short arc lamps of this type (100 watt) must be operated on direct current. A mercury arc power supply was specially constructed for this experimental study.

The mercury arc lamp was mounted on a removable back mounting plate of an Illumination Industries Type III Model LH-350 or LH-360 lamphouse with the controls located on the back mounting plate to permit all degrees of lamp and mirror adjustment. The aluminized spherical mirror provided a light gain of up to 50%.

The lamp condenser used in this system consists of two unsymmetrical double convex lenses[1] (77 mm focal length, 52 mm diameter) and a plano convex lens[1] (83 mm focal length, 53 mm diameter), with an effective focal length of 26.3 mm. Spherical aberration was minimized as best as possible using the design method of Smith (81). Chromatic aberration was not a problem because of the nearly monochromatic excitation produced by the exciter filter.

With the mercury arc lamp situated at a distance equal to the focal length of the lamp condenser from the lamp condenser itself, a collimated beam of blue-white light was formed. An iris diaphragm was placed directly in front of the lamp

---

[1]American Science Center, Chicago, Illinois.

condenser to limit the diameter of the collimated beam of light to slightly greater than 25 mm diameter, the diameter of the back lens of the detection chamber condenser.

Mounted between the lamp condenser and the exciter filter was a 1/8 inch piece of heat absorbing glass[1] to block heat producing infrared radiation beyond 1000 mμ wavelength. Transmission greater than 350 mμ is unaffected, with exception of reflection losses.

An aluminized mirror placed at a 45° angle was mounted between the heat absorbing and exciter filter. This was used in the alignment procedure only and was removed during experimental runs.

The exciter filter used in this study was a 2 x 2 inch x 3 mm thick BG-12 Jena glass[2] absorption type colored optical glass filter. This type of filter was chosen because of its spectral characteristics with respect to the absorption region of acridine orange as illustrated in Figure 2. The 3 mm thick BG-12 transmitts blue-ultraviolet light excitation energy from 325 to 500 mμ wavelength with a maximum transmission of 72 per cent in the 410 mμ wavelength region. The transmission at the 435.8 mμ wavelength is 50 per cent. An anti-reflection coating reduces the reflection losses to near zero. This

---

[1] American Science Center, Chicago, Illinois.

[2] Fish-Schurman Corp., New Rochelle, New York.

exciter filter transmitts about 10 per cent from 700 mμ wavelength onwards toward the red end of the spectrum.

An American Optical[1] student type monocular microscope was modified somewhat and physically mounted on the optical bench for mechanical stability. The concave mirror, plain stage, movable mechanical stage, and eyepiece were removed from the microscope. A plain stage was constructed from 1/4 inch aluminum for mounting of the detection chamber. An adjustable mechanical stage was added to the plain stage for detection chamber positioning.

The detection chamber excitation condenser employed in this apparatus was an American Optical 1.25 numerical aperture Abbe microscope condenser located about 28 cm from the lamp condenser. This condenser is mounted on the movable microscope substage for ease of positioning. The Abbe condenser concentrates luminous blue-ultraviolet illumination from the exciter filter onto the cell flow stream within the detection chamber. Nonfluorescing immersion oil (n = 1.515) was used between the condenser and bottom glass of the detection chamber.

Darkfield illumination was employed by placing a 17.5 mm diameter circular stop in front of the back lens of the Abbe condenser. Using oil immersion, the numerical aperture of

---

[1]American Optical Co., Buffalo, New York.

the darkfield region was about 0.85. The irradiation intensity was reduced about 50 per cent of that attainable with bright-field illumination.

The detection chamber is a very crucial component in the cell identification system. The chamber used in this work follows the basic proportional fluid amplifier design given in Weinger (98) and Van Tilburg et al. (95), with a slight modification. A single stage proportional fluid amplifier is shown in Figure 3. High energy fluid from the power jet or power nozzle is directed into the interaction region. The purpose of the power nozzle is to provide a jet stream whose traverse velocity profile is uniform and symmetrical about the center line of the nozzle which can be deflected by the control fluid, i.e., control channel. A control fluid is directed into the interaction region from two jets on each side of the power jet. Normally the purpose of the control jets are to interact with the power jet causing a deflection into one or the other of two output apertures. The two output apertures are replaced by one output aperture in this work. When the fluid control pressures are equal the power jet (cell flow stream) is not deflected. Furthermore, the confined flow from the control jet (channel) causes an effective narrowing of the main jet flow. If the control channel pressure is increased sufficiently, the main jet (cell flow stream) will be extinguished.

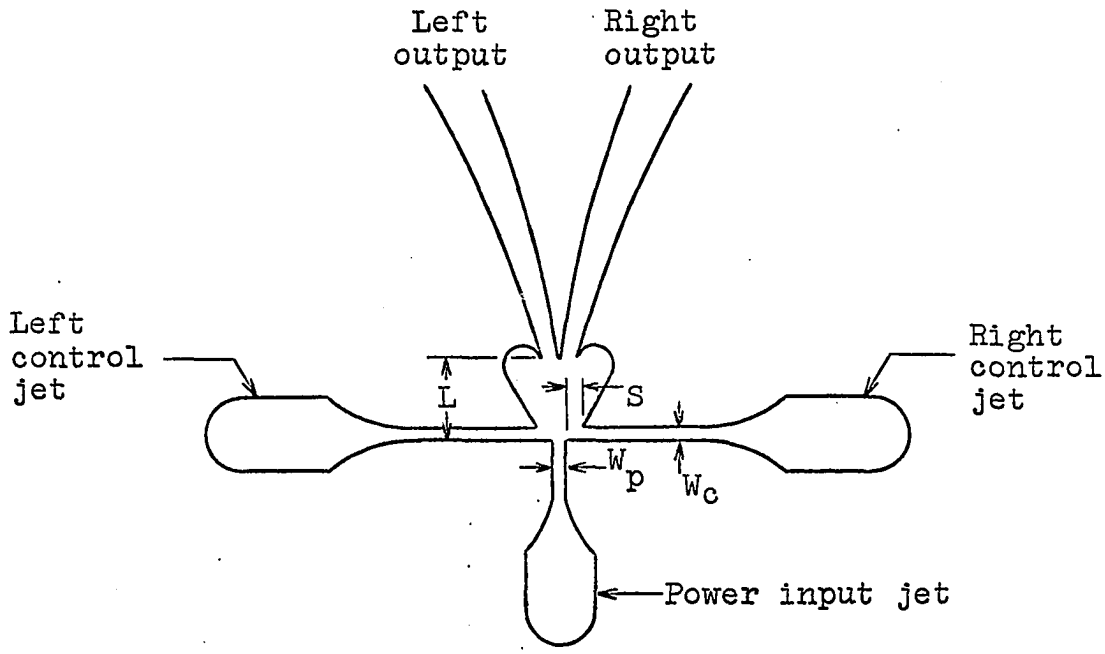

Dimensions

$W_c = 1.5W_p$

$S = 1.37W_p$

$L = 10W_p$

Figure 3. Proportional control fluid amplifier, modified after Weinger (98)

The detection chamber used in this work was designed from the geometrical relationships given for proportional fluid amplifier design by Weinger (98). The chamber consists of two 1 inch x 1 7/8 inch non-fluorescent glass microscope slides separated by a teflon spacer. The fluid amplifier and corresponding cell flow stream is formed between the two pieces of glass (Figure 4). Glass slides were specially selected so as to be free of scratches and pits. Spacers were fabricated by first making a pencil sketch (mask) of the spacer, overlaying it with the teflon, and then using a sharp scalpel to cut them out. Spacer thicknesses were 50, 75, 100, and 160 microns. The depth of the chamber, i.e., spacer thickness, was determined by the size of the particles being measured. Glass thickness on the excitation condenser side of the chamber varied from 1.145 to 1.120 mm for optimal excitation of the cell flow stream. The top piece of glass is 1 mm thick. Into this piece of glass was drilled (sand blasted) four small holes: one 1/32 inch in diameter for the cell flow stream, two 1/16 inch in diameter for the control channels, and one 3/32 inch in diameter for the exit flow. Into these holes were epoxyed a 22 ga., two 18 ga., and a 15 ga. hypodermic needle(s), each 3/8 inch long, respectively. Polyethylene tubing was connected to the small pieces of hypodermic needles for transfer of cells and fluid into and out of the chamber. The exit flow stream of the chamber was connected to a large

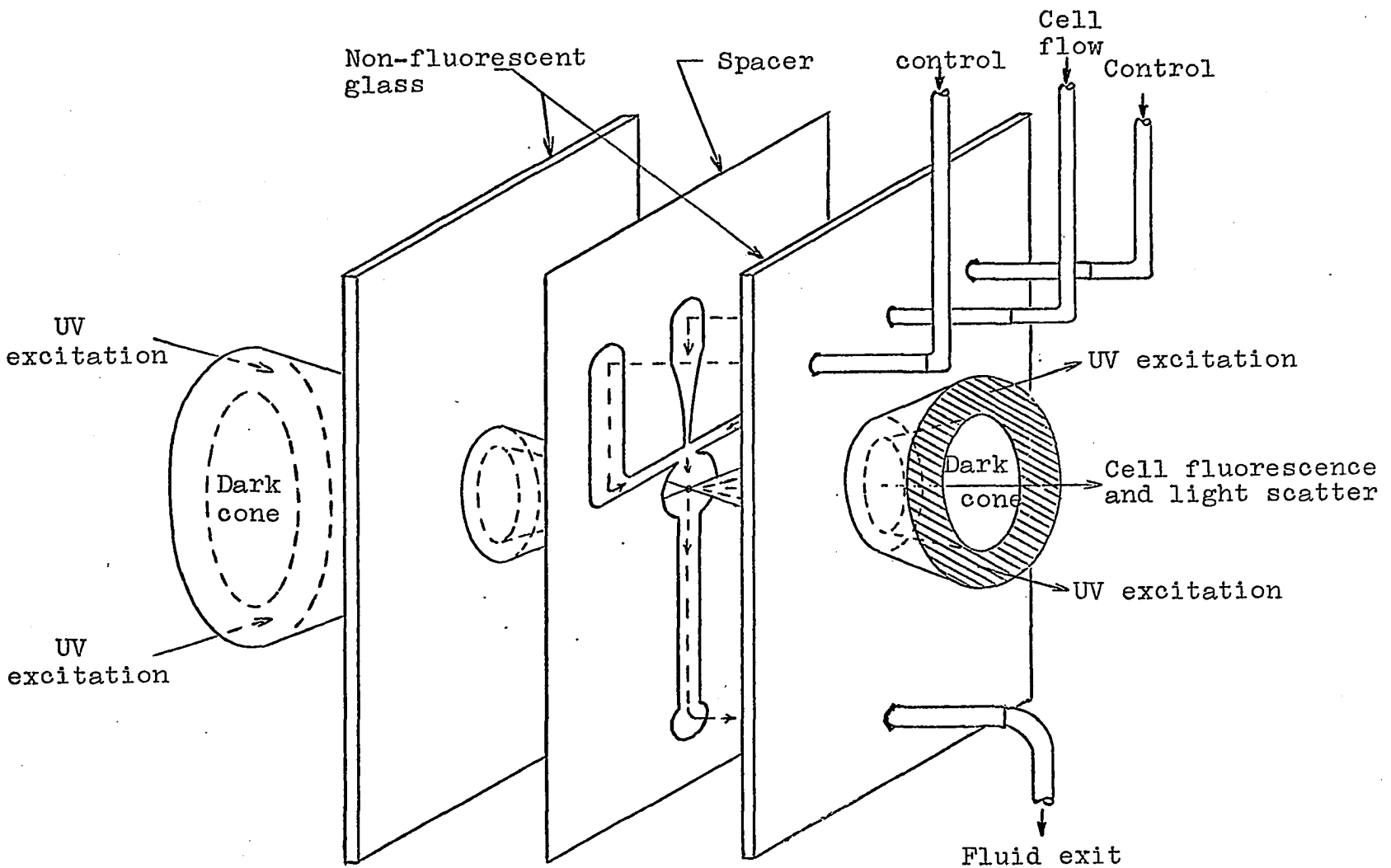

Figure 4. Expanded view of detection chamber illustrating darkfield illumination

bottle (1 1/2 gal.) to which a vacuum pump was connected. This functioned to create the necessary pressure for the cell flow jet and control jets to permit flow through the chamber. A 2 1/2 cc plastic syringe with eight 1/32 inch holes (spaced 1/4 inch apart) drilled in it and connected to the vacuum bottle with 1/8 inch plastic tubing was used to control the vacuum. The relative height between the cell container and control channel reservoir, coupled with the vacuum, determined the width of the cell flow stream. The flow rate was altered by adjustment of the vacuum or by the adjustment of a screw clamp situated on the exit tubing.

The detection chamber was housed in a 2 inch x 3 inch x 3/8 inch brass container referred to as the cuvette. This was then mounted onto the adjustable microscope stage for ease of positioning. Rubber bands were used to attach the cuvette firmly to the plain stage of the microscope.

A standard American Optical[1] 20X achromatic objective -5X double convex lens[2] system (total magnification 100X) focused the cell flow stream onto the masks of the fluorescence and darkfield photomultiplier tubes. The focal length, numerical aperture, and working distance (in air) of the 20X objective is 9.1, 0.5, and 0.8 mm, respectively, whereas, the focal

---

[1]American Optical Co., Buffalo, New York.

[2]American Science Center, Chicago, Illinois.

length of the 5X magnifier lens is 38 mm. The distance from the cuvette to the photocathode of each of the photomultiplier tubes was 48 cm.

A National Photocolor[1] 92/8 nonabsorbing 2 inch diameter pellicle (8 μ thick) beam splitter was placed directly behind the 5X magnifier lens. Ninety-two per cent of the incident fluorescence and light scatter from a cell was directed toward the fluorescence photomultiplier tube, whereas, eight per cent was directed (reflected) downward toward the darkfield photomultiplier tube. A 1 inch diameter aluminized mirror located 11 cm below the beam splitter directed the incident light toward the darkfield photomultiplier tube.

The barrier filter was mounted between the beam splitter and the fluorescence photomultiplier. The filter consists of two 2 inch x 2 inch x 1 mm thick pieces of OG-4 Jena Glass, absorption type colored optical glass filters. The OG-4 filter has a sharp cut-off near 515 mμ wavelength (Figure 2). Two other types of barrier filters were tried. The GG-14 Jena Glass filter, which has a cut-off near 480 mμ wavelength, passed the excitation light scattered from the cells, whereas, the OG-1 Jena Glass filter with a cut-off near 525 mμ wavelength offered no improvement over the OG-4.

Since the two photomultiplier tubes were relatively insensitive to wavelengths greater than 650 mμ wavelength no red

---

[1]National Photocolor Corp., South Norwalk, Connecticut.

suppression filter was used in front of these tubes.

Photomultiplier tube masks, which limit the observation zone across the cell flow stream, can be constructed using a number of different techniques (82). The method used was to cut the mask apertures from 0.005 inch thick exposed (black) photographic film negatives. Mask apertures were constructed such that the height of the observation zone within the detection chamber was slightly greater than the diameter of the cell nucleus (fluorescence) or overall cell diameter (darkfield). The width of the observation zone was set equal to or slightly greater than the cell flow stream. Photomultiplier tube masks were centered and mounted about 1/8 inch in front of the tubes on a specially constructed open-end metal cylinder (sleeve) which encloses the tubes. The metal sleeves were maintained at the photocathode potentials.

To protect the photomultiplier tube photocathodes from excessive direct light irradiation from the mercury arc lamp in the alignment procedure, two circular tube shields were constructed from 1/16 inch cardboard. These protectors were placed directly in front of the photocathodes of the photomultiplier tubes between the masks and the photocathodes.

Separate photomultiplier tubes were used for the fluorescence and darkfield channels. A specially selected (low dark current) E.M.I.[1] 9502B photomultiplier tube was used for

---

[1]Whittaker Corp., Gencom Div., Plainview, L.I., New York.

fluorescence measurement, whereas, a Dumont[1] 6467 photomultiplier tube was used for light scatter measurements. The 9502B is a high gain (G = 35.6 x 10^6 @ 1780 volts) 13-stage "venetian blind" type photomultiplier tube designed for low light level applications. The 6467 is a medium gain (G = 2.15 x 10^5 @ 1260 volts) 10-stage box and grid type photomultiplier tube. Both photomultiplier tubes have S-11 spectral response photocathodes.

A dual variable high voltage photomultiplier tube power supply was designed and constructed for the 9502B and the 6467. Dynode voltages of the photomultiplier tubes were supplied from a chain of 470K ohm, 1/4 watt resistors (mounted at the base of the tubes) across the high voltage supply as illustrated in Figure 5. To stabilize the photocathode-dynode No. 1 voltage of the 9502B photomultiplier tube at the recommended value of 150 volts, a 150 volt zener diode was employed. Photomultiplier tube voltages were measured using a multimeter.

Fundamentally, both photomultiplier tubes function as photoelectron (current) amplifiers, the anode current (i_a) being a linear function of the input light energy in lumens or watts (25). Both tubes drive current-to-voltage transducers (3) using differential operational amplifiers[2] with output

---

[1] Dumont Labs, Clifton, New Jersey.

[2] Analog Devices, Inc., Cambridge, Massachusetts.

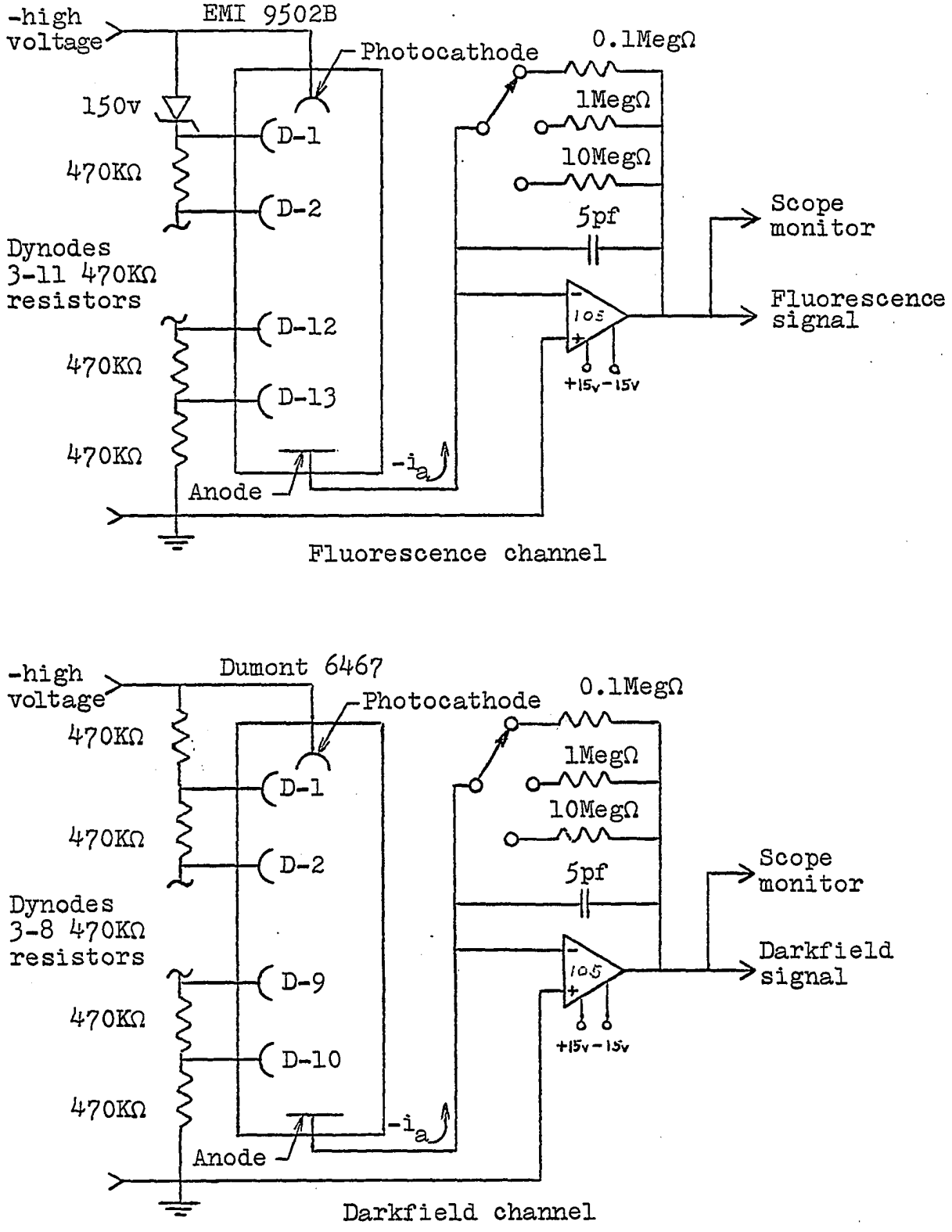

Figure 5. Photomultiplier tube circuitry

voltages a direct function of the input currents, i.e., $e_o = -i_a R_L$. Inasmuch as peak signal currents are in the low microampere range, load resistors of 100K ohm, 1 megohm, and 10 megohm were chosen.

Output signals from both current-to-voltage transducers were fed directly to clamping circuit of zero or -1.4 volts (Figure 6). Operational amplifiers were used in voltage follower circuits to reduce loading effects of the negative 1.4 voltage clamping circuits.

The fluorescence and darkfield signals from the clamping circuits were fed directly to a Krohn-Hite[1] model 3202 variable low-pass/high-pass filter for system bandwidth adjustment.

Both signals were recorded on Ampex[2] Type 748 magnetic instrumentation tape using an Ampex Model 1300 rack mounted recorder/reproducer system for storage and future data processing on the LINC-8 digital computer[3].

A dual beam oscilloscope was used to monitor the fluorescence and darkfield signals. An electronic counter was used to count the number of signals recorded. This counter was connected to either of the two measurement channels. A

---

[1]Krohn-Hite Corp., Cambridge, Massachusetts.

[2]Ampex Corp., Redwood City, California.

[3]Digital Equipment Corp., Maynard, Massachusetts.

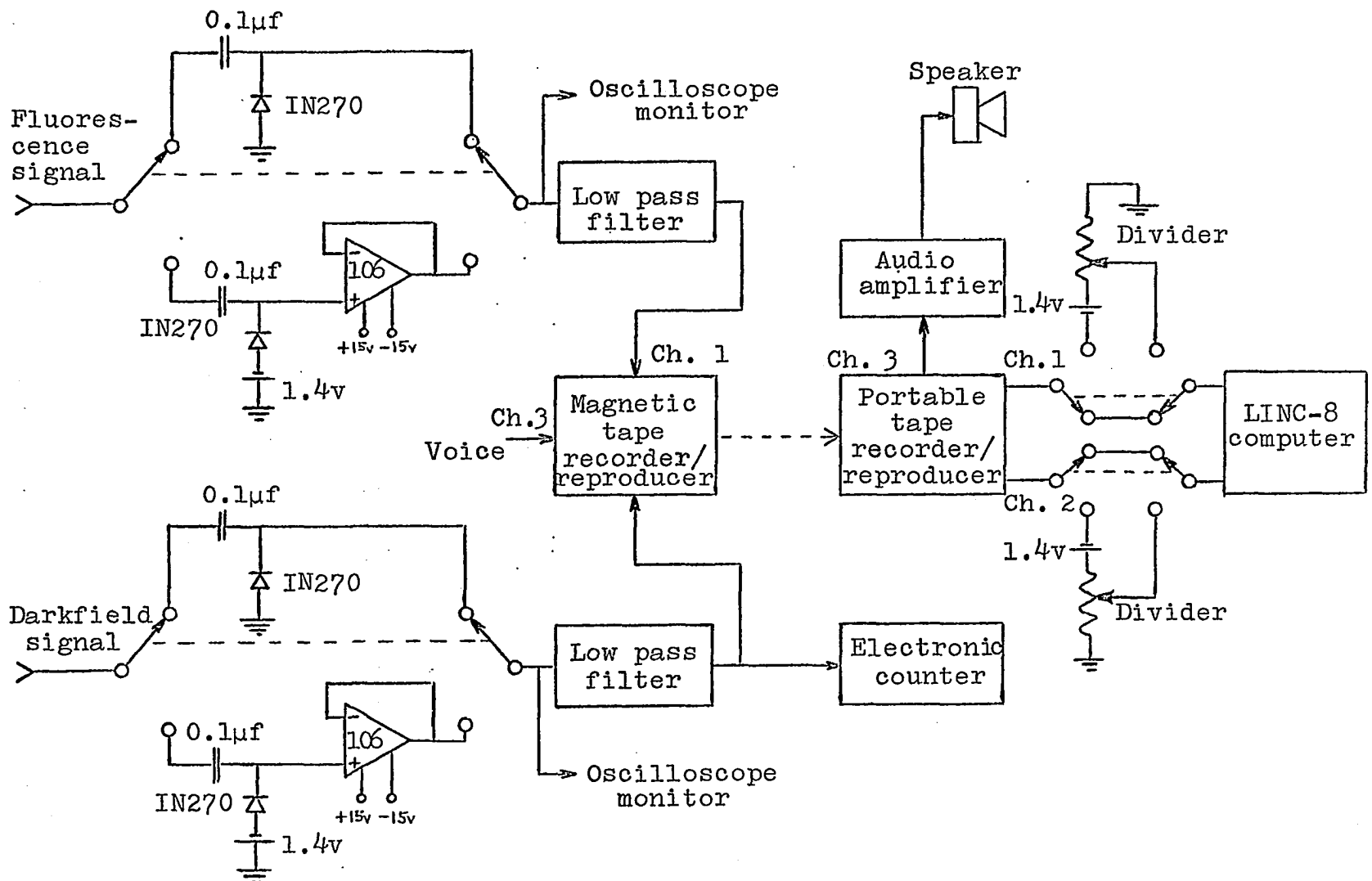

Figure 6. Diagram of fluorescence/darkfield electronics system

Philbrick Researches[1] Model PR-30 regulated power supply was used to supply the necessary d-c power to all differential operational amplifiers used.

---

[1] Philbrick Researches, Dedham, Massachusetts.

EXPERIMENTAL PROCEDURE

The overall objective of this study was the development of an automatic flow-through opto-photoelectric system (technique) capable of simultaneously measuring the fluorescence and darkfield (light scatter) optical properties of individual biological cells in dilute aqueous suspension. Both living and non-living cells were used in this study. With the system properly aligned and calibrated, cells were tagged with acridine orange for selective staining of the nucleus, diluted, and allowed to flow through the system for measurement. Photomultiplier tube signals were recorded on magnetic tape for future processing. A small digital computer was used to compute and display the fluorescence (nucleus size) and darkfield (overall cell size) peak signal amplitude and relative ratio distributions. In order to evaluate system performance, the peak signal amplitude distributions are compared with distributions of the same cell type that have been determined by other investigators. Relative ratio distributions are compared to their respective peak signal amplitude distributions. Cell size distributions of two types of pollen, as measured automatically by the system and manually with a microscope and eyepiece micrometer are compared. Standard deviations are compared for similarities. The average peak fluorescence and darkfield signal amplitudes vs. cellular cross sectional areas are plotted for the various cells tested.

To evaluate the measurement systems ability to differentiate between nucleated and non-nucleated cells, a cell suspension containing both types was used. An example using statistical decision theory is given to illustrate the use of Bayes method of distinguishing between different cell types in an aqueous mixture. In the process of evaluating the system, not only is the system being evaluated, but the salient features of the cell distributions are also observed.

Acridine orange dye[1], color index 46005, was chosen as the basic fluorochrome in this study because of its specific affinity for the nucleic acids present in the cell. When utilizing proper staining conditions (8, 73) with acridine orange, fluorochromed deoxyribonucleic acid fluoresces from green to green-yellow (530 mμ wavelength) and ribonucleic acid from orange to red-orange (650 mμ wavelength). The strongest region of acridine orange absorption is from about 435 to 500 mμ wavelength.

One of the many advantages of acridine orange is the simple bulk fluorochroming technique for staining large numbers of cells in aqueous suspensions (87). This method consists of adding a fixed amount of a dilute solution of 0.01 to 0.001 per cent acridine orange to fixed amount liquid cell suspension. After allowing adequate time for staining to occur, the cell-dye suspension is further diluted and is ready for measurement.

---

[1]National Aniline Div., Allied Chemical Corp., New York, New York.

Non-buffered stock dye solutions[1] of acridine orange in distilled water (0.001% and 0.01%), frog Ringer's (0.01%), and physiological saline (0.01%) were employed in the bulk fluorochroming process. The pH of these solutions varied from 5.9 to 7.0, which is close to that specified by Bertalanffy (8) for optimal staining results.

Thirteen different types of biological cells plus two sizes of latex particles were selected for evaluation in this research study. These ranged in size from large pollen grains (46 μ diameter) to small latex particles (0.81 μ diameter).

Pecan[2], ragweed[2], paper mulberry[2], and chinese lilac pollen grains were chosen for initial testing of the measurement system because of their large spherical size, ease of handling, and bright autofluorescence. The chinese lilac pollen sample, which was locally obtained, contained a considerable amount of noncellular debris, which altered the darkfield distribution considerably. All pollens were placed in a small test tube, suspended in 95 per cent ethanol, shaken vigorously, ultrasonically agitated to remove clumps and then dispersed in distilled water.

---

[1]10 mg of AO dissolved in 100 ml of diluent (0.01%) and 1 mg of AO dissolved in 100 ml of diluent (0.001%).

[2]Coulter Diagnostics, Inc., Miami Springs, Florida.

Two sizes (types) of isolated rat liver nuclei were obtained for measurement using the methods of Blobel and Potter (11) and Chauveau et al. (18). These diploid and tetraploid nuclei were suspended in Earl's Balanced Salt solution[1] (EBSS) and stored slightly above freezing prior to measuring.

Frog (Rana pipiens), goldfish (Carassius auratus), and avian (Leukotrol[2]) erythrocytes were chosen because of their size and the fact that they are nucleated. Whole frog and goldfish blood was placed in frog Ringer's solution[3], whereas, avian erythrocytes were placed in physiological saline (0.85% NaCl in H_2O). Sturkie (85) gives a physiological saline (Ringer's solution) for birds which should preferably be used rather than normal mammalian physiological saline. A few drops of sodium heparin were added to the cell suspensions to inhibit clotting.

Heparinized fresh dog blood was first centrifuged at 700 rpm for 4-8 minutes. The leucocyte rich plasma was pipetted off and re-centrifuged at 2000 rpm. The cell pellet of erythrocytes and leucocytes was then withdrawn and placed

---

[1] 6.8 gm NaCl, 0.4 gm KCl, 0.1 gm $MgSO_4$, 0.125 gm NaH_2PO_4, 2.2 gm $NaHCO_3$ and 1.0 gm glucose dissolved in 600 ml of distilled water.

[2] Pfizer Diagnostics, Chas. Pfizer and Co., Inc., New York, New York.

[3] 6.5 gm NaCl, 0.14 gm KCl, and 0.12 gm $CaCl_2$ dissolved in 1000 ml of distilled water.

in EBSS. No attempt was made to remove the erythrocytes from the blood cell suspension. The cell suspension was briefly ultrasonically agitated prior to measurement.

Defibrinated whole swine blood was centrifuged at 700 rpm for 4-8 minutes to obtain a leucocyte rich plasma. The leucocyte rich plasma was pipetted off and re-centrifuged at 2000 rpm. The leucocyte rich pellet was then re-suspended in 0.3 per cent saline to remove the remaining erythrocytes. This method proved quite effective for lysing the erythrocytes, but the cell membranes remained intact. The leucocyte-erythrocyte membrane solution was re-centrifuged at 2000 rpm. The cell pellet was then removed and placed in EBSS for measurement. Cells were ultrasonically agitated and filtered through eight layers of cheese cloth to remove clumps prior to measurement.

Cultured lymphocytes grown in Eagle's MEM solution (23) were also measured in this study. These cells were suspended in EBSS prior to measurement. The culture was a number of days old and thus the cell suspension contained a large amount of debris.

Yeast cells (Saccharomyces cerevisiae) and small cocci (Staphylococcus aureus), which were selected because of small size and ease of handling, were placed in physiological saline. The yeast cells were ultrasonically agitated and then filtered through coarse tissue paper to remove large

clumps due to budding, etc., whereas, the bacteria were only sonically agitated.

Two sizes of spherical monodispersed latex particles[1] were measured (light scatter only). The larger 7.6 μ diameter particles are styrene divinylbenzene copolymer latexes, whereas, the smaller 0.81 μ diameter particles are polystrene latexes. Both types of particles were dispersed in distilled water. Prior to placing in distilled water, they were suspended in 95 per cent ethanol (wetting agent) to reduce clumping. Both types of latex particle suspensions were ultrasonically agitated prior to measurement.

Employing the stock dye solutions of acridine orange each group of cells was visually tested for optimal dye concentration (coloration and intensity) using a fluorescence microscope with darkfield illumination (mercury arc lamp). Cell samples to be tested were fluorochromed at different dye concentrations and the coloration and intensity recorded. It was experimentally determined that for most types, with the exception of pollen, yeast, and bacteria, the final overall dye concentration was 0.001 per cent. When a cell was properly stained the nucleus fluoresced bright green-yellow and the cytoplasm was relatively clear of fluorescence, with the exception of granules of RNA which fluoresced red-orange. Cells that were understained fluoresced pale green (nucleus).

---

[1] Dow Diagnostic Products, Midland, Michigan.

Those which were over-stained fluoresced orange (nucleus and cytoplasm). The point at which over-staining occurs is very pronounced. For example, cells stained at a final dye concentration of 0.0025 per cent fluoresced dull orange-yellow. Fluorescent intensity and coloration of the cell varies directly as the dye concentration until a definite concentration is obtained, at which, degeneration ensues (76). Necessary staining time was determined to be about two minutes in all cases, with exception of pollen for which it was difficult to ascertain. Once the two minute staining time had elapsed, the cell suspensions were diluted and made ready for measurement. Final dye concentrations, along with color of cytoplasm and nucleus, are listed in Table 1.

Some difficulty was encountered in the staining of some cells. Pollen grains exhibited a strong degree of autofluorescence, which was nearly uniform across the cell. Paper mulberry and chinese lilac pollen fluoresced green-yellow, whereas, ragweed and pecan pollen fluoresced yellow-orange. In order to effectively stain the various pollen grains, the final dye concentration had to be lowered to 0.0001 per cent. The nuclear region of the pollen grains fluoresced a brighter green-yellow, with the exception of ragweed. The remainder of the cell remained green-yellow. The nucleus of fixed avian erythrocytes (Leukotrol) fluoresced a fainter green-yellow than the other types of cells tested. There were granules

Table 1. Dye concentrations, colors, and dilutents of cells used in fluorescence/darkfield studies

Cell	Final dye concentration	Cytoplasm color	Nucleus color	Dilutent
P. mulberry pollen	0.0001% ($1/10^6$)	green-yellow	green-yellow	Distilled water
Ragweed pollen	0.0001% ($1/10^6$)	yellow-orange	--	Distilled water
Chinese lilac pollen	0.0001% ($1/10^6$)	green-yellow	green-yellow	Distilled water
Pecan pollen	0.0001% ($1/10^6$)	yellow-orange	green-yellow	Distilled water
Rat liver nuclei	0.001% ($1/10^5$)	--	green-yellow	EBSS
Frog blood (erythrocytes)	0.001% ($1/10^5$)	clear	green-yellow	Frog Ringer's
Goldfish blood (erythrocytes)	0.001% ($1/10^5$)	clear	green-yellow	Frog Ringer's
Avian erythrocytes	0.001% ($1/10^5$)	lt. green granules	green-yellow	0.85% saline
Dog leucocytes	0.001% ($1/10^5$)	Red-orange granules	green-yellow	EBSS
Swine leucocytes	0.001% ($1/10^5$)	Red-orange granules	green-to-lt. green	EBSS
Cultured lymphocytes	0.001% ($1/10^5$)	clear	green-yellow	EBSS
Yeasts	0.0005% ($1/2\times10^5$)	light green	green-yellow	0.85% saline
Cocci (bacteria)	0.001% ($1/10^5$)	green-yellow	--	0.85% saline

within the cytoplasm, which did not appear in unfixed avian erythrocytes (82). The coloration and intensity of swine leucocytes varied somewhat more than anticipated. This was thought to be primarily due to treatment in removing of the erythrocytes. The nucleus of yeast cells fluoresced bright green-yellow, whereas, the cytoplasm fluoresced a very light green-yellow.

The concentration of cells per unit volume was not determined in the tests. Cell suspensions were easily checked under the microscope to verify that they were adequately separated from each other. A more effective and quicker method was to add cells to, or dilute the diluent at the start of a test by observing the pulse density on the oscilloscope monitor. Detection chamber spacer thicknesses (50, 75, 100 and 160 μ) were selected so that they were four to five times the diameter of the cell being tested. This was experimentally determined to be adequate for proper laminar, non-plugged, flow through the chamber. Turbulence did occur when initially using the 160 μ spacer, but was corrected by slowing down the flow.

The following experimental procedure was used during this investigation. Electrical equipment, with exception of the photomultiplier tube power supply, was turned on about one-half hour prior to a test in order to reach thermal stabilization. Prior to starting the mercury arc lamp the

photomultiplier tube shields and proper calibration masks should be in place, with the darkfield stop, exciter filter, and barrier filter removed. The detection chamber which had been previously physically centered was flushed with distilled water (gravitational flow) from the control channel reservoir to remove air bubbles. Water exits from both the cell line and output during the flushing process. While the chamber was being flushed the chamber condenser was slowly advanced toward the detection chamber and the mercury arc imaged on the photomultiplier tube masks by adjustment of the microscope objective lens. The arc image was centered on the mask apertures by adjustment of the lamp centering controls or slight movement (positioning) of the photomultiplier tubes themselves. This completed the preliminary adjustment of the mercury arc and the condenser was backed away from the chamber. The cell line was then placed in the ink container and the vacuum pump turned on to form a relatively narrow ink jet flow through the chamber. The jet was observed for turbulence by placing a white card in front of the fluorescence photomultiplier tube and refocusing the objective lens. The ink jet can be narrowed or widened by adjustment of the control channel fluid height (h) with respect to the detection chamber, or by adjusting the vacuum, or by adjustment of the screw clamp (if used) on the fluid exit of the chamber. The width of the ink jet in the chamber was maintained at 50 μ, which corresponds to 5 mm at

the photomultiplier tube masks. The ink jet can easily be centered on the mask apertures by adjustment of the movable stage controls. To assure that no air bubbles are contained within the chamber, it should be re-flushed with water and the ink alignment repeated. When the vacuum pump is on, the chamber can be flushed with water by placing the cell line in a container of water. The chamber flushing process can be speeded up by opening and closing the valve located at the base of the control channel reservoir. Care should also be taken to pinch-off the cell flow line when removing it from the ink, water, or cell suspension. With the ink jet centered on the mask apertures, the microscope condenser was backed-off, immersion oil added to the front lens, and then advanced toward the chamber, making close contact with it to remove air bubbles. At this point the microscope objective was re-focused to verify that the mercury arc and ink jet has remained fixed. At this point the auxiliary light source was turned on and the mirror placed in front of the mercury lamp condenser. Light from the auxiliary lamp was directed toward the chamber condenser (Kohler illumination) and the ink jet was slightly re-focused on the mask apertures. The fluid level of the control channel should be recorded, so as to maintain a constant flow channel width during an experimental run. The auxiliary lamp and mirror were then removed, as the alignment procedure was completed. The chamber was thoroughly flushed with water to

remove the ink. The darkfield stop of the detection chamber condenser was swung into place and optically centered by placing a white card directly in front of the 5X magnifier lens and observing the darkened image of the darkfield stop upon it. Once the darkfield stop was in place, the photomultiplier tube shields were removed and the BG-12 exciter filter placed in the system and the entire system enclosed.

Paper mulberry pollen was used throughout this experimentation for system calibration. A small amount of pollen (about 1 mm^3) was placed in a small test tube containing about 1/2 ml of 95 per cent ethanol to serve as a wetting agent. To this was added about 4 ml of distilled water. The cells were vigorously shaken, ultrasonically agitated, and placed in a container. The fluid levels of the pollen container and control reservoir were adjusted to the same height used in the alignment procedure. The cell line (pinched) was then placed into the pollen suspension. The photomultiplier tube power supplies were turned on and the voltage across the fluorescence and darkfield photomultiplier tubes adjusted. Since the barrier filter was not used in the calibration procedure, both channels record light scatter from the paper mulberry pollen grains. Calibration signals from the fluorescence and darkfield channels were recorded on magnetic tape. Voice comments were recorded at the beginning of each test run. The gain of the photomultiplier tube current-to-voltage transducers

(amplifiers) were adjusted by changing its load resistance (Figure 5). A counter was used to determine when a sufficient number (greater than 512 or 2048) of cell pulses had been recorded. After the calibration test run, the photomultiplier tube power supplies were turned off, the cuvette flushed with distilled water, and the system opened. The calibration masks were replaced with the proper size test masks, the barrier filter added, and the system then closed.

Cells being tested were placed in a clean test tube and stained with acridine orange. A slight amount of agitation thoroughly mixes the dye with the cell suspension. After allowing two minutes for cell staining, the suspension was diluted, ultrasonically agitated, and placed in the cell holder to be measured. The cell flow tube (pinched) was placed into the cell suspension, the fluid levels adjusted, and the photomultiplier tube power supplies turned on. The fluorescence and darkfield signal voltages were recorded on magnetic tape. When a sufficient number of cells had been counted, the photomultiplier tube power supplies were turned off and the detection chamber flushed with water. If no other test runs were to be performed, the system was opened up and the photomultiplier tube shields replaced. If other cells were to be tested, the photomultiplier tube masks could easily be changed and the other cells measured. If it is desired to run the calibration test after the actual cell test, the experimental procedure

can be altered to accommodate this.

To determine the proper bandwidth setting of the variable low pass filter (fluorescence channel) in the noisy measurement situation the following procedure was used. The pulse width of the darkfield signal was measured on the oscilloscope. With this information and the approximate sizes of the nucleus and cytoplasm known, the pulse width of fluorescence signal can be calculated. Once the pulse width is known the minimum bandwidth (Hz) can be determined by dividing the pulse width (in seconds) into one (79).

A portable Ampex[1] Model FR-1300 was employed to get the recorded data from the magnetic tapes into the A/D converter of the LINC-8 computer. Both the portable and rack-mounted recorder/reproducer systems were calculated prior to recording and playing back of the data. Data was recorded at a tape speed of 30 ips and played back at 7 1/2 ips.

Three LINC-8 computer programs[2] were employed in the data reduction and analysis. The first two programs compute the peak signal amplitude frequency distribution from 512 or 2048 measured cells for either the fluorescence or darkfield channels (Figure 7). These programs compute the amplitude (size) distribution for only one channel at a time, not simultaneously. The incoming signals are sampled and digitized by

---

[1]Ampex Corp., Redwood City, California.

[2]Psycho-Toxicology Laboratory, Veterinary Medical Research Institute, Iowa State University, Ames, Iowa.

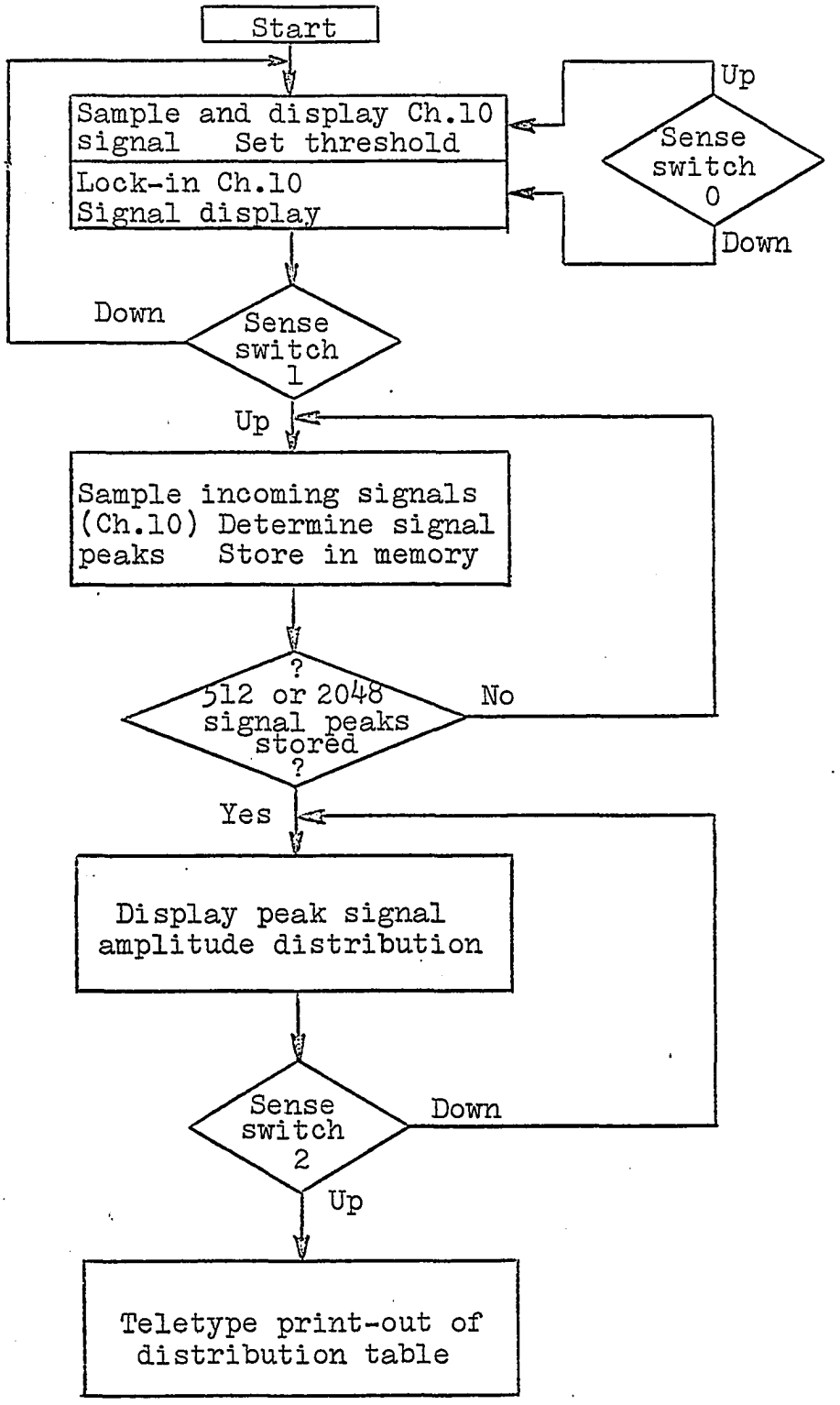

Figure 7. Peak signal amplitude distribution computer flow diagram

the A/D converter and compared to a variable threshold level (0 to 1000 millivolts). If the instantaneous amplitude of a cell exceeds the threshold, its peak amplitude is determined and stored. Sense switches control computer operation. The computer can display the incoming signal continuously or store it indefinitely on its display scope. The computer sorts the peak amplitudes of either 512 or 2048 cell pulses into 25 millivolt increments from zero to 1000 millivolts. The computer then displays the peak amplitude distribution on its display scope. If the amplitude of a cell exceeds 1000 millivolts it is registered by the A/D converter as 1000 millivolts. The horizontal axis of the distribution display is divided into increments of 25 millivolts (300 millivolts per inch of scope display) from zero to 1000 millivolts, whereas, the vertical axis represents the number of cells contained within each 25 millivolt increment. The vertical scale factor is conveniently controlled (right switches). If the cell signals are greater than 1000 millivolts, a voltage divider (pad) can be used to compress the data along the horizontal axis, with some loss of resolution (Figure 6). Once the computer has analyzed enough incoming data and displayed the peak signal amplitude on the display scope, a polaroid picture can be made with the scope camera for a permanent record. The computer teletype will print out the complete distribution if required.

The third computer program computes the relative ratio distribution from 512 cells, i.e., the fluorescence peak

signal amplitude (nuclear size) divided by the darkfield peak signal amplitude (overall cell size) or vice versa, and displays it on the computer display scope (Figure 8). Incoming fluorescence and darkfield signal waveforms are digitized by the A/D converter and displayed. Computer operation is again conveniently controlled by the sense switches. Both the channels have variable threshold levels which must be exceeded for the computer to determine the individual signal ratios. If either of these signals do not exceed the threshold, or exceed 1000 millivolts, the computer will not determine the ratio for that particular cell. The horizontal axis of the display is divided into intervals of 0.2 ranging from 1 at the center of the display to 51.2 at the far right and the inversion of these intervals to the left side of the center (1). The vertical axis magnitude is again conveniently controlled (right switches).

The measurement system was designed such that 0 to 1 or 0 to 2.8 volt (maximum) signal pulses could be recorded on magnetic tape (Figure 6). The maximum nominal input level for this recorder/reproducer system is ±1.0 V(rms). To fully utilize the maximum capability of the system, the 0 to 2.8 volt range should be used. Initially, data was recorded within the 0 to 1 volt range. Pollen grains, frog blood, fish blood, and rat liver nuclei were recorded within this range. The remaining cells measured were recorded in the 0 to 2.8 volt

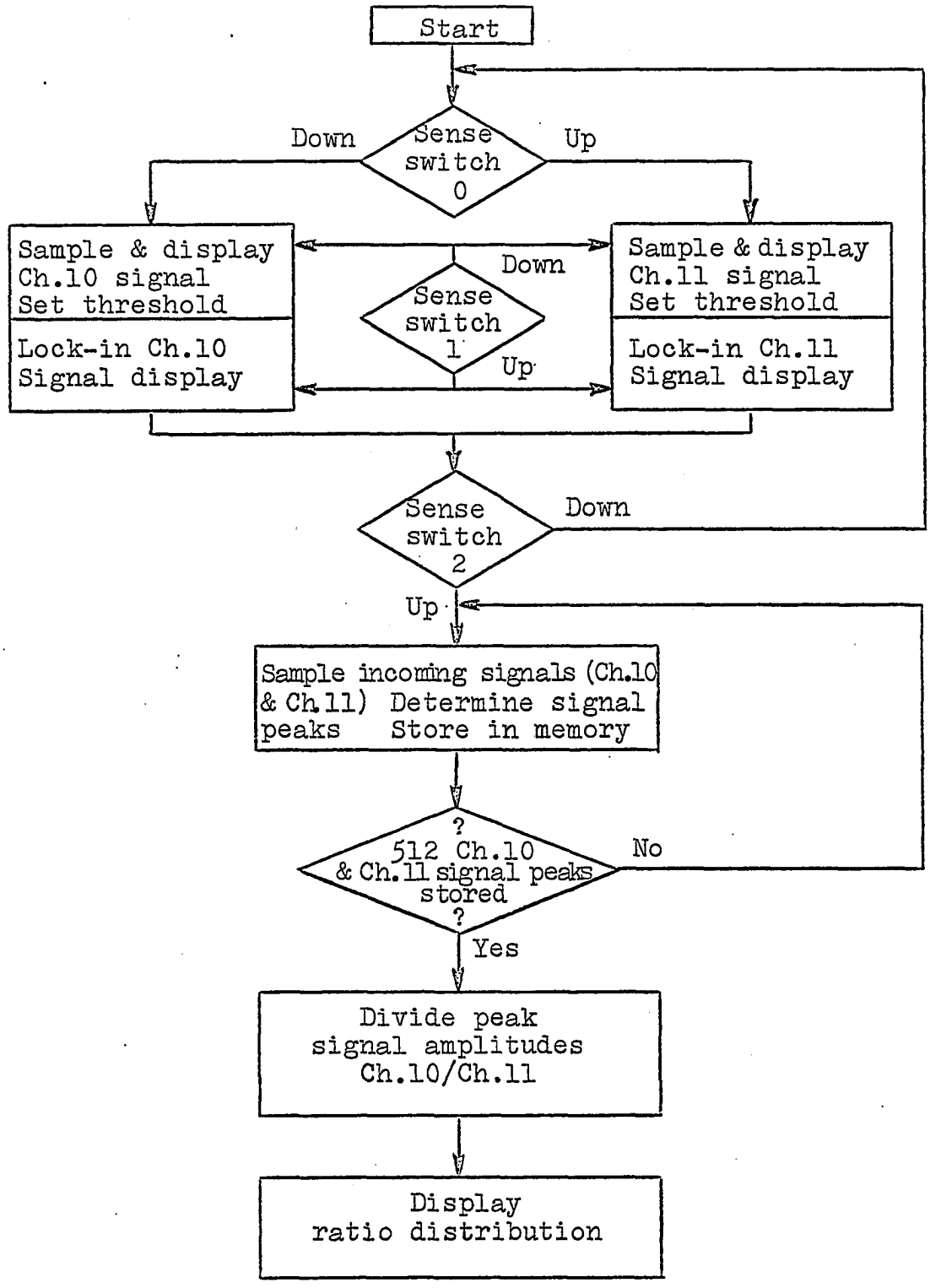

Figure 8. Relative peak signal amplitude ratio distribution computer flow diagram

range. The 0-2.8 volt recording capability was incorporated midway through the testing program to permit a wider distribution of large and small cells to be recorded then analyzed by the computer. Since the computer program and A/D converter can only analyze signals in the 0 to 1 volt range, a voltage divider was used to reduce a 2.8 volt peak signal to 1 volt (Figure 6).

As stated previously a calibration run was made prior to or after each cell type tested. A scheme was devised to account for test to test variations in excitation light intensity within the detection chamber and misalignment. Photomultiplier tube current gain (G) is defined as

$$G_i = \frac{I_{a_i}}{I_{in_i}} = \frac{V_{a_i}/R_{L_i}}{I_{in_i}} \quad @ \quad V_{pm_i} , \qquad (6)$$

where I_{a_i} is the anode current, the anode voltage divided by load resistance (V_{a_i}/R_{L_i}), I_{in_i} the photocathode current, and V_{pm_i} the overall photomultiplier tube voltage for a particular calibration test ($i = 1,2,....n$). The photocathode current varys from test to test, but should remain fixed from run to run of an individual test, assuming that the same type and size of particle is always used for system calibration. It can be expressed as

$$I_{in_i} = K_i \; I_{in}(ref), \text{ for } i = 1,2,....n, \qquad (7)$$

where I_{in} is the photocathode current of a particular test, K_i the i^{th} calibration constant, and $I_{in}(ref)$ the reference photocathode current. Equation 7 can be substituted into Equation 6, yielding

$$G_i = \frac{V_{a_i}/R_{L_i}}{K_i\ I_{in}(ref)} \quad @ \quad V_{pm_i} \tag{8}$$

The gain for an individual test can be referred to some other gain (ref) of another test in the following manner. The reference calibration gain G(ref) can be expressed as

$$G(ref) = \frac{V_a(ref)/R_L(ref)}{I_{in}(ref)} \quad @ \quad V_{pm}(ref), \tag{9}$$

where $V_a(ref)$ is the reference anode voltage, $R_L(ref)$ the reference anode load resistance, $I_{in}(ref)$ the reference photocathode current, and $V_{pm}(ref)$ the reference overall photomultiplier tube voltage for the reference calibration test. If Equation 8 is substituted into Equation 9, the calibration gain constant K_i can be determined for a particular test with respect to the reference calibration test, as given below

$$K_i = \frac{V_{a_i}}{V_a(ref)} \times \frac{R_L(ref)}{R_{L_i}} \times \frac{G(ref)}{G_i}, \tag{10}$$

where i = 1,2,....n.

Photomultiplier tube calibration gains G_i can be calculated from Equation 5 for their respective voltages V_{pm_i}. Average peak anode signal voltages V_{a_i} can be obtained from the calibration voltage distributions. Each test will usually have a different calibration gain constant. The reference gain G(ref), average peak anode calibration signal voltage V_a(ref), and reference load resistance R_L(ref) for both fluorescence and darkfield channels were taken from a particular calibration test using paper mulberry pollen. Both the fluorescence and darkfield calibration gain constants $K_{i_{fl}}$ and $K_{i_{df}}$ are equal to one (1) for the reference test. Calibration gain constants varied from 0.282 to 2.71. Once the fluorescence and darkfield calibration gain constants for a particular test had been determined, the relative calibrated gains of the two channels can be determined by

$$G_{fl} = K_{i_{fl}} \times G(j)_{fl\ data} \tag{11}$$

and

$$G_{df} = K_{i_{df}} \times G(j)_{df\ data} \tag{12}$$

where $G(j)_{fl\ data}$ and $G(j)_{df\ data}$ are the photomultiplier gains determined from Equation 5 at a voltage V_{pm_i} for a particular data run.

RESULTS

Shown in Figures 9 through 23 are the fluorescence and darkfield (light scatter) signal waveforms and their respective peak signal amplitude distributions. The upper waveform illustrates a typical fluorescence signal and the lower waveform is the simultaneous darkfield signal, with exceptions being the sample calibration (Figure 9), yeast cells test (Figure 22) and the latex particles test (Figure 23). All signal waveforms, with exception of the sample calibration were photographed using a storage oscilloscope and camera from recorded data stored on magnetic tape. The sample calibration signal waveforms were photographed from the display scope of the LINC-8 computer. Peak fluorescence and darkfield signal amplitude frequency distributions were obtained for all cell types tested with exception of the small bacteria (Figure 24). Ratio distributions (peak fluorescence signal divided by peak darkfield signal) for rat liver nuclei, goldfish blood, and dog and swine leucocytes are illustrated in Figure 25. Due to similarities in the ratio distribution, only a selected number of these were obtained.

Prior to, or immediately after, completing a series of test runs on a specific type of cell, a calibration test was performed. A typical calibration peak signal distribution (prior to running goldfish blood) is illustrated in Figure 9. Shown in the upper half of the figure is a typical fluorescence

Figure 9. Signal waveforms and peak signal amplitude distributions of the sample calibration

a. Fluorescence channel signal waveform
Photomultiplier gain - 6.2×10^2, $R_L = 0.1$Megohm
Mask aperture - 1.5 x 7.0mm, LP filter - 20kHz
Scale factors
Horizontal - time, vertical - 250mv/cm

b. Darkfield channel signal waveform
Photomultiplier gain - 8.6×10^2, $R_L = 1.0$Megohm
Mask aperture - 2.5 x 7.0mm, LP filter - 20kHz
Scale factors
Horizontal - time, vertical - 250mv/cm

c. Fluorescence channel calibration distribution
Scale factors
Horizontal - 25mv increments,
vertical - 13.8 cells/cm

d. Darkfield channel calibration distribution
Scale factors
Horizontal - 25mv increments,
vertical - 14.5 cells/cm

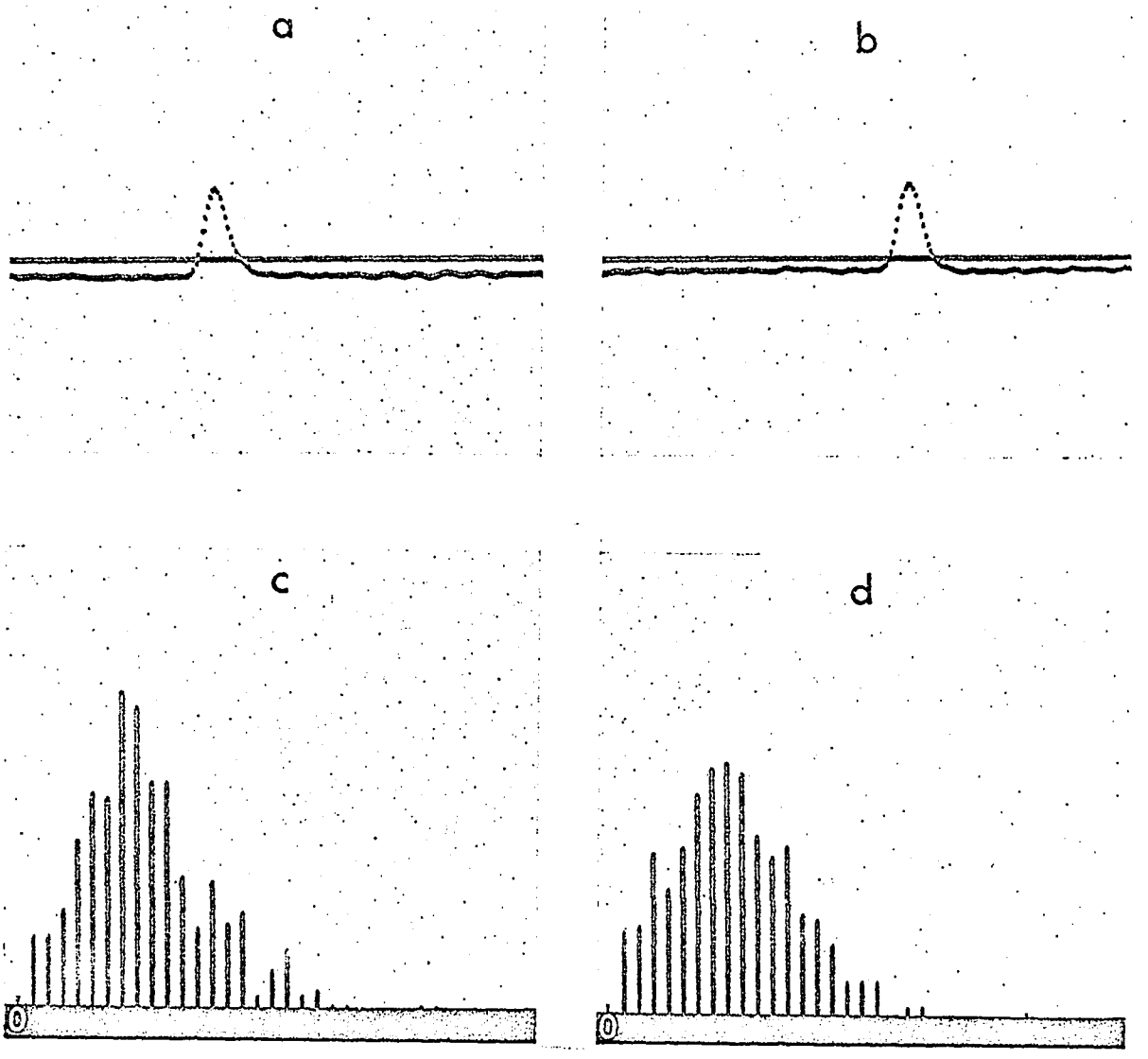
a
b
c
d
0
0

and darkfield calibration signal waveform and threshold levels. Directly below the signal waveforms are the respective fluorescence and darkfield channel peak signal amplitude distributions. Average peak signal amplitudes were calculated from the respective amplitude distribution computer teletype print-outs to be about 200 and 212.5 millivolts across load resistances of 0.1 and 1.0 megohms, respectively, for the fluorescence and darkfield channels. The fluorescence and darkfield photomultiplier tube gains, determined from their respective overall photomultiplier tube voltages (V_{pm}), were calculated to be 6.2×10^2 and 8.6×10^2, respectively (Equation 5). The fluorescence and darkfield calibrations prior to running paper mulberry pollen were arbitrarily taken as the reference calibrations with average peak signals, load resistances, and photomultiplier tube gains of 100 millivolts, 0.1 megohms, 4.75×10^2 and 137.5 millivolts, 1.0 megohm and 1.575×10^2, respectively. Using Equation 10, the fluorescence and darkfield calibration gain constants were calculated to be 1.53 and 0.284, respectively. Generally, the fluorescence gain constant was greater than one (1), whereas, the darkfield gain constant was less than one (1). Using the calculated gain constants, the adjusted photomultiplier tube gains (data) can be determined (Equations 11 and 12).

The fluorescence and darkfield signal waveforms and peak signal amplitude distributions for the four types of pollen

tested are shown in Figure 10 through Figure 13. At least two separate tests were performed on each type of pollen tested. Primary fluorescence/darkfield tests were first run, followed by primary-secondary/darkfield tests. A considerable amount of difficulty was experienced in measuring pecan and chinese lilac pollen. Clumping occurred from time to time with plugging of the flow chamber, and the fluorescence/darkfield average peak signal distributions were not of good quality.

Four distributions were obtained for each type of pollen tested. The leftmost pair of signal waveforms corresponds to the primary fluorescence/darkfield tests, whereas, the rightmost pair corresponds to the primary-secondary fluorescence/darkfield tests. The fluorescence and darkfield peak signal distributions for paper mulberry pollen are shown in Figure 10. Both the primary and primary-secondary fluorescence and darkfield peak signal distributions illustrate the uniformity of this type of pollen. The primary fluorescence and darkfield peak signal distributions for ragweed pollen (Figure 11) again illustrate the uniform fluorescence and light scatter properties for this type of pollen. The primary-secondary fluorescence and darkfield peak signal distributions are widened considerably from the previous primary fluorescence/darkfield distributions. This was primarily due to an oscillatory condition in the instrumentation. The data is valid, but somewhat dispersed about its mean. Chinese lilac pollen, which

Figure 10. Signal waveforms and peak signal amplitude distributions of paper mulberry pollen

a. Primary fluorescence and darkfield signal waveforms
Upper waveform - fluorescence signal
Calibrated photomultiplier gain - 3.85×10^4,
R_L = 1.0Megohm
Mask aperture - 1.5 x 7.0mm, LP filter - 10kHz
Lower waveform - darkfield signal
Calibrated photomultiplier gain - 1.575×10^2,
R_L = 1.0Megohm
Mask aperture - 1.5 x 7.0mm, LP filter 20kHz
Scale factors (both waveforms)
Horizontal - 5msec/cm, vertical - 200mv/cm

b. Primary-secondary fluorescence and darkfield signal waveforms
Upper waveform - fluorescence signal
Calibrated photomultiplier gain - 7.4×10^3,
R_L = 1.0Megohm
Mask aperture - 1.5 x 7.0mm, LP filter - 10kHz
Lower waveform - darkfield signal
Calibrated photomultiplier gain - 1.85×10^2,
R_L = 1.0Megohm
Mask aperture - 1.5 x 7.0mm, LP filter - 20kHz
Scale factors (both waveforms) - same as in a.

c. and e. Primary fluorescence and darkfield signal distributions
Primary fluorescence distribution (c.) scale factors
Horizontal - 25mv increments,
vertical - 14.0 cells/cm
Darkfield distribution (e.) scale factors
Horizontal - 25mv increments,
vertical - 14.0 cells/cm

d. and f. Primary-secondary fluorescence and darkfield signal distributions
Primary-secondary fluorescence distribution (d.) scale factors
Horizontal - 25mv increments,
vertical - 14.2 cells/cm
Darkfield distribution (f.) scale factors
Horizontal - 25mv increments,
vertical - 14.2 cells/cm

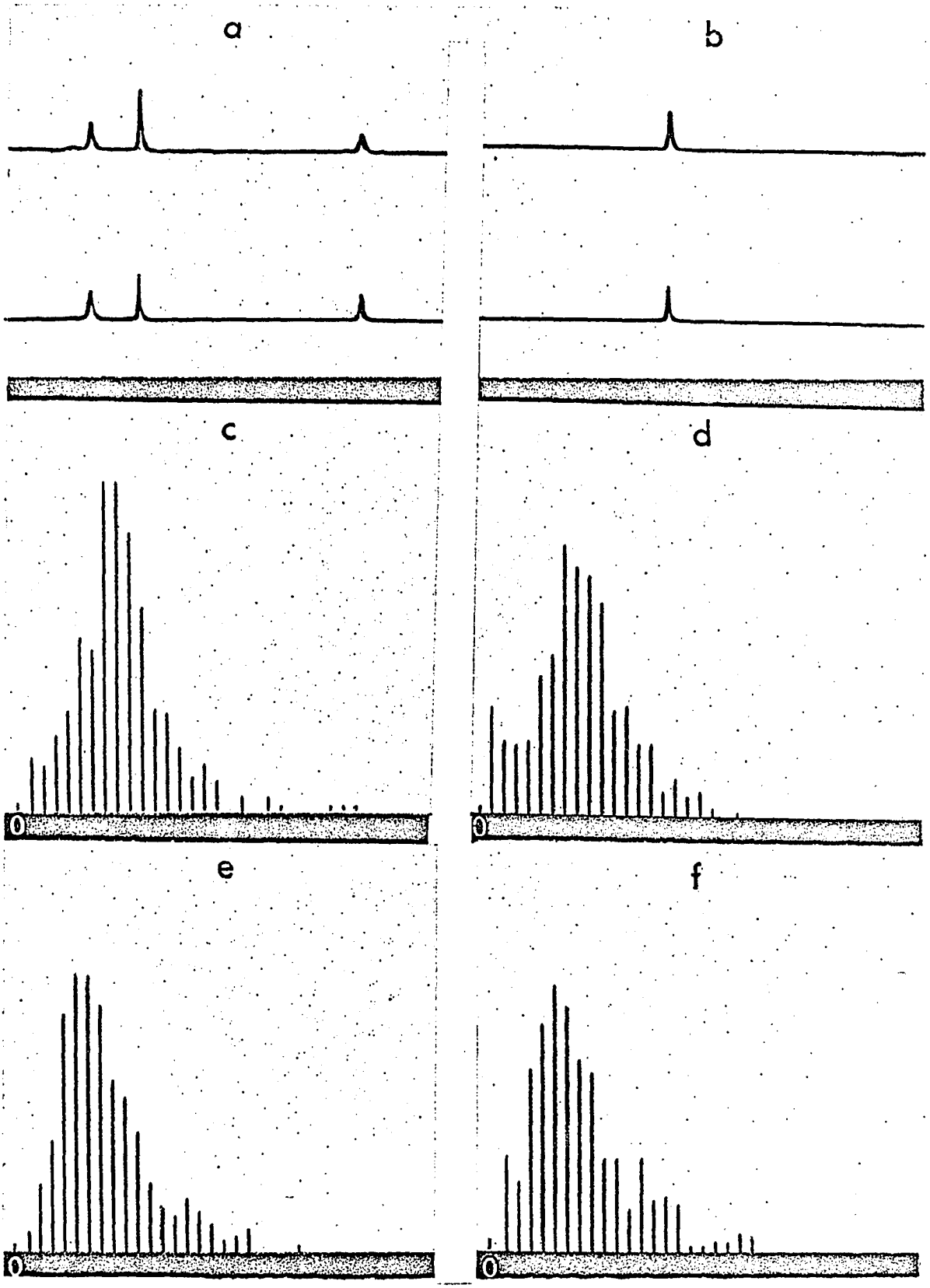
a
b
c
d
e
f

Figure 11. Signal waveforms and peak signal amplitude distributions of ragweed pollen

a. Primary fluorescence and darkfield signal waveforms
Upper waveform - fluorescence signal
Calibrated photomultiplier gain - 3.18×10^4,
R_L = 1.0Megohm
Mask aperture - 2.5 x 8mm, LP filter - 5kHz
Lower waveform - darkfield signal
Calibrated photomultiplier gain - 3.9×10^2,
R_L = 0.1Megohm
Mask aperture - 2.5 x 8mm, LP filter - 10kHz
Scale factors (both waveforms)
Horizontal - 5msec/cm, vertical - 500mv/cm

b. Primary-secondary fluorescence and darkfield signal waveforms
Upper waveform - fluorescence signal
Calibrated photomultiplier gain - 6.47×10^3,
R_L = 1.0Megohm
Mask aperture - 2.5 x 8mm, LP filter - 10kHz
Lower waveform - darkfield signal
Calibrated photomultiplier gain - 1.05×10^2,
R_L = 1.0Megohm
Mask aperture - 2.5 x 8mm, LP filter - 20kHz
Scale factors (both waveforms) - same as in a.

c. and e. Primary fluorescence and darkfield distributions
Primary fluorescence distribution (c.) scale factors
Horizontal - 25mv increments,
vertical - 23.5 cells/cm
Darkfield distribution (e.) scale factors
Horizontal - 25mv increments,
vertical - 23.5 cells/cm

d. and f. Primary-secondary and darkfield distributions
Primary-secondary fluorescence distribution (d.) scale factors
Horizontal - 25mv increments,
vertical - 10.0 cells/cm
Darkfield distribution (f.) scale factors
Horizontal - 25 mv increments,
vertical - 7.8 cells/cm

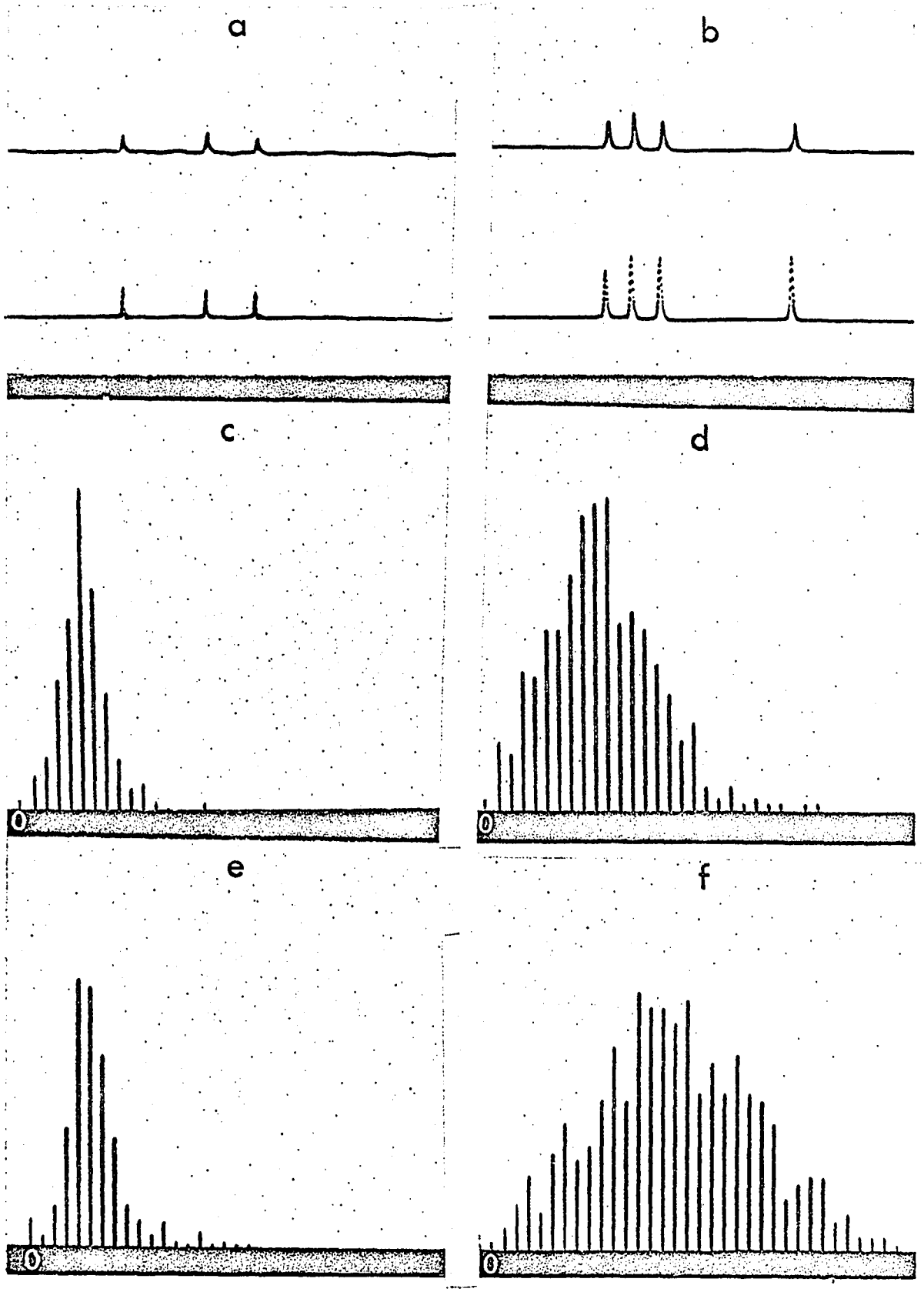
a
b
c
d
e
f

was collected at this University, yielded the least presentable results of all cells tested. A considerable amount of unwanted non-fluorescent debris was present in the collected sample (Figure 12). The primary fluorescence peak signal distribution lies close to the leftmost side of the distribution plot and is due to low photomultiplier tube gain, whereas, the darkfield peak signal distribution is nearly uniform. The primary-secondary and darkfield peak signal distributions are similar to the previous two signal distributions for this pollen. Illustrated in Figure 13 are the respective primary fluorescence and darkfield peak signal distributions of pecan pollen. The leftmost side of the darkfield distribution illustrates one of two things: (1) that there was clumping, or (2) there was debris in the sample. The latter observation is thought to be correct. The primary-secondary and darkfield peak signal distributions of pecan pollen are not of exceptionally good quality. Cell fluorescence was affected by the irregular staining characteristics and the photomultiplier tube gains were slightly lower than they should have been. Ragweed, paper mulberry, pecan, and chinese lilac pollen, in this order, yielded the best overall distributions of the pollen grains tested. The majority of these distributions are approximately Gaussian with a small standard deviations.

Figures 14a and 14b illustrates the size (cross sectional area) distributions of paper mulberry and ragweed pollen as

Figure 12. Signal waveforms and peak signal amplitude distributions of Chinese lilac pollen

a. Primary fluorescence and darkfield signal waveforms
Upper waveform - fluorescence signal
Calibrated photomultiplier gain - 9.83×10^3,
R_L = 1.0Megohm
Mask aperture - 5 x 10mm, LP filter - 10kHz
Lower waveform - darkfield signal
Calibrated photomultiplier gain - 3.46×10^2,
R_L = 0.1Megohm
Mask aperture - 5 x 10mm, LP filter - 20kHz
Scale factors (both waveforms)
Horizontal - 5msec/cm, vertical - 500mv/cm

b. Same as a. above, with vertical scale factors changed to 200mv/cm

c. Primary-secondary fluorescence and darkfield signal waveforms
Upper waveform - fluorescence signal
Calibrated photomultiplier gain - 5.15×10^3,
R_L = 1.0Megohm
Mask aperture - 5 x 10mm, LP filter 10kHz
Lower waveform - darkfield signal
Calibrated photomultiplier gain - 3.72×10^2,
R_L = 0.1Megohm
Mask aperture - 5 x 10mm, LP filter 20kHz
Scale factors (both waveforms) - same as in a.

d. and f. Primary fluorescence and darkfield signal distributions
Primary fluorescence distribution (d.) scale factors
Horizontal - 25mv increments,
vertical - 13.9 cells/cm
Darkfield distribution (f.) scale factors
Horizontal - 25mv increments,
vertical - 10.0 cells/cm

e. and g. Primary-secondary fluorescence and darkfield signal distributions
Primary-secondary fluorescence distribution (e.) scale factors
Horizontal - 25mv increments,
vertical - 17.5 cells/cm
Darkfield distribution (g.) scale factors
Horizontal - 25mv increments,
vertical - 10.0 cells/cm

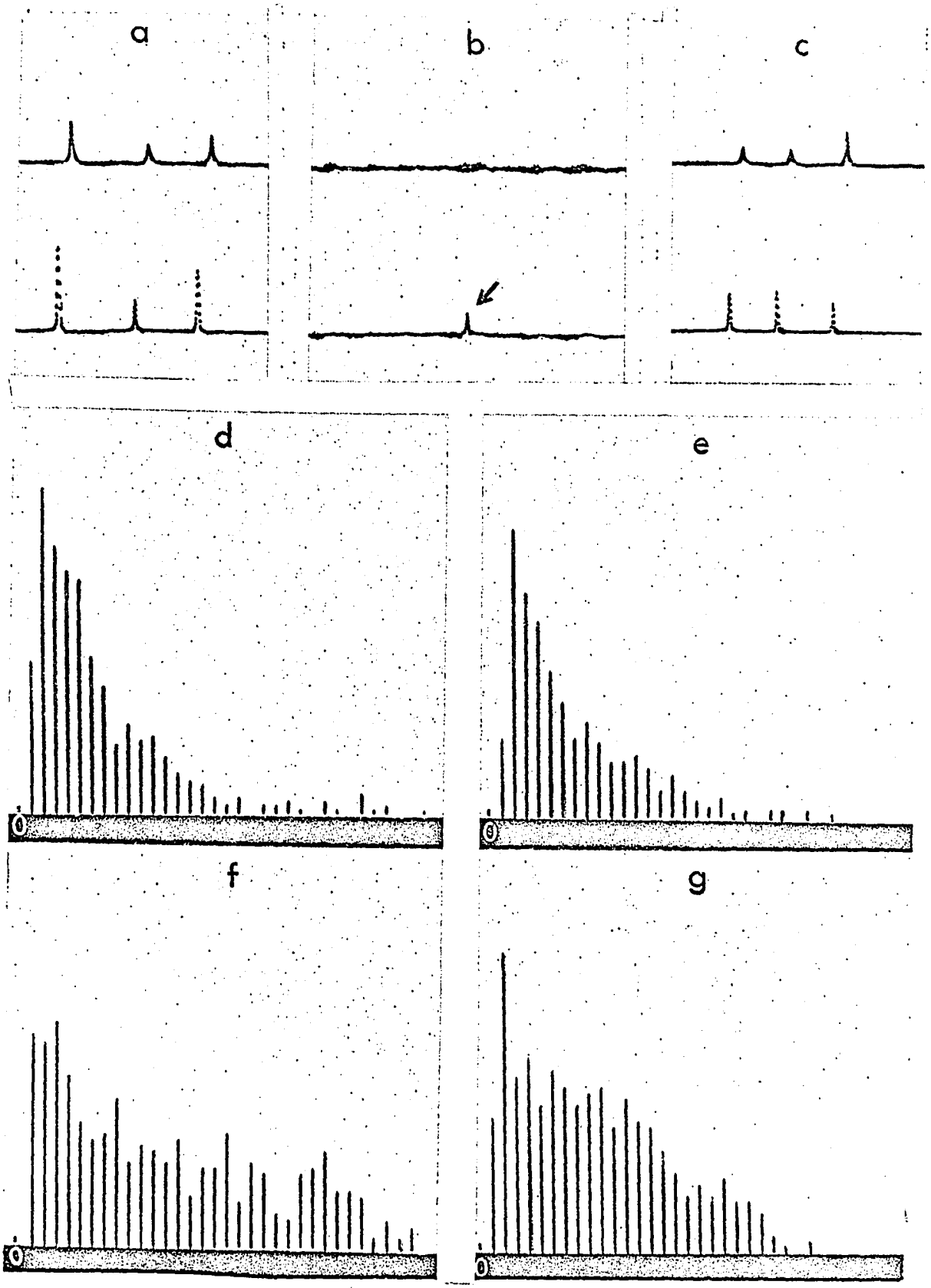
a
b
c
d
e
f
g

Figure 13. Signal waveforms and peak signal amplitude distributions of pecan pollen

a. Primary fluorescence and darkfield signal waveforms
Upper waveform - fluorescence signal
Calibrated photomultiplier gain - 3.37×10^4,
R_L = 1.0Megohm
Mask aperture - 5 x 10mm, LP filter - 10kHz
Lower waveform - darkfield signal
Calibrated photomultiplier gain - 1.0×10^3,
R_L = 0.1Megohm
Mask aperture - 5 x 10mm, LP filter - 20kHz
Scale factors (both waveforms)
Horizontal - 5 msec/cm, vertical - 500mv/cm

b. Primary-secondary fluorescence and darkfield signal waveforms
Upper waveform - fluorescence signal
Calibrated photomultiplier gain - 8.25×10^3,
R_L = 1.0Megohm
Mask aperture - 5 x 10mm, LP filter - 10kHz
Lower waveform - darkfield signal
Calibrated photomultiplier gain - 2.51×10^3,
R_L = 0.1Megohm
Mask aperture - 5 x 10mm, LP filter - 20kHz
Scale factors (both waveforms)
Horizontal - 5msec/cm, vertical - 500mv/cm

c. and e. Primary fluorescence and darkfield signal distributions
Primary fluorescence distribution (c.) scale factors
Horizontal - 25mv increments,
vertical - 8.8 cells/cm
Darkfield distribution (e.) scale factors
Horizontal - 25mv increments,
vertical - 6.32 cells/cm

d. and f. Primary-secondary and darkfield signal distributions
Primary-secondary fluorescence distribution (d.) scale factors
Horizontal - 25mv increments,
vertical - 7.9 cells/cm
Darkfield distribution (f.) scale factors
Horizontal - 25mv increments,
vertical - 7.9 cells/cm

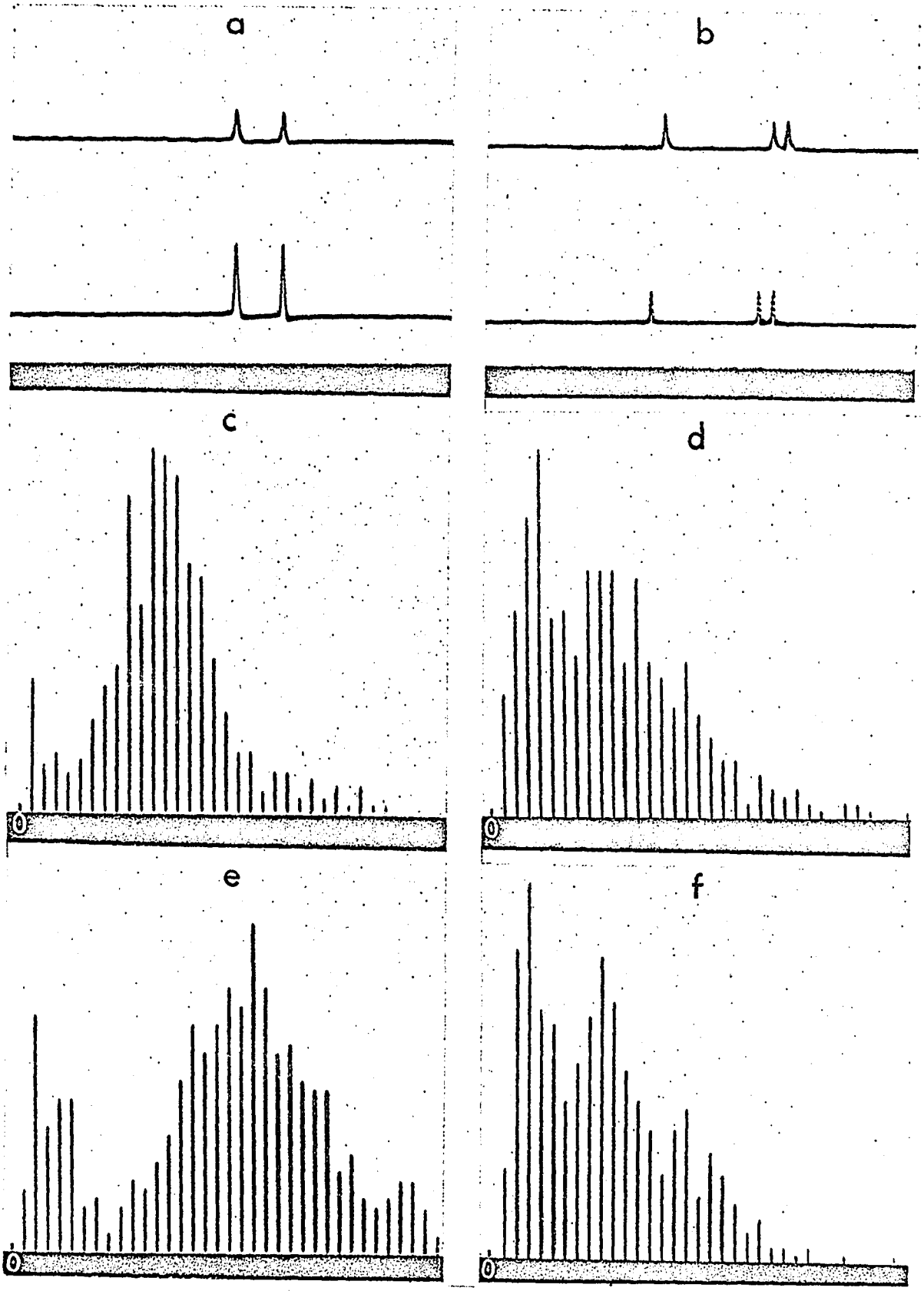
a
b
c
d
e
f

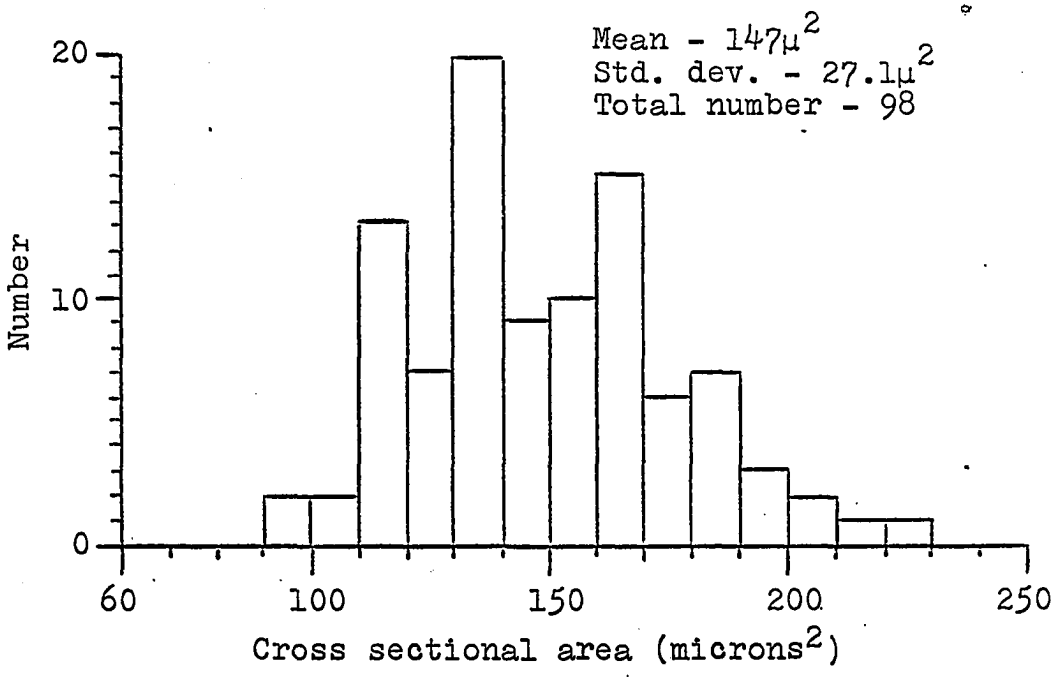

Figure 14a. Size distribution of paper mulberry pollen

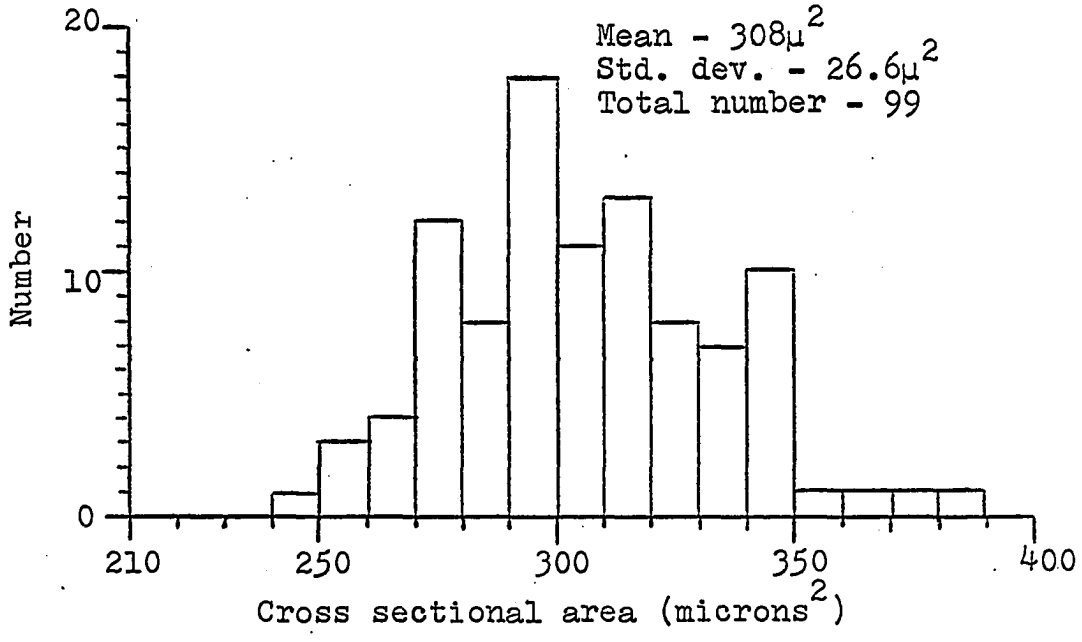

Figure 14b. Size distribution of ragweed pollen

measured with a microscope and eyepiece micrometer. Standard deviations are approximately equal. The fluorescence and darkfield peak signal amplitude distributions (Figure 10 and 11) for paper mulberry and ragweed pollen compare favorably with these. Primary fluorescence distribution standard deviations for both pollens are the same, whereas, the darkfield distribution standard deviation for paper mulberry pollen is about three times greater than ragweed pollen. The fluorescence and darkfield distributions of ragweed pollen are in close agreement (shape) with the fluorescence, light scatter, and volume distributions measured by Van Dilla et al. (93).

The fluorescence and darkfield signal waveforms obtained for isolated diploid and tetraploid rat liver nuclei, along with their respective peak signal distributions, are illustrated in Figure 15. The leftmost and rightmost signal waveforms and distributions are for 5 and 8 μ diameter nuclei, respectively. Both fluorescence distributions of the two types of nuclei are nearly Gaussian. The darkfield distributions vary somewhat and are slightly wider than the fluorescence distributions, which is to be expected considering the process of obtaining the nuclei. Standard deviation of the fluorescence signal is about one-half the standard deviation of the darkfield signal for both types of rat liver nuclei. The relative ratio of the peak fluorescence and darkfield signals is nearly constant. The fluorescence peak signal amplitude

Figure 15. Signal waveforms and peak signal amplitude distributions of rat liver nuclei

a. Fluorescence and darkfield signal waveforms - diploid nuclei
Upper waveform - fluorescence signal
Calibrated photomultiplier gain - 8.5×10^4,
R_L = 1.0Megohm
Mask aperture - 1.1 x 5.0mm, LP filter 10kHz
Lower waveform - darkfield signal
Calibrated photomultiplier gain - 3.26×10^3,
R_L = 1.0Megohm
Mask aperture - 1.1 x 5.0mm, LP filter 20kHz
Scale factors (both waveforms)
Horizontal - 5msec/cm, vertical - 500mv/cm

b. Fluorescence and darkfield signal waveforms - tetraploid nuclei
Upper waveform - fluorescence signal
Calibrated photomultiplier gain - 5.95×10^4,
R_L = 1.0Megohm
Mask aperture - 1.1 x 5.0mm, LP filter - 10kHz
Lower waveform - darkfield signal
Calibrated photomultiplier gain - 2.49×10^3,
R_L = 1.0Megohm
Mask aperture - 1.1 x 5.0mm, LP filter - 20kHz
Scale factors (both waveforms) - same as in a.

c. and e. Fluorescence and darkfield signal distributions - diploid nuclei
Fluorescence distribution (c.) scale factors
Horizontal - 25mv increments,
vertical - 23.0 cells/cm
Darkfield distribution (e.) scale factors
Horizontal - 25mv increments,
vertical - 10.0 cells/cm

d. and f. Fluorescence and darkfield signal distributions - tetraploid nuclei
Fluorescence distribution (d.) scale factors
Horizontal - 25mv increments,
vertical - 62.5 cells/cm
Darkfield distribution (f.) scale factors
Horizontal - 25mv increments,
vertical - 40.0 cells/cm

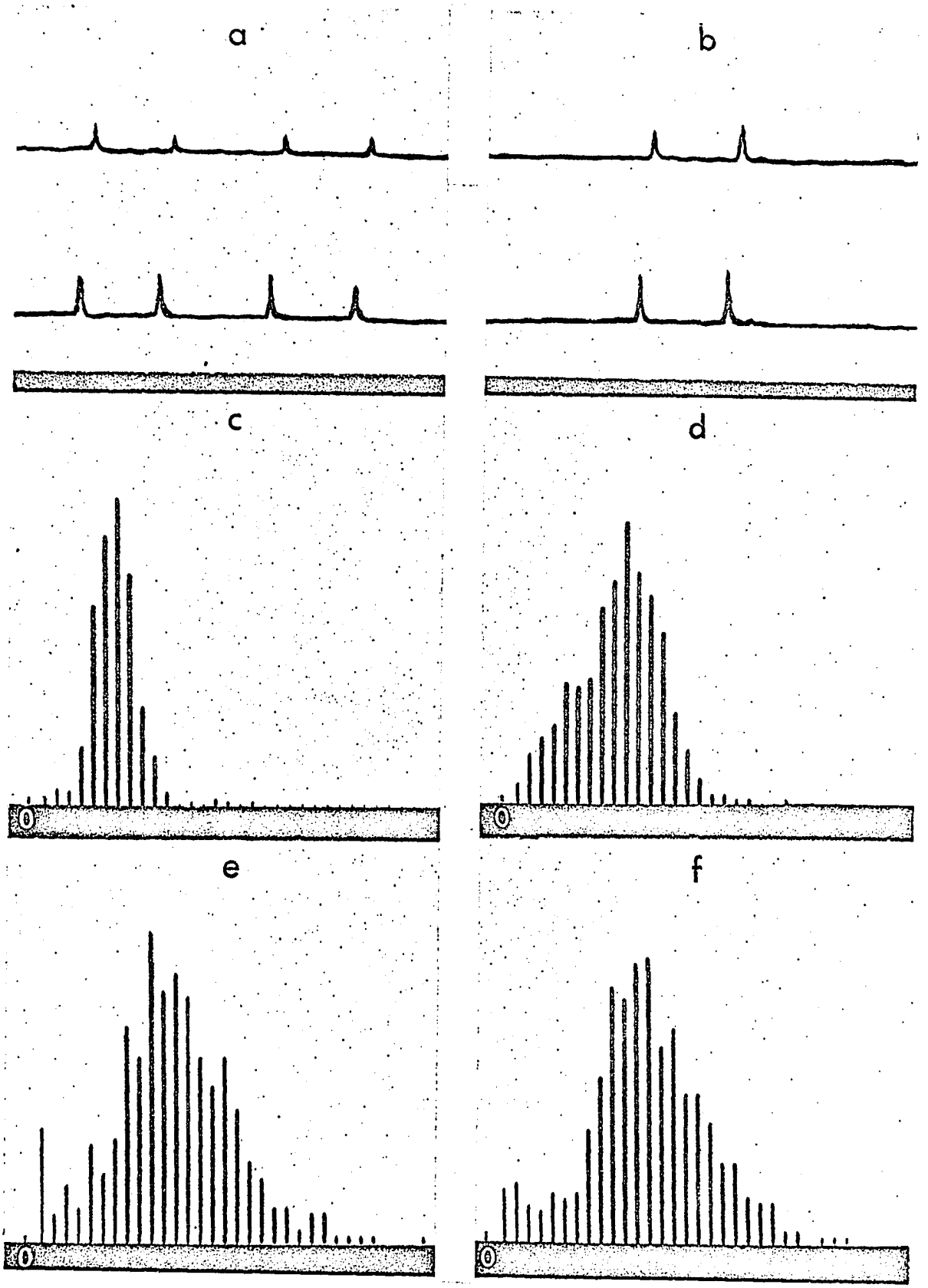
a
b
c
d
e
f

distributions for both types of nuclei are in close agreement with those obtained by Ruch (76) using Auramine O as a fluorescent dye.

The fluorescence and darkfield signal waveforms and respective peak signal distributions obtained for frog blood are illustrated in Figure 16. Frog erythrocytes are plainly distinguishable in the fluorescence and darkfield distributions (Figure 16b and 16c) by noting the definite peak in each distribution. Both distributions are somewhat compressed to the left. The fluorescence distribution was moved to the right by increasing the fluorescence photomultiplier tube gain (Figure 16d). Since there were a considerable number of darkfield signals greater than 1000 millivolts, the darkfield data was compressed (Figure 16e) using a voltage divider (ratio 1/2) in the data input line to the LINC-8. The standard deviation of the fluorescence signal is somewhat smaller than the darkfield signal. Both peak signal distributions are somewhat complex to analyze and illustrates considerable overlapping due to the mixture of erythrocytes, leucocytes, and thrombocytes. According to Andrew (2), the ratio of erythrocytes to leucocytes plus thrombocytes is about 15-20 to 1.

Figure 17 illustrates the fluorescence and darkfield signal waveforms and respective peak signal distributions for goldfish blood. Signal waveforms illustrate the variety of cells present. As in frog blood, the erythrocyte peak is

Figure 16. Signal waveforms and peak signal amplitude distributions of frog blood

a. Fluorescence and darkfield signal waveforms
Upper waveform - fluorescence signal
Calibrated photomultiplier gain - 1.65×10^4,
R_L = 1.0Megohm
Mask aperture - 1.1 x 5.0mm, LP filter - 10kHz
Lower waveform - darkfield signal
Calibrated photomultiplier gain - 4.95×10^3,
R_L = 1.0Megohm
Mask aperture - 2.5 x 7.0mm, LP filter - 20kHz
Scale factors (both waveforms)
Horizontal - 5msec/cm, vertical - 200mv/cm

b., c., d. and e. Fluorescence and darkfield signal distributions
Fluorescence distribution (b.) scale factors
Horizontal - 25mv increments,
vertical - 24.5 cells/cm
Darkfield distribution (c.) scale factors
Horizontal - 25mv increments,
vertical - 57.7 cells/cm
Fluorescence distribution (d.) scale factors
Horizontal - 25mv increments,
vertical - 21.0 cells/cm
Calibrated photomultiplier gain - 3.0×10^4,
R_L = 1.0Megohm
Darkfield distribution (e.) scale factors
Horizontal - 50mv increments,
vertical - 35.0 cells/cm
Calibrated photomultiplier gain - same as in a.

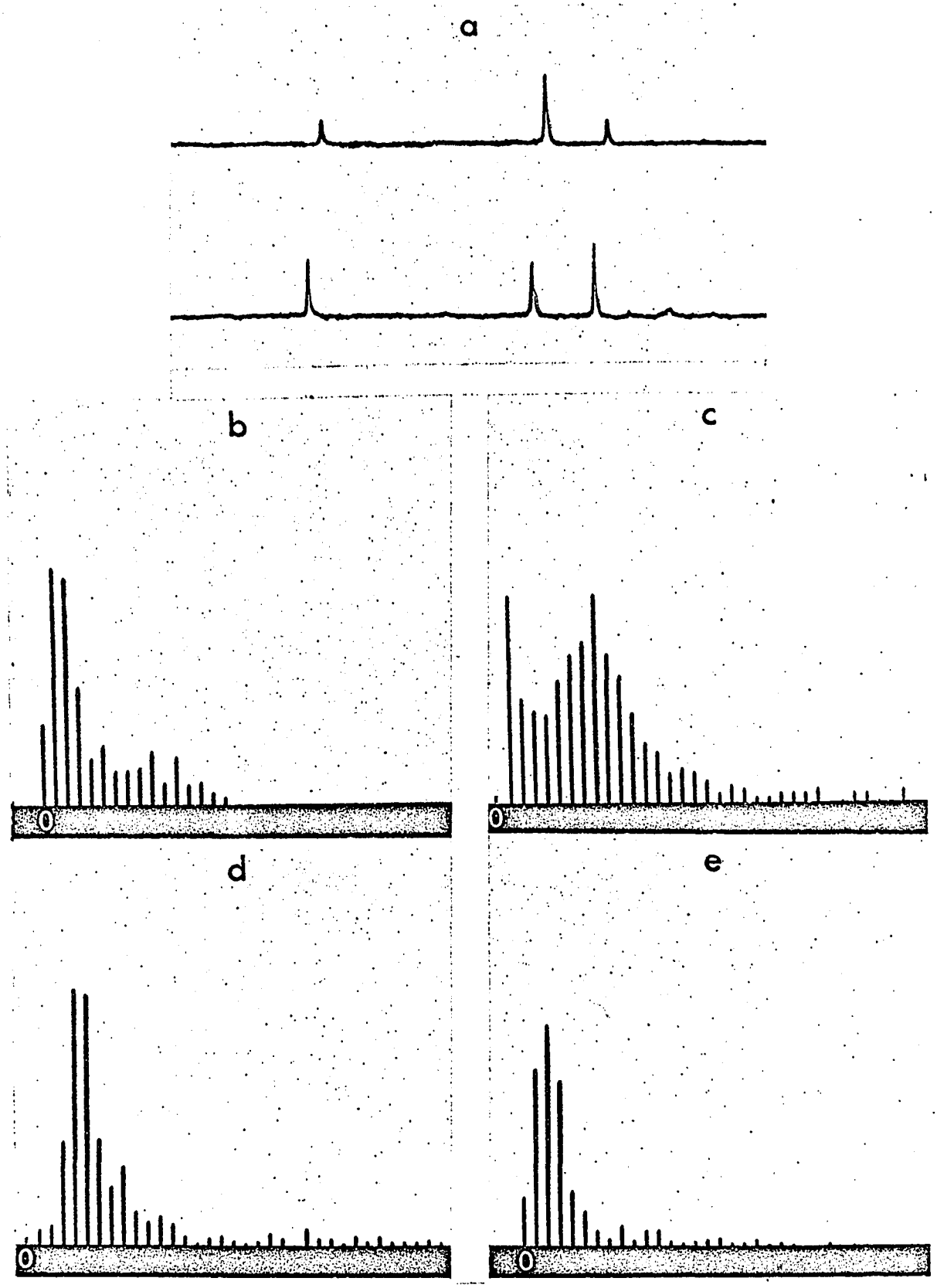
a
b
c
0
0
d
e
0
0

Figure 17. Signal waveforms and peak signal amplitude distributions of goldfish blood

a. Fluorescence and darkfield signal waveforms
Upper waveform - fluorescence signal
Calibrated photomultiplier gain - 1×10^5,
R_L = 1.0Megohm
Mask aperture - 1.1 x 5.0mm, LP filter - 10kHz
Lower waveform - darkfield signal
Calibrated photomultiplier gain - 1.75×10^3,
R_L = 1.0Megohm
Mask aperture - 2.5 x 7.0mm, LP filter 20kHz
Scale factors (both waveforms)
Horizontal - 5msec/cm, vertical - 500mv/cm

b., c., d. and e. Fluorescence and darkfield signal distributions
Fluorescence distribution (b.) scale factors
Horizontal - 25mv increments,
vertical - 23.0 cells/cm
Darkfield distribution (c.) scale factors
Horizontal - 25mv increments,
vertical - 35.0 cells/cm
Fluorescence distribution (d.) scale factors
Horizontal - 25mv increments,
vertical - 40.0 cells/cm
Calibrated photomultiplier gain - 2.68×10^4
Darkfield distribution (e.) scale factors
Horizontal - 20mv increments,
vertical - 23.0 cells/cm

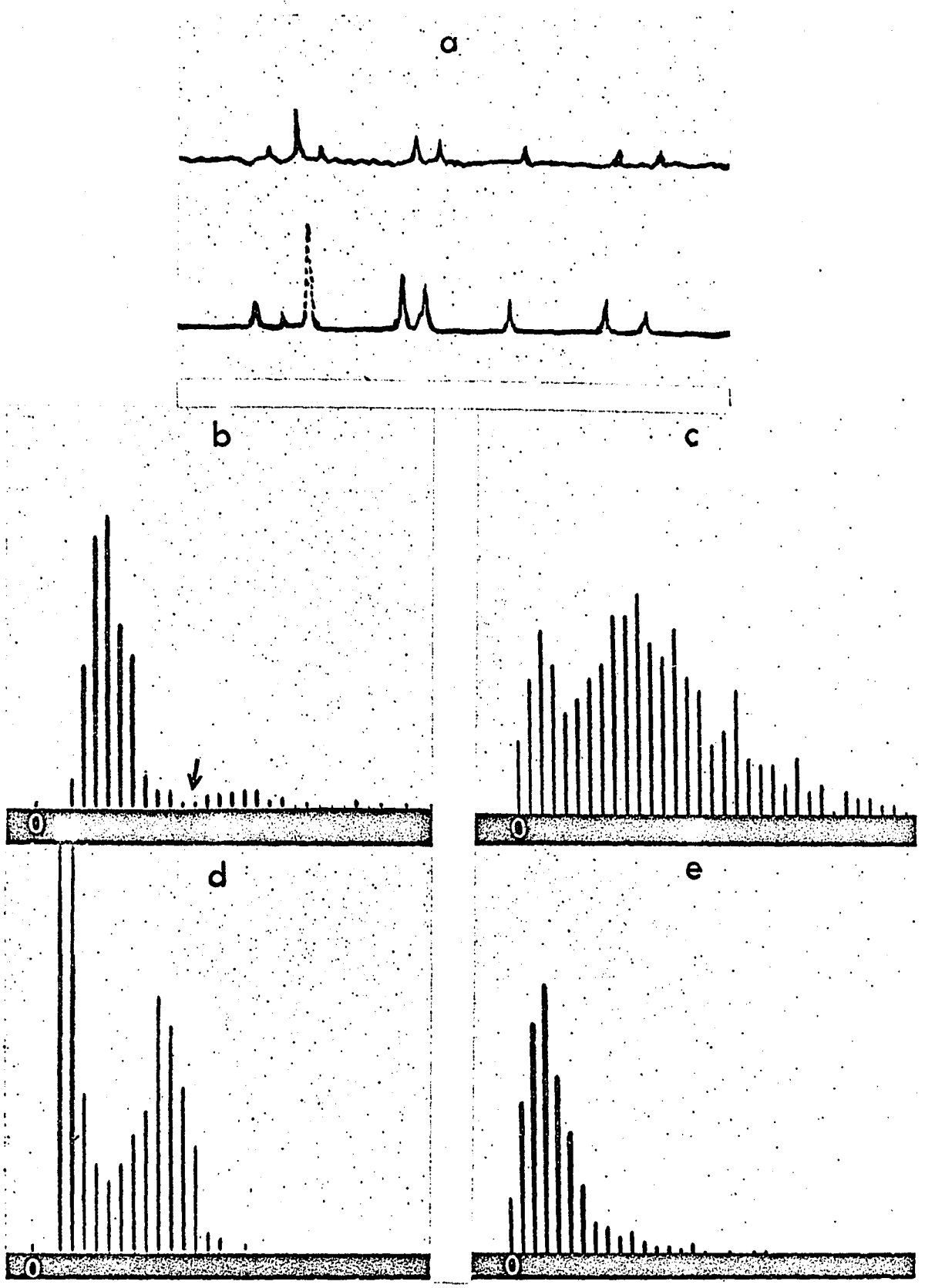
a
b
c
0
d
0
e
0
0

well defined in both the fluorescence and darkfield distributions (Figure 17b and 17c). The fluorescence photomultiplier tube gain was lowered (Figure 17d) to observe the fluorescence distribution notch (Figure 17b). According to Watson et al. (97), the average area of the erythrocyte nucleus is about one-half the average area of a lymphocyte, which would account for the notch. The darkfield distribution was compressed (Figure 17e) by use of a voltage divider (ratio of 1/2) in the data input line to the LINC-8. As was previously illustrated (frog blood), resolution is lost by data compression. The distributions are nearly Gaussian, with standard deviation of the fluorescence signal about one-half that of the darkfield signal. Since there are a variety of cells also present in goldfish blood, the ratio method, to be described later, may be a valid technique for determining the percentages of the various types of cells present.

The fluorescence and darkfield signal waveforms and respective peak signal distributions for avian erythrocytes are illustrated in Figure 18. Both signal waveforms (peaks) have approximate Gaussian distributions with the standard deviation of the fluorescence signal peak about one-half the darkfield signal peak. A voltage divider (ratio of 1/2.8) was used in the data input line of the LINC-8 to reduce the incoming signals from 2.8 volt peaks (maximum) to 1 volt with no loss of information.

Figure 18. Signal waveforms and peak signal amplitude distributions of avian erythrocytes

a. Fluorescence and darkfield signal waveforms
Upper waveform - fluorescence signal
Calibrated photomultiplier gain - 6.6×10^4,
R_L = 10Megohm
Mask aperture - 0.6 x 5.0mm, LP filter - 10kHz
Lower waveform - darkfield signal
Calibrated photomultiplier gain - 3.35×10^2,
R_L = 10Megohm
Mask aperture - 1.5 x 5.0mm, LP filter - 20kHz
Scale factors (both waveforms)
Horizontal - 5msec/cm, vertical - 1000mv/cm

b. and c. Fluorescence and darkfield signal distributions
Fluorescence distribution (b.) scale factors
Horizontal - 70mv increments,
vertical - 23.0 cells/cm
Darkfield distribution (c.) scale factors
Horizontal - 70mv increments,
vertical - 13.5 cells/cm

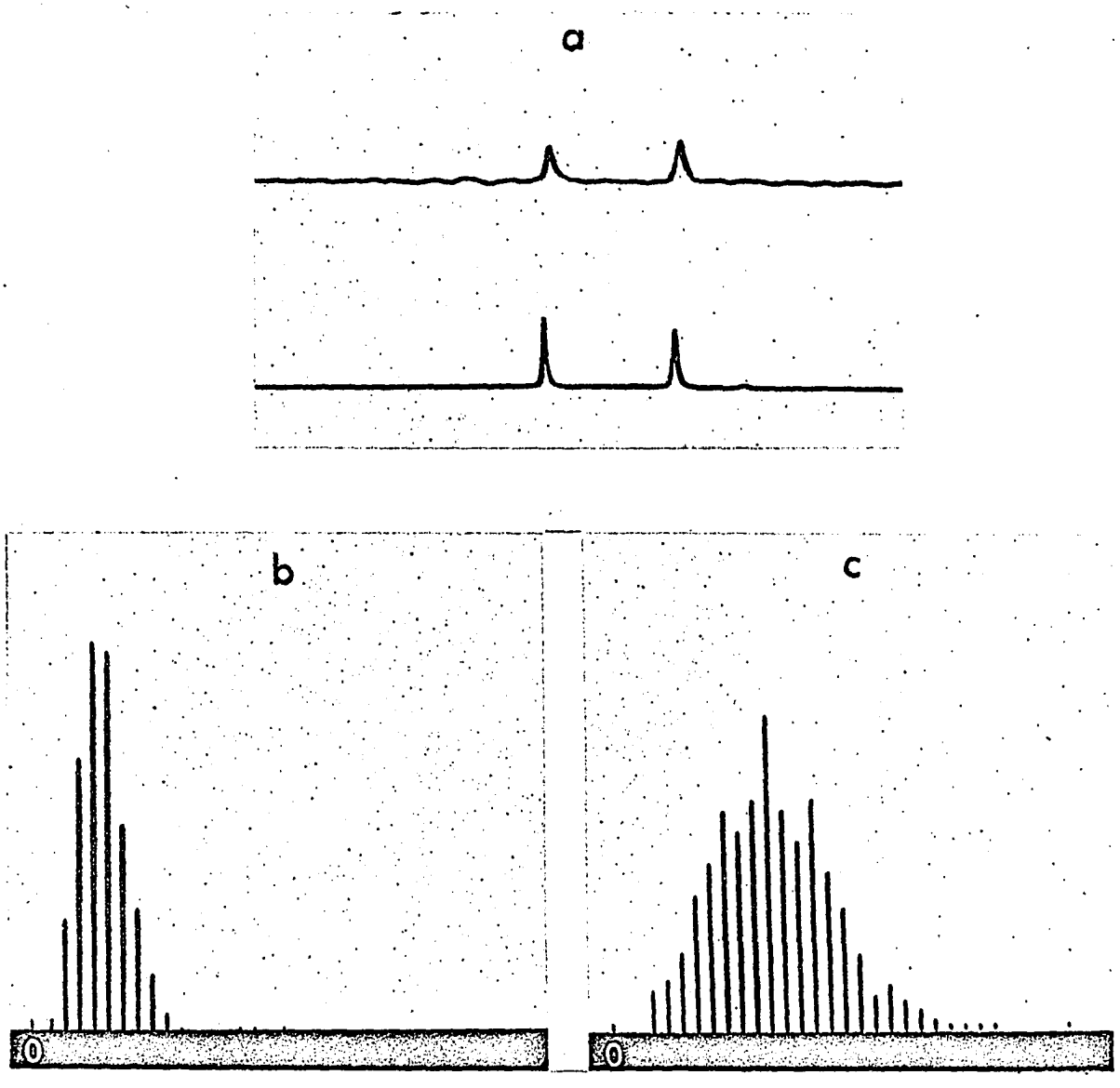
a
b
c
0
0

Signal waveforms and peak signal distributions obtained from fresh dog blood are illustrated in Figure 19. The fluorescence and darkfield signal waveforms (Figure 19a) demonstrate the ability of measurement system to differentiate between fluorescent and non-fluorescent tagged cells and the potential for differentiating between mammalian erythrocytes (non-nucleated) and leucocytes, with exception of the camel. The fluorescence (leucocyte) and darkfield (leucocytes and erythrocytes) distributions (Figures 19b and 19c) are somewhat complex. Garcia (32, 33) has extensively studied the Feulgen-DNA content of leucocytes of humans and various mammals. The lymphocyte and granulocyte DNA frequency distributions are nearly overlapping, with lymphocytes favoring the leftmost region of the distribution and granulocytes mainly on right side. Dividing the fluorescence distribution at the center notch yields nearly 50 per cent each of lymphocytes and granulocytes, which is in error by at least 20 to 30 per cent (7, 89). Closer examination of the fluorescence distribution shows a definite hump near its leftmost region. Approximately 15 to 20 per cent of the leucocytes lie within this region. These are thought to be mainly small-to-medium size lymphocytes. The darkfield distribution illustrates two principle regions of cell sizes and is somewhat similar in shape to that reported by Fulwyler et al. (31) for overall blood cell volumes. Both the fluorescence and darkfield distributions were

Figure 19. Signal waveforms and peak signal amplitude distributions of dog blood

a. Fluorescence and darkfield signal waveforms
Upper waveform - fluorescence signal
Uncalibrated photomultiplier gain - 8.4×10^3,
R_L = 10Megohm
Mask aperture - 1.25 x 5.0mm, LP filter - 10kHz
Lower waveform - darkfield signal
Uncalibrated photomultiplier gain - 4.6×10^3,
R_L = 10Megohm
Mask aperture - 1.5 x 5.0mm, LP filter - 10kHz
Scale factors (both waveforms)
Horizontal - 5msec/cm, vertical - 500mv/cm

b., c., d. and e. Fluorescence and darkfield signal distributions
Fluorescence distribution (b.) scale factors
Horizontal - 25mv increments,
vertical - 9.0 cells/cm
Darkfield distribution (c.) scale factors
Horizontal - 25mv increments,
vertical - 3.6 cells/cm
Fluorescence distribution (d.) scale factors
Horizontal - 70mv increments,
vertical - 17.3 cells/cm
Darkfield distribution (e.) scale factors
Horizontal - 70mv increments,
vertical - 57.0 cells/cm

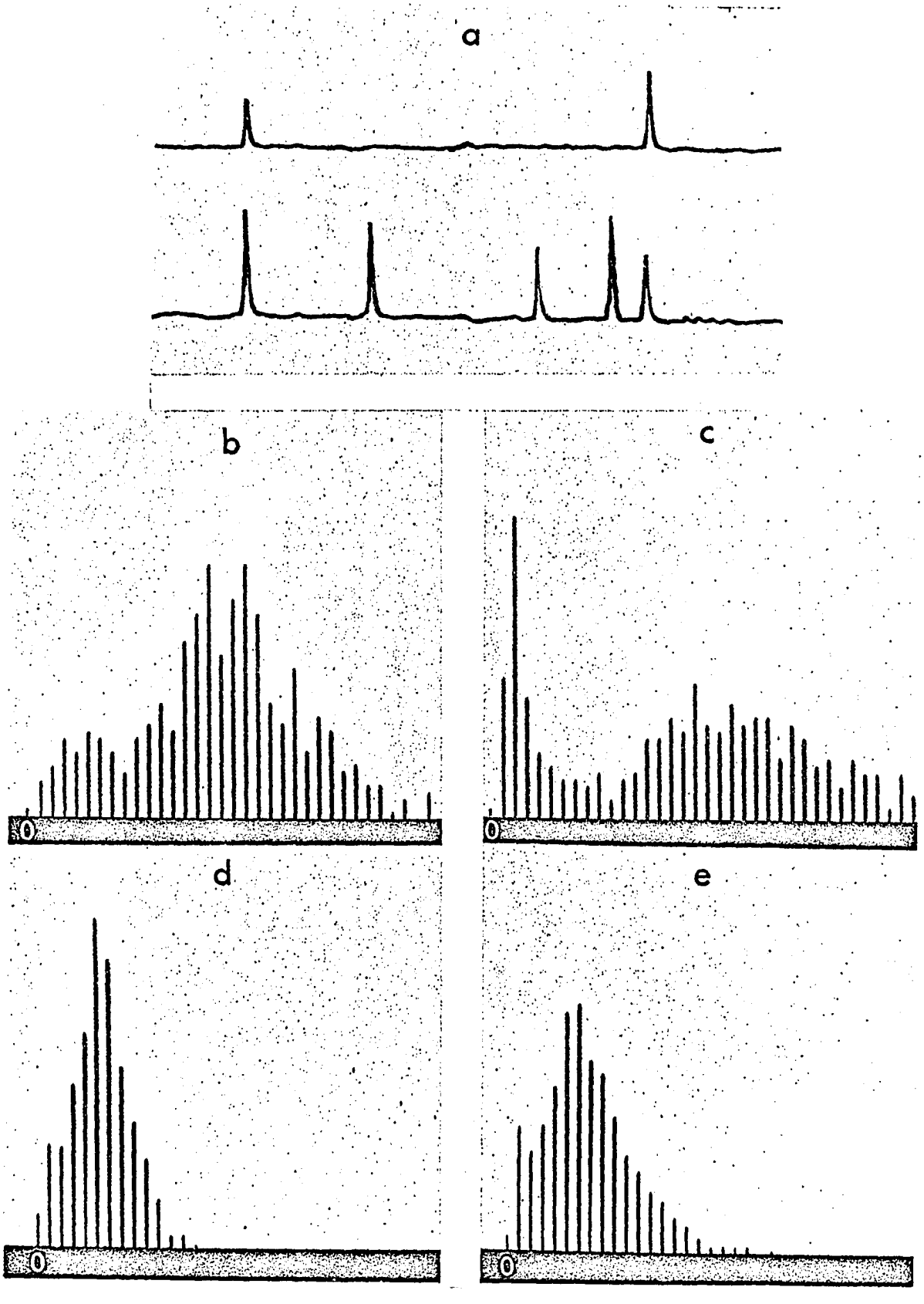
a
b
c
d
e
0
0
0
0

compressed (Figure 19d and 19e), with some loss of resolution, by use of a voltage divider (ratio of 1/2.8) in the data input line to the LINC-8. The shape of the compressed fluorescence (Gaussian) and darkfield distributions are in agreement to that reported by Trujillo and Van Dilla (90) and Fulwyler et al. (31), for human leucocytes and blood cells, respectively. The relative fluorescence/darkfield peak signal ratio of the different types of leucocytes can possibly be employed as a method for the partial differentiation among the leucocytes.

The fluorescence and darkfield peak signal distributions and respective signal waveforms obtained from swine leucocytes are illustrated in Figure 20. Signal waveforms again vividly distinguish the nucleated and non-nucleated elements of the blood. Darkfield signal waveforms illustrate the cellular debris (erythrocyte membranes) contained in the cell suspension. Swine blood was not measured until 8 hours after acquiring. Upon observing the leucocytes prior to measurement, a marked degree of fluorescence coloration was observed. Cells were either a light green-yellow or a darker more intense green color, as compared to dog leucocytes all of which were of the same green-yellow color. Lymphocytes were in the majority with granulocytes difficult to find. The fluorescence distribution (Figure 20b) illustrates two distinct notches in the distribution with three definite peaks. Approximately 50 per cent of the leucocytes lie in each of the two major regions of the

Figure 20. Signal waveforms and peak signal amplitude distributions of swine blood

a. Fluorescence and darkfield signal waveforms
Upper waveform - fluorescence signal
Calibrated photomultiplier gain - 1.65×10^4,
R_L = 10Megohm
Mask aperture - 1.25 x 5.0mm, LP filter - 10kHz
Lower waveform - darkfield signal
Calibrated photomultiplier gain - 8×10^2,
R_L = 10Megohm
Mask aperture - 1.5 x 5.0mm, LP filter - 10kHz
Scale factors (both waveforms)
Horizontal - 5msec/cm, vertical - 500mv/cm

b., c., d. and e. Fluorescence and darkfield signal distributions
Fluorescence distribution (b.) scale factors
Horizontal - 25mv increments,
vertical - 25.0 cells/cm
Darkfield distribution (c.) scale factors
Horizontal - 25mv increments,
vertical - 23.0 cells/cm
Fluorescence distribution (d.) scale factors
Horizontal - 70mv increments,
vertical - 56.0 cells/cm
Darkfield distribution (e.) scale factors
Horizontal - 70mv increments,
vertical - 35.0 cells/cm

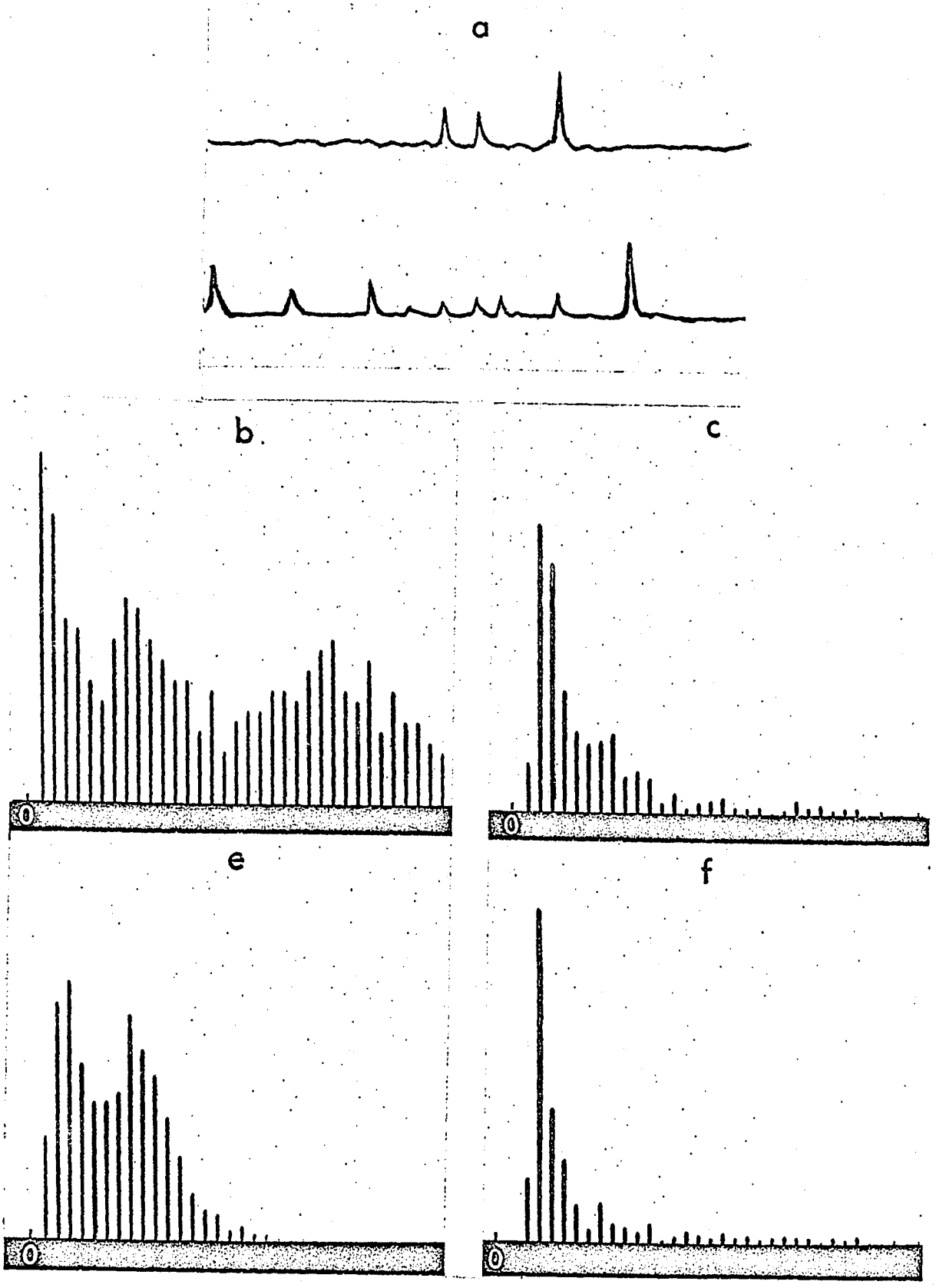
a
b
c
e
f

distribution. The darkfield peak signal distribution (Figure 20c) is composed of light scatter from erythrocytes (membranes) and leucocytes. Both the fluorescence and darkfield distributions were compressed (Figure 20d and 20e) by use of a voltage divider (ratio 1/2.8) in the data input line to the LINC-8.

Illustrated in Figure 21 are the fluorescence and darkfield signal waveforms and respective peak signal distributions of cultured lymphocytes. The lymphocytes were from a relatively old culture with the majority of cells appearing to be small lymphocytes. The fluorescence photomultiplier tube gain was somewhat lower than anticipated when running these tests and resulted in a crowding of the fluorescence distribution (Figure 21b). Figure 21c illustrates the darkfield distribution of light scattered from culture cells and any debris flowing through the detection chamber.

The fluorescence and darkfield signal waveforms and respective peak signal distributions for yeast cells are shown in Figure 22. Due to technical difficulties in the instrumentation, the fluorescence and darkfield tests were recorded separately. Both the fluorescence and darkfield signals (Figures 22a and 22b) are well above the noise level. Some increase in photomultiplier tube gains is possibly needed to move the fluorescence and darkfield distributions (Figures 22c and 22d) to the right. Both distributions were expanded by removal of the voltage divider (ratio 1/2.8) in the data input

Figure 21. Signal waveforms and peak signal amplitude distributions of cultured lymphocytes

a. Fluorescence and darkfield signal waveforms
Upper waveform - fluorescence signal
Uncalibrated photomultiplier gain - 6.2×10^4,
R_L = 10Megohm
Mask aperture - 1.25 x 5.0mm, LP filter - 5kHz
Lower waveform - darkfield signal
Uncalibrated photomultiplier gain - 6.8×10^2,
R_L = 10Megohm
Mask aperture - 1.5 x 5.0mm, LP filter - 10kHz
Scale factors (both waveforms)
Horizontal - 10msec/cm, vertical - 500mv/cm

b. and c. Fluorescence and darkfield signal distributions
Fluorescence distribution (b.) scale factors
Horizontal - 25mv increments,
vertical - 36.0 cells/cm
Darkfield distribution (c.) scale factors
Horizontal - 25mv increments,
vertical - 18.0 cells/cm

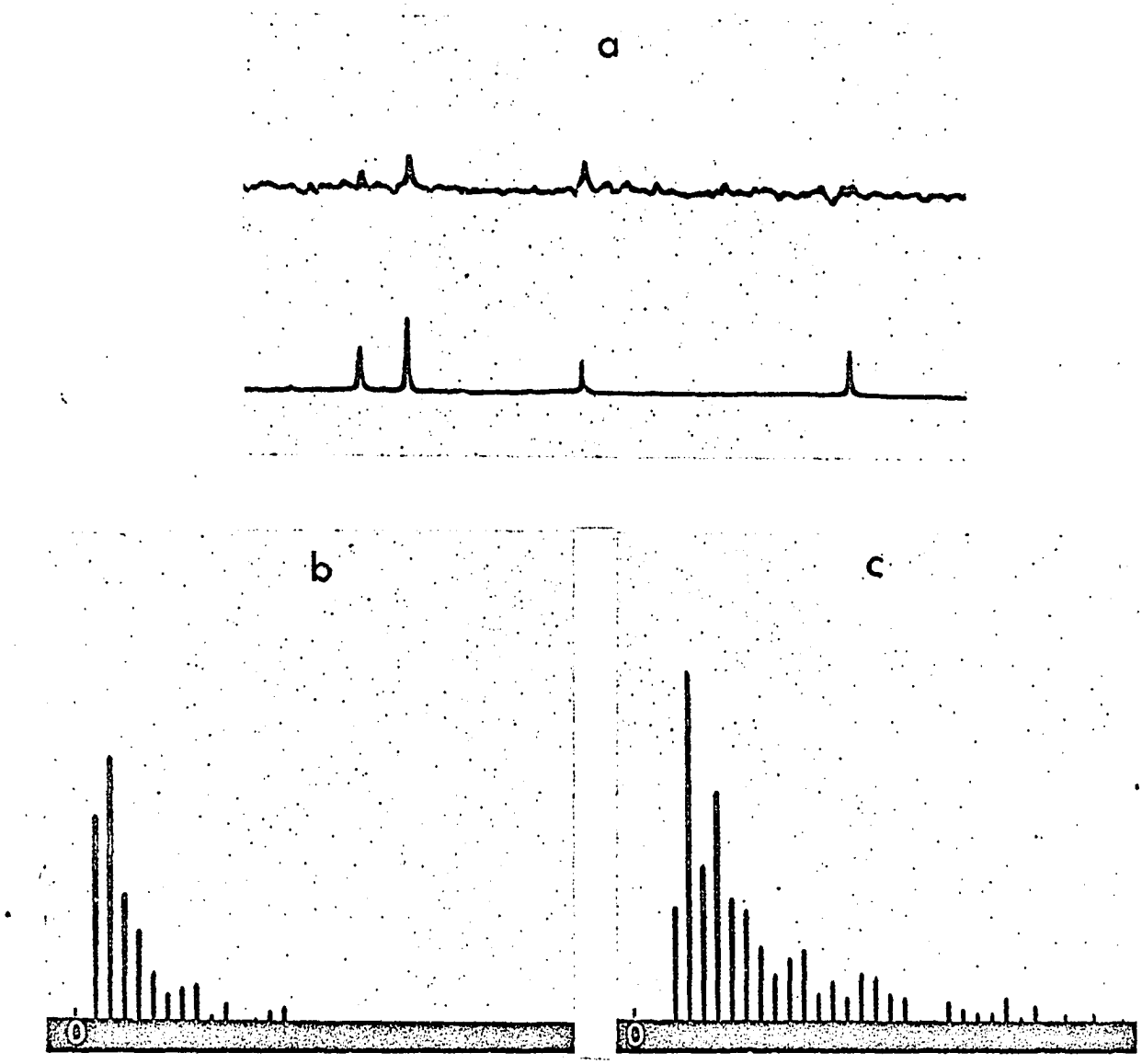
a
b
c
0
0

Figure 22. Signal waveforms and peak signal amplitude distributions of yeasts

a. and b. Fluorescence and darkfield signal waveforms
Fluorescence signal (a.)
Calibrated photomultiplier gain - 1.68×10^5,
R_L = 10Megohm
Mask aperture - 0.5 x 5.0mm, LP filter - 5kHz
Darkfield signal (b.)
Calibrated photomultiplier gain - 1.35×10^3,
R_L = 10Megohm
Mask aperture - 1.25 x 5.0mm,
LP filter - 10kHz
Scale factors (both waveforms)
Horizontal - 5msec/cm, vertical - 1000mv/cm

c. and d. Fluorescence and darkfield signal distributions
Fluorescence distribution (c.) scale factors
Horizontal - 70mv increments,
vertical - 23.0 cells/cm
Darkfield distribution (d.) scale factors
Horizontal - 70mv increments,
vertical - 23.0 cells/cm

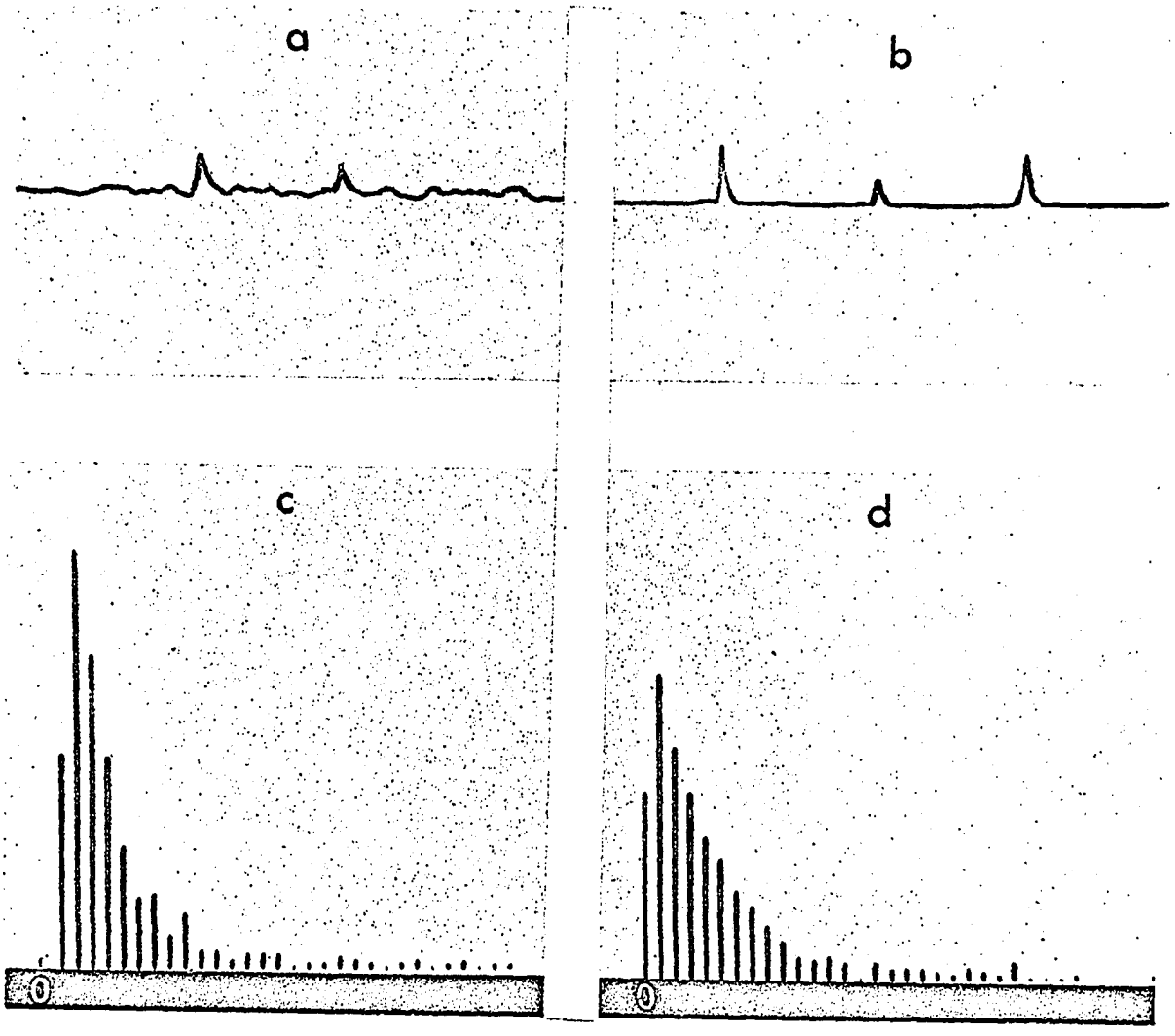
a
b
c
d

line to the LINC-8, with no improvement in resolution.

Figure 23 illustrates typical darkfield signal waveforms and respective peak signal distributions for 0.81 and 7.6 μ diameter latex particles. Since these particles do not fluoresce, only light scatter was measured. Signals from the larger particles (Figure 23b) are well above the noise level, whereas, the smaller particle signals (Figure 23a) are only slightly above the noise. The narrowness of the peak signal distribution of the smaller particles (Figure 23c) is due to their 0.0063 μ standard deviation, as compared to the relatively wide distribution (Figure 23d) of the larger particle (2.3 μ standard deviation). Some clumping did occur after ultrasonic agitating the smaller particles, which can be noted by observing the small peak of the 4^{th} and 5^{th} lines (bars) of the distribution plot. The 7.6 μ diameter particle darkfield distribution is identical in shape to the volume distribution reported by Fulwyler et al. (31) for the same type particle.

The small bacteria tested in this study appear to be the size limit of the present fluorescence/darkfield detection scheme (Figure 24). Both the fluorescence and darkfield signals are within the noise. The fluorescence and darkfield peak signal distributions were not obtained for the bacteria.

Relative ratio distributions of the peak fluorescence signal divided the peak darkfield signal for four selected types of cells are illustrated in Figure 25. Both types of rat liver nuclei were selected for the testing of a single

Figure 23. Signal waveforms and peak signal amplitude distributions of latex particles

a. Darkfield signal waveform - 0.81μ particles
Uncalibrated photomultiplier gain - 7.5×10^3,
R_L = 10Megohm
Mask aperture - 0.4 x 5.0mm, LP filter - 7.5kHz
Scale factors
Horizontal - 5msec/cm, vertical - 200mv/cm

b. Darkfield signal waveform - 7.6μ particles
Calibrated photomultiplier gain - 7.14×10^2,
R_L = 1.0Megohm
Mask aperture - 1.5 x 5.0mm, LP filter - 10kHz
Scale factors
Horizontal - 5msec/cm, vertical - 500mv/cm

c. Darkfield signal distribution - 0.81μ particles
Scale factors
Horizontal - 25mv increments,
vertical - 35.0 cells/cm

d. Darkfield signal distribution - 7.6μ particles
Scale factors
Horizontal - 70mv increments,
vertical - 14.0 cells/cm

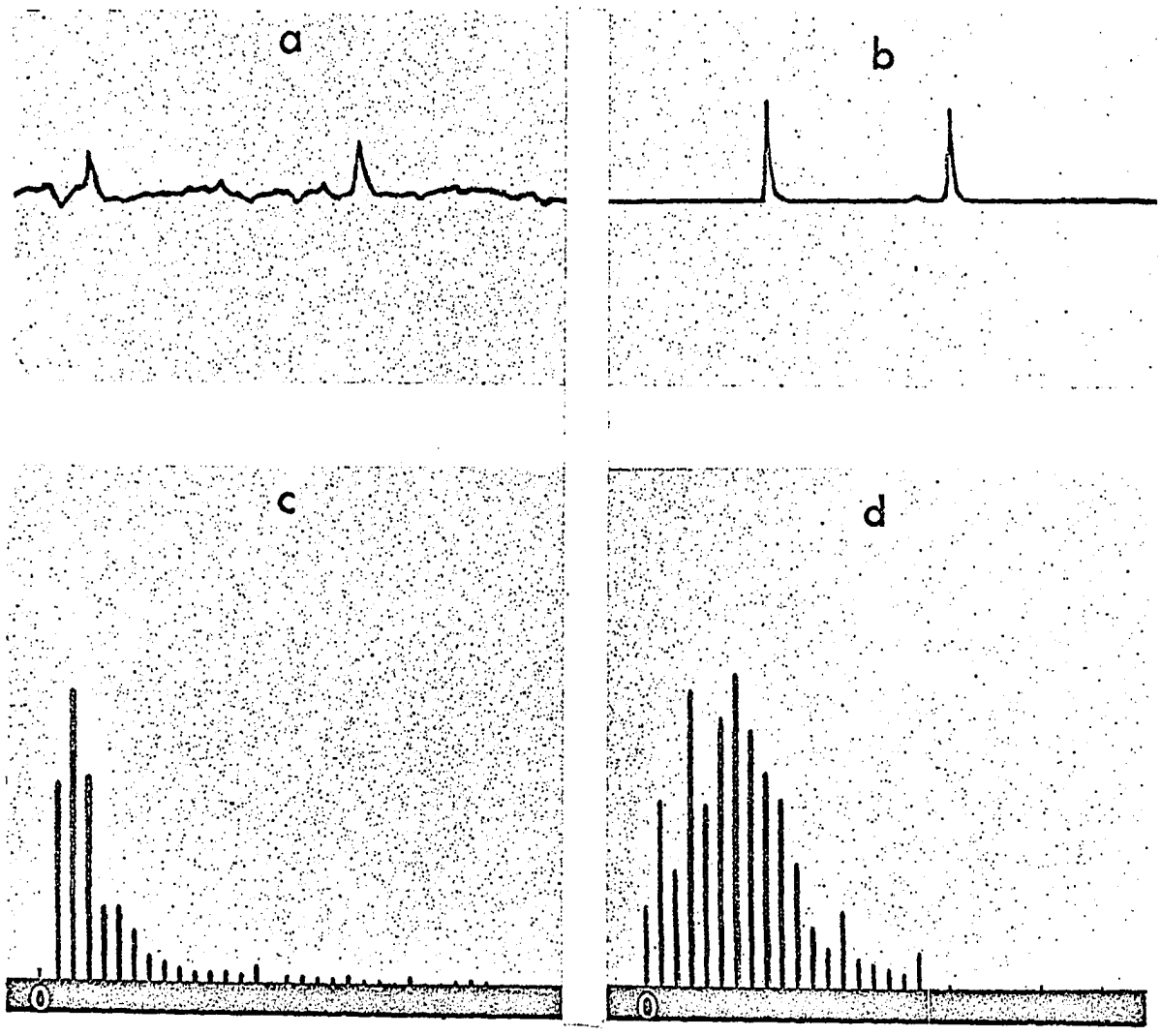
a
b
c
d

Figure 24. Signal waveforms of cocci bacteria

a. and b. Fluorescence and darkfield signal waveforms
Upper waveforms (a. and b.) - fluorescence signals
Uncalibrated photomultiplier gain - 1.25×10^4,
R_L = 10Megohm
Mask aperture - 0.3 x 5.0mm, LP filter - 5kHz
Scale factors
Horizontal - 10msec/cm, vertical - 1000mv/cm
Lower waveforms (a. and b.) - darkfield signals
Uncalibrated photomultiplier gain - 6.8×10^3,
R_L = 10Megohm
Mask aperture - 0.3 x 5.0mm, LP filter - 5kHz
Scale factors
Horizontal - 10msec/cm, vertical - 500mv/cm

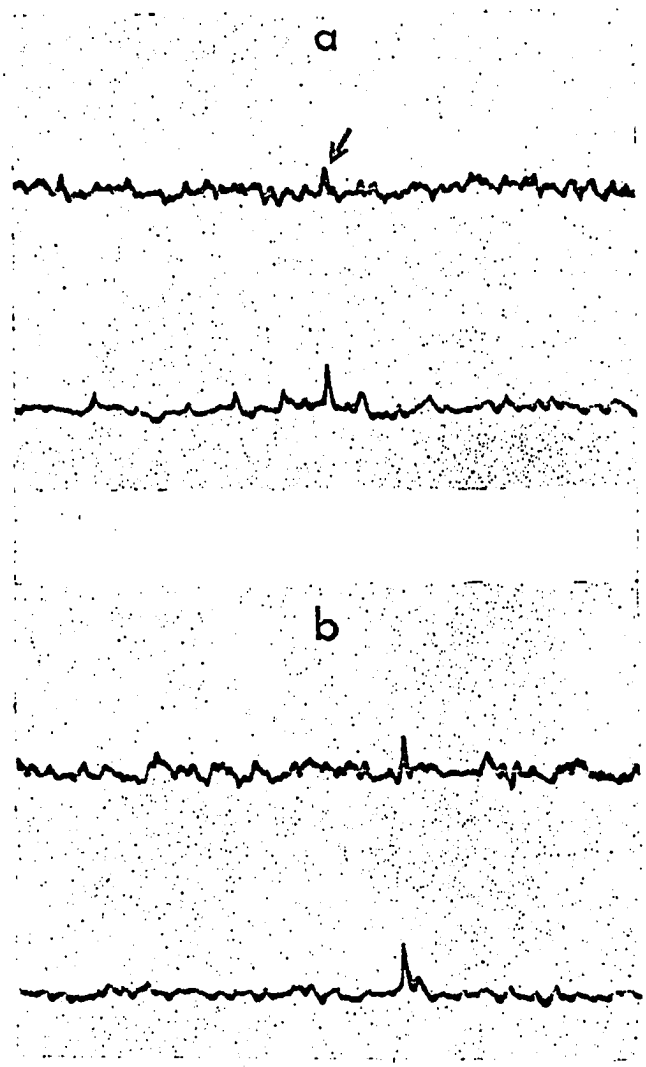
a
b

Figure 25. Relative peak fluorescence-to-darkfield signal ratio distribution

a. Rat liver nuclei (diploid)

b. Rat liver nuclei (tetraploid)

c. Goldfish blood

d. Swine leucocytes

e. and f. Dog leucocytes

Scale factors
Horizontal - Center: ratio = 1; right of center: 1.2, 1.4, ..., 51.2; and left of center: 1/1.2, 1/1.4, ..., 1/51.2
Vertical - number of cells (512 total)

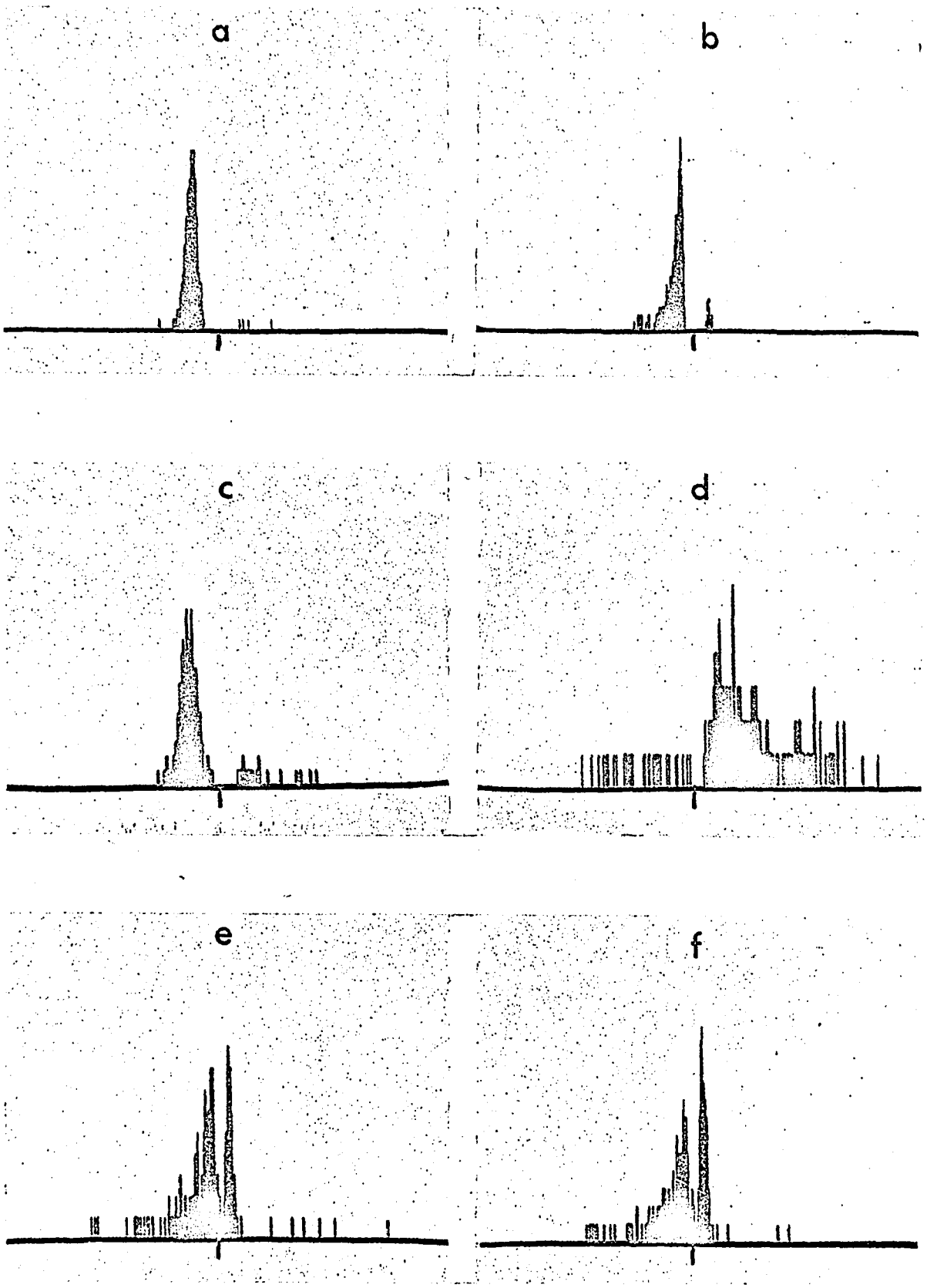
a
b
c
d
e
f

cell type. The 5 μ diameter ratio distribution (Figure 25a) is nearly symmetrical, whereas the 8 μ diameter ratio distribution (Figure 25b) is slightly unbalanced to the left. The individual peak signal distributions of rat liver nuclei (Figure 15) verify that the two relative ratio distributions are correct.

The relative ratio distribution of goldfish blood is illustrated in Figure 25c. Goldfish blood was chosen because of its cellular make-up. Lymphocytes (average diameter 6.5 μ) make-up about 92.5 per cent of the total leucocyte count. Lymphocytes and thrombocytes (average diameter 4.5 μ) average about 1/100 and 1/40 of the total blood cell count (97). Both the lymphocyte and thrombocyte consists of essentially a dense nucleus, with a relatively small amount of cytoplasm. The ratio of the nucleus-to-cytoplasm cross sectional areas of these is nearly one-to-one, whereas, the nucleus-to-cytoplasm ratios of the nucleated erythrocytes is about one-to-four (97). The majority of cells (erythrocytes) have relative fluoresce-to-darkfield peak signal ratios less than 1.0, with lymphocytes and thrombocytes having relative signal ratios greater than 1.0 (1/50 of the plot). Close examination of the peak signal distributions (Figures 17b and 17c) indicate that the relative ratio distribution plot is valid.

The relative ratio distribution plot for dog leucocytes is illustrated in Figures 25e and 25f. Mariano and Iorio (54)

have measured the cross sectional areas of human granulocytes and lymphocytes to be 96.3 and 72.1 μ^2, respectively. Lymphocytes are characterized by their relatively large nucleus and small amount of cytoplasm (area ratio approximately 1.0), whereas, granulocytes contain a relatively large amount of cytoplasm (area ratio less than 1.0), plus the characteristic granules. The relative ratio distribution plot obtained of dog leucocytes is markedly divided into two parts of about 20-25 and 75-80 per cent, as determined by a cut-out and weigh measurement procedure. This is in close agreement with the lymphocyte and granulocyte percentages for dog blood given by Benjamin (7) and Trautmann and Fiebiger (89).

Figure 25d illustrates the relative peak fluorescence-to-darkfield signal ratio distribution for swine leucocytes. Due to possible staining irregularities the ratio distribution is rather complex. The majority of the leucocytes were lymphocytes, as observed under the microscope prior to testing. No differential cell count was made at that time. The relative ratio distribution for swine leucocytes illustrates that the majority of the measured cells were lymphocytes.

To evaluate the ability of this measurement system in sizing cells according to their nuclear and overall cross section areas, the average peak fluorescence and darkfield signal amplitudes are plotted as a function of nuclear and overall cross sectional areas. The approximate (measured)

cellular dimensions of the nucleus and overall cell, and cell shapes, are given in Table 2. Cross sectional areas (computed from data in Table 2) of the nucleus and total cell, along with average peak signals are listed in Table 3. Average peak fluorescence and darkfield signal amplitudes were calculated from the computer print-outs of the individual peak signal amplitude distributions. The tolerances listed in Table 3, which are illustrated by the square-shaped dashed-lines located around the data points of the cell size plots, represent the possible error in the measurement process due to measuring cellular dimensions with a microscope and photomultiplier voltages with a multimeter, and will be discussed at the end of this chapter.

The average peak primary fluorescence signal amplitude vs. total cross sectional area for the four types of pollen tested is illustrated in Figure 26. There is a definite linear relationship ($y = mx + b$) between the average peak signal amplitude and the cross sectional area. It is interesting to note that the plot does not pass through the origin, as would normally be expected. This is due primarily to the basic characteristic of primary fluorescence, as compared to secondary fluorescence. Stained pollen grains, which did not stain well, did not yield the results that were originally anticipated and were not plotted. Although the fluorescence peak signal amplitude of the pollen grains was increased by

Table 2. Approximate sizes (in microns) and shapes of cells used in fluorescence/darkfield studies

Cell	Overall cell size		Nucleus size		Cell shape
	Short diameter	Long diameter	Short diameter	Long diameter	
P. mulberry pollen	13.7	13.7	--	--	Round
Ragweed pollen	19.8	19.8	--	--	Round
Chinese l. pollen	36.7	36.7	--	--	Round
Pecan pollen	46.5	46.5	--	--	Round
Diploid rat liver nuclei[a] (26)	--	--	5.0	5.0	Round
Tetraploid rat liver nuclei[a] (26)	--	--	8.0	8.0	Round
Frog erythrocytes (1, 27, 2)	15.5	21.5	6.7	9.7	Oval
Goldfish erythrocytes (80, 97)	10.1	12.3	4.3	6.1	Oval
Avian erythrocytes	8.3	11.2	3.7	5.3	Oval
Dog erythrocytes (1, 89)	7.2	7.2	--	--	Round

[a]Sizes were not measured; refer to references.

Table 2. (Continued)

Cell	Overall cell size		Nucleus size		Cell shape
	Short diameter	Long diameter	Short diameter	Long diameter	
Dog and swine leucocytes (1, 89)	5-20	5-20	5-15	5-15	Round or oval
Yeasts (14)	2.4	3.0	≈1.0	≈1.0	Oval
Cocci bacteria[a] (14)	0.8-1.0	0.8-1.0	--	--	Round
Sm. latex particles[a]	0.81	0.81	--	--	Round
Lg. latex particles[a]	7.6	7.6	--	--	Round

Table 3. Cross sectional areas (in square microns) and average peak signal amplitudes ($x10^{-9}$ amps) of cells used in fluorescence/darkfield studies

Cell	Fluorescence		Darkfield	
	Nuclear cross section	Average peak signal amplitude[a]	Total cross section	Average peak signal amplitude[b]
P. mulberry pollen	--	210(±27%)	147.0 (±15%)	190 (±31%)
	--	1100[c] (±21%)		
Ragweed pollen	--	170[d] (±28%)	308.0 (±10%)	550 (±31%)
	--	1410[c] (±31%)		
Chinese lilac pollen	--	344[d] (±30%)	1050.0 (±11%)	1350 (±28%)
	--	655[c] (±31%)		
Pecan pollen	--	385[d] (±29%)	1700.0 (±9%)	825 (±25%)
	--	1100[c] (±31%)		
Diploid rat liver nuclei	19.6 (±40%)	122 (±29%)	19.6 (±40%)	220 (±20%)

[a] Average peak fluorescence signal amplitudes of pollen at a photomultiplier gain of $3.85x10^4$. All other cells at a photomultiplier gain of $5.95x10^4$.

[b] Average peak darkfield signal amplitudes of pollen at a photomultiplier gain of $1.575x10^2$. All other cells at a photomultiplier gain of $2.49x10^3$.

[c] Primary-secondary fluorescence average peak signal amplitude.

[d] Primary fluorescence average peak signal amplitude.

Table 3. (Continued)

Cell	Fluorescence		Darkfield	
	Nuclear cross section	Average peak signal amplitude[a]	Total cross section	Average peak signal amplitude[b]
Tetraploid rat liver nuclei	50.5 (±25%)	262 (±29%)	50.5 (±25%)	312 (±20%)
Frog erythrocytes	50.5 (±25%)	250 (±30%)	258.0 (±11%)	125 (±21%)
Goldfish erythrocytes	21.0 (±40%)	100 (±27%)	97.0 (±18%)	357 (±23%)
Avian erythrocytes	15.0 (±45%)	34 (±26%)	73.0 (±20%)	465 (±20%)
Dog erythrocytes	--	--	40.7 (±28%)	160 (±20%)
Dog leucocytes[e]	--	294 (±13%)	--	--
Swine leucocytes	--	226 (±27%)	--	--
Yeasts	≈1.0	9(±25%)	5.5(±75%)	21(±22%)
Sm. latex particles[e]	--	--	0.52	63(±10%)
Lg. latex particles	--	--	45.3	1600(±20%)

[e]Calibration test not run due to technical difficulties.

addition of the fluorochrome, no linear relationship appears to exist among the stained pollen. Other staining techniques may yield different results.

Wide-angle light scatter from pollen grains is linearly related to overall cross sectional area (Figure 27). The relative refractive index of the pollen tested in this study is approximately the same, as noted by observing the pollen grains with a microscope when suspended in water. Since the mercury arc projection across the cell flow stream is 50-60 μ in diameter, the larger pecan pollen (46.5 μ diameter) can effectively mask the light source. This is the principal cause for saturation or extinction of the plot in Figure 27.

Illustrated in Figure 28 is the plot of average peak fluorescence signal amplitudes vs. the cross sectional area of the cell nucleus. There is a definite linear correlation between the average peak signal amplitudes and nuclear cross sectional area when using acridine orange. Dog and swine leucocytes were not plotted because of their size variation (Table 2). This plot effectively illustrates the nuclear cell sizing capability of this measurement technique.

Wide-angle light scattering measurements of the various cells tested (plus latex particles), with exception of pollen grains, did not completely yield the anticipated results (Figure 29). Both the reflection and refraction coefficients for light scattered by spherical particles show a strong

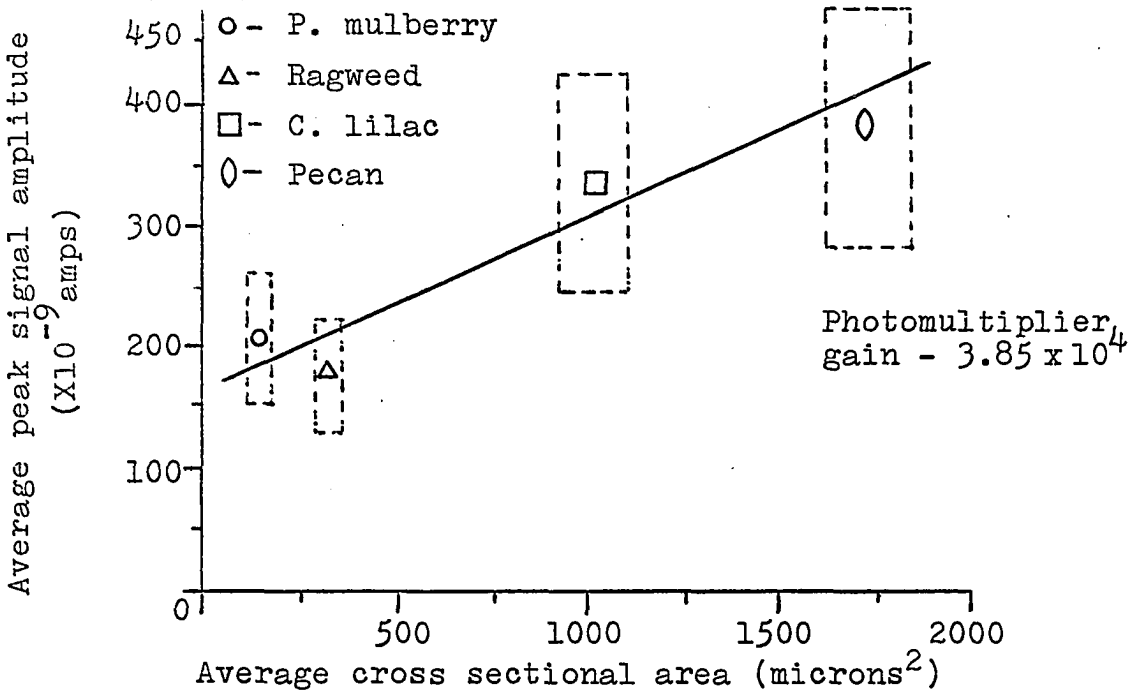

Figure 26. Fluorescence signal amplitude vs. total cross section area of pollen grains

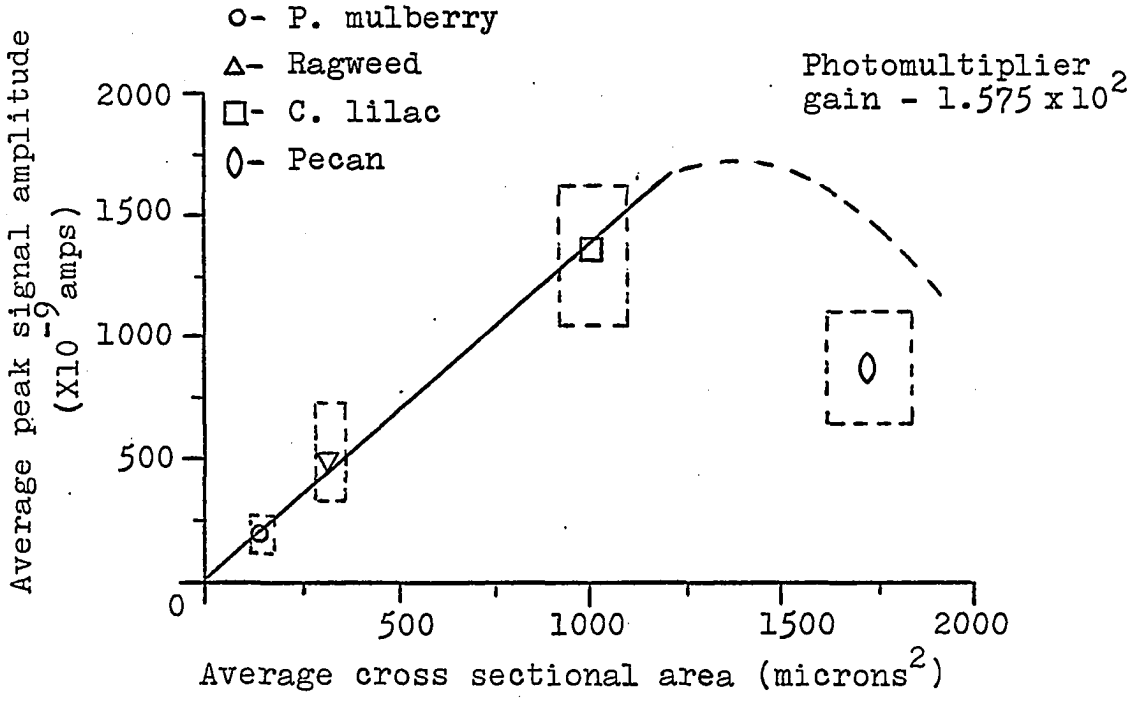

Figure 27. Darkfield signal amplitude vs. total cross sectional area of pollen grains

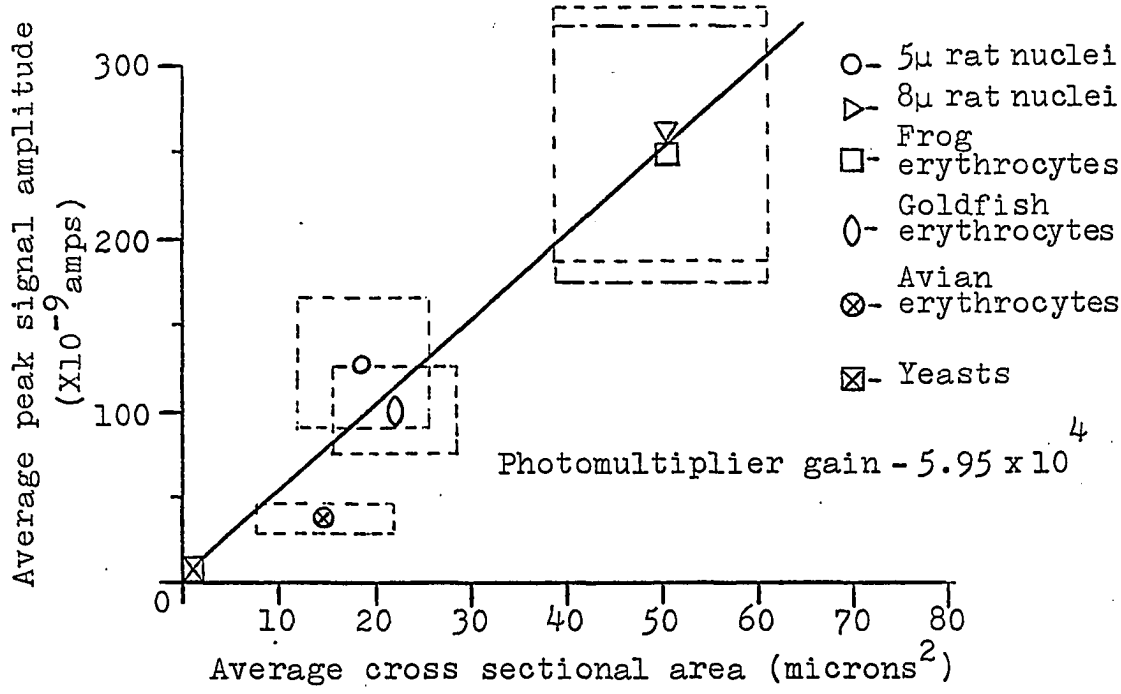

Figure 28. Fluorescence signal amplitude vs. cross sectional area of cell nucleus

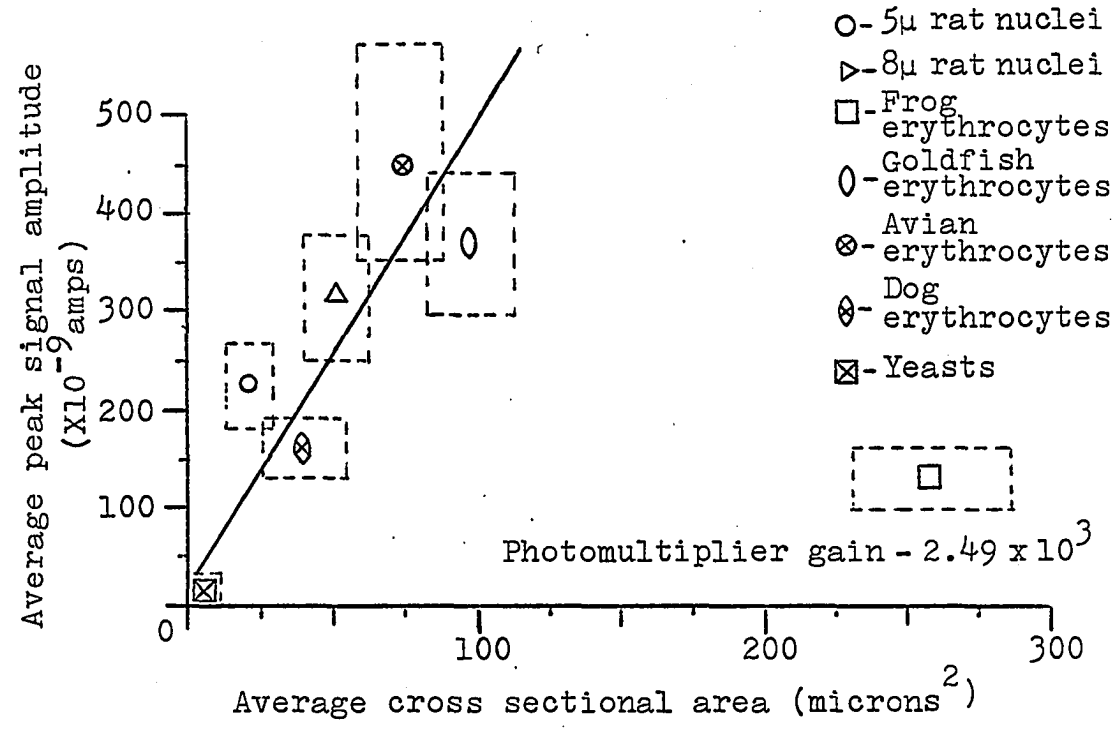

Figure 29. Darkfield signal amplitude vs. total cross sectional area of cell

dependence on relative refractive index (m), whereas, the diffraction coefficient is independent of refractive index (Appendix A). Since the relative refractive index of the cells tested was not previously cited in the literature, the assumption was made that the relative refractive indices for most biological cells tested were about equal. This was experimentally determined to be only partially correct. The plot of average peak darkfield signal amplitudes as a function of overall cross sectional area (Figure 29) illustrates this point. Yeast cells, dog erythrocytes, rat liver nuclei, and goldfish and avian erythrocytes are nearly linearily related to overall cross sectional area. The two sizes of latex particles tested, each having approximately the same refractive index are also closely related (Table 3). The average peak signal amplitude from the larger latex particle (7.6 μ) is about equal to the ratio of the cross sectional areas of the larger particle to the smaller particle (0.81 μ) times the average peak signal amplitude measured from the smaller latex particle. The average peak signal amplitudes from the two types of rat liver nuclei are similarly related. The darkfield data for frog erythrocytes is well removed from the main region of data. Three independent darkfield measurements on frog erythrocytes yielded similar results. If the refractive indices were known for the cells tested, the solution of the total light scattering intensity (Appendix A) would be

difficult without the aid of a computer. The darkfield signal vs. size plots of Figures 27 and 29 demonstrate the overall cell sizing capability, within certain limitations, of this measurement system.

To illustrate the use of Bayes method (Appendix B) for distinguishing (deciding) between different cell types in an aqueous mixture an example will be given. Illustrated in Figure 30 are the approximate Gaussian fluorescence and darkfield peak signal amplitude distributions for 8 (tetraploid and 5 (diploid) μ diameter rat liver nuclei taken from actual data of these two test runs (Figure 15). There is considerable overlapping of the two sets of distributions. The fluorescence and darkfield mean peak signal amplitudes of the two types of nuclei are listed in Table 3. The approximate peak signal standard deviations of the 8 and 5 μ nuclei were determined to be 100 and 50 millivolts (fluorescence) and 150 and 75 millivolts (darkfield), respectively. In this example it is assumed for demonstrational purposes that equal amounts (P(a) = P(b)) of each type of the nuclei are contained in aqueous suspension for measurement. From an actual mixture of nuclei, the a priori probabilities could be experimentally determined using other techniques.

Equation 37 is used to determine the respective fluorescence and darkfield voltage threshold settings for distinguishing between the two sizes of nuclei. The costs (C_a and C_b)

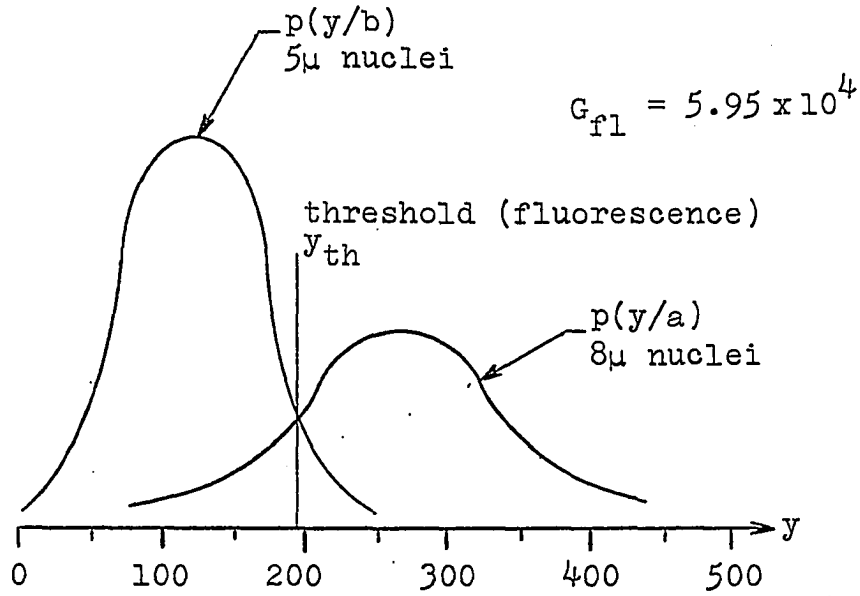

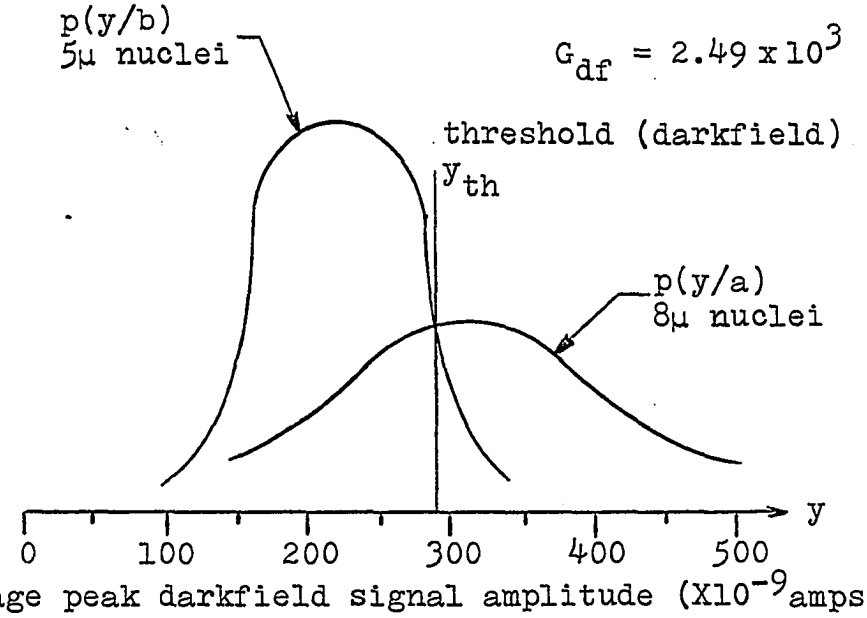

Figure 30. Probability distributions of diploid and tetraploid rat liver nuclei

for making a wrong decision in this example are taken to be equal, which may not always be the case. Substituting the respective fluorescence and darkfield data into the threshold expression (Equation 37), yields respective threshold settings of $y_{fl} > 192$ millivolts and $y_{df} > 284$ millivolts. Thus, if the peak fluorescence and/or darkfield signal amplitudes of a rat liver nuclei are greater than 192 or 284 millivolts, then the 8 μ nuclei is to be chosen as being present (measured). The computed thresholds lie exactly at the intersections of the respective 8 and 5 μ distributions, which is to be expected. If the a priori probabilities P(a) or P(b), or the costs C_a or C_b are changed, the thresholds will be moved toward the right or left.

On the basis of the decision rule employed in determining the threshold setting, the conditional risks or error can be computed, if desired, using Equations 39 and 40.

The Bayes decision rule method relies on knowing the a priori and conditional probabilities and the assignment of costs in advance. This information may not always be present prior to a test. Other methods, such as minimax decision rule, may possibly be employed in the decision process.

Sources of Error and Error Evaluation

There are a number of possible sources of error in this measurement system. Although the system was elaborately

calibrated prior to measuring the various cells, errors can still occur. Air bubbles in any of the cuvette flow lines can slow the flow rate and widen, narrow, or displace the flow stream. Widening or displacement of the flow stream may cause the cell to be only partially measured. A narrowing of the flow stream is not a serious problem, other than a slowing of the cell stream flow rate. Drifting or deflection of the cell flow stream can be caused by air bubbles or large particles (clumps) deflecting the flow stream by becoming lodged in the chamber.

Wandering of the mercury arc can be a problem if the lamp is not allowed to adequately warm-up and stabilize with respect to temperature. The intensity of the excitation source will vary if proper lamp operating conditions (voltage and current) are not maintained.

Coloration and intensity changes can occur if proper staining procedures are not employed. Controlling of pH by use of buffers is important for consistent staining results. Kasten (46) has reported contaminants within various fluorochromes, with acridine orange one of these. Highly purified dyes should preferably be used in quantitative microfluorometry.

The physical dimensions of a majority of the cells tested in this study were measured with a brightfield microscope and eyepiece micrometer. The error in reading the micrometer (0.5 μ (430X) and 1.0 μ (100X)) causes a certain degree of

uncertainty when calculating cross sectional areas of cells. The per cent change in cross sectional area (A) as a function of cell radius (r) can be estimated using the following two equations:

$$\frac{dA}{A} = \frac{1}{r} \times 100\% \text{ ..... (430X)} \qquad (13)$$

and

$$\frac{dA}{A} = \frac{2}{r} \times 100\% \text{ ..... (100X)} \qquad (14)$$

When measuring elliptical cells of small and large radii a and b, such as frog or goldfish erythrocytes, the per cent change in cross sectional area (A) is

$$\frac{dA}{A} = \frac{1}{2}\left[\frac{1}{a} + \frac{1}{b}\right] \times 100\% \text{ ..... (430X)} \qquad (15)$$

and

$$\frac{dA}{A} = \left[\frac{1}{a} + \frac{1}{b}\right] \times 100\% \text{ ..... (100X)} \qquad (16)$$

These percentages are listed as the tolerances of the measured nuclear and overall cross sectional areas in Table 3.

Another relatively large source of error in the measurement process is the error in measuring overall photomultiplier tube voltages. This error is essentially double because of the two required voltmeter readings (calibration run plus actual cell test). A multimeter was used to measure voltages throughout this experimentation. The error in measuring high voltage with this meter is about ±10 volts. A digital voltmeter (±0.1%) would lower this error by a factor of 10 or

more. The per cent change in gain (G) (error) of the 10-stage (darkfield) and 13-stage (fluorescence) photomultiplier tubes is respectively:

$$\frac{dG}{G} = 70\left[\frac{1}{V_{pm_{cal}}} + \frac{1}{V_{pm_{test}}}\right] \times 100\% \qquad (17)$$

and

$$\frac{dG}{G} = 91\left[\frac{1}{V_{pm_{cal}}} + \frac{1}{V_{pm_{test}}}\right] \times 100\%, \qquad (18)$$

where $V_{pm_{cal}}$ and $V_{pm_{test}}$ are the overall photomultiplier tube voltages. These percentages are listed as the fluorescence and darkfield peak signal amplitude tolerances in Table 3.

There is also a small inherent error in sampling the fluorescence and darkfield signal pulses by the computer, since it samples the signal about every 40 μ seconds. Signal pulse widths, when played back at 7 1/2 ips on the magnetic tape recorder, range from about 1000 to 2000 μ seconds. This corresponds to a maximum error of about 20 to 40 millivolts when sampling a 1 volt peak triangular pulse. This error can further be reduced by slowing down the cell flow rate through the detection chamber or playing back the data stored on magnetic tape at a slower rate. The tape recorder noise (25-35 millivolts peak-to-peak) also contributed a small amount of error to the measurement process. Both the sampling error and tape recorder noise tend to disperse the peak signal amplitude data distributions about their mean.

SUMMARY AND CONCLUSIONS

Automatic identification of large numbers of fluorochromed biological cells in aqueous suspension, according to their fluorescence and darkfield optical properties, is a valid technique within certain size limitations as supported by the preponderance of evidence presented.

The fluorescence/darkfield (light scatter) opto-photoelectric measurement system which has been described in this study employed blue-ultraviolet excitation light energy to illuminate a narrow cell flow stream. A modified proportional control fluid amplifier, not heretofore reported, was effectively used to generate the cell flow stream. Cells were tagged with the fluorescent dye acridine orange, placed in dilute suspension, and allowed to flow through the system for measurement. A rack-mounted and portable recorder/reproducer system was used for data storage and playback. The LINC-8 digital computer was utilized for data analysis and reduction to compute and display both the fluorescence and darkfield peak signal amplitude distributions and relative ratio distributions. This type of system is capable of real-time automatic cell analysis.

Experimental results show a definite linear correlation between the projected cross sectional areas of the fluorescing cell nucleus and the peak amplitude of the fluorescence signals. Not only can this measurement method size cells

according to the area of the nucleus, but could also be used as the sensing mechanism in a cell sorter. There is a definite quasi-linear relationship between the projected total area of a cell and the peak amplitude of the darkfield (light scatter) signal as determined by the relative refractive index. Some caution should be used when interpreting the darkfield results. A quantitative darkfield method has the potential of determining the refractive index of biological cells. Small angle light scatter, which is independent of light scatter, is a better method for overall cell sizing.

This measurement system provides a means for determining the relative nucleus-to-cytoplasm ratio of cells. Although a differential leucocyte count was not performed on the dog blood tested, the evidence presented indicates that this type of a system can at least partially differentiate among the different types of leucocytes, i.e., lymphocytes and granulocytes can automatically be distinguished from each other. This measurement system can also be coupled with a volume sensing detector for determination of nucleus size-to-volume ratio.

The system can automatically differentiate between nucleated and non-nucleated cells, i.e., between mammalian erythrocytes and leucocytes. The practicality of this method comes in the large number of erythrocytes to leucocytes in mammalian blood. A measurement system of this type has the potential for quantitatively studying the blood cell composition of various species in the animal kingdom.

This system provides a method for automatic analysis of various pollen grains according to their primary fluorescence and darkfield optical properties. It is conceivable that a system of this type, by substituting air for a liquid flow system, could be used in air pollution studies. Water pollution studies are evident.

By using different fluorescence staining procedures (Feulgen technique) the system provides a method of analyzing large cell populations for DNA content. Various pathological conditions of cells can be studied, such as, a comparison of normal and neoplastic cells. Growth and aging characteristics of cultured cells can be analyzed. The system can effectively differentiate between cells and non-cellular debris.

Fluorochromes other than acridine orange should also be used to evaluate the performance of this system. Acridine orange has the disadvantage of fluorescing in solution, thus reducing background contrast. There are other dyes (e.g., berberine sulfate) that do not have this property. Fluorescence brighteners might also be employed.

In a fluorescence/light scatter measurement system of this type, the intensity and spectral content of the excitation light source are of crucial importance. Optical laser sources of the proper wavelength represent the present optimum in fluorescence and light scatter excitation. Simple UV excitation sources are non-existent. The optics should be kept

as simple as the measurement system will permit, but should not be detrimental to the measurement process. Careful selection of excitation and suppression filters is important in achieving good optical contrast. Maximum photomultiplier tube sensitivity to the green-yellow fluorescence of acridine orange requires the greatest possible cathode spectral response for that portion of the spectral region. A smaller and more compact system is not only feasible, but desirable. The type of detection chamber used in this study possesses the potential of a cell sorting device, with the addition of a second flow output.

Future work in this area of study should consist of investigating the possibility of raising the S/N ratio further by employing a feedback scheme similar to the one discussed in the second chapter. Correlation tests should be run to further clarify the "noise" situation. Signal detection techniques can be employed for distinguishing between the different cell types of a mixture. Real-time computation of peak signal amplitude and relative ratio distributions would increase the efficiency of data reduction and analysis. An electronic system for measuring the fluorescence-to-darkfield relative peak signal ratios would also be advantageous.

BIBLIOGRAPHY

1. Altman, P. L. and Dittmer, D. S. Biology data book. Washington, D.C., Federation of American Societies for Experimental Biology. 1964.

2. Andrew, W. Comparative hematology. New York, N.Y., Grune and Stratton. 1965.

3. Applications manual for operational amplifiers. Dedham, Mass., Philbrick/Nexus Research. 1968.

4. Barer, R. Phase contrast and interference microscopy in cytology. In Oster, G. and Pollister, A. W., eds. Physical techniques and biological research. Vol. 3. Pp. 29-90. New York, N.Y., Academic Press Inc. 1956.

5. Barron, A. L. E. Using the microscope. London, Chapman and Hall Ltd. 1965.

6. Bartels, P. Fluorescence microscopy--principles, applications, and instrumentation. New York, N.Y., E. Leitz, Inc. ca. 1965.

7. Benjamin, M. M. Outline of veterinary clinical pathology. 2nd ed. Ames, Iowa, The Iowa State University Press. 1961.

8. Bertalanffy, F. D. Evaluation of the acridine-orange fluorescence microscope method for the cytodiagnosis of cancer. New York Academy of Sciences Annals 93(16): 717-750. 1962.

9. Boast, W. B. Illumination engineering. 2nd ed. New York, N.Y., McGraw-Hill Book Co., Inc. 1953.

10. Born, M. and Wolf, E. Principles of optics. 3rd ed. New York, N.Y., Pergamon Press. 1965.

11. Blobel, G. and Potter, V. R. Nuclei from rat liver: isolation method that combines purity with high yield. Science 154: 1662-1665. 1966.

12. Blum, L. L. The photoelectric determination of erythrocyte count. American Journal of Clinical Pathology 15: 85-93. 1945.

13. Brackett, F. S., Mattern, F. T., and Olson, B. J. Appraisal of instrument for counting erythrocytes by scatter photometry. American Journal of Clinical Pathology 23: 731-745. 1953.

14. Breed, S. R., Murray, E. G. D., and Smith, N. R. Bergey's manual of determinative bacteriology. 7th ed. Baltimore, Md., The Williams and Wilkins Co. 1957.

15. Brown, Earle B. Modern optics. New York, N.Y., Reinhold Publishing Corp. 1965.

16. Brown, G. T. Pollen-slide studies. Springfield, Ill., Charles C. Thomas, Publisher. 1949.

17. Bucknall, R. A. and Sutcliffe, J. F. The nucleic acids and cellular differentiation in the root apex of Pisum sativum. Journal of Experimental Botany 16(48): 423-432. 1965.

18. Chauveau, J., Moule', Y., and Rouiller, Ch. Isolation of pure and unaltered liver nuclei morphology and biochemical composition. Experimental Cell Research 11: 317-321. 1956.

19. Coulter, W. H. High speed automatic blood cell counter and cell size analyzer. National Electronics Conference Procedures 12: 1034-1049. 1956.

20. De Ment, J. The first law of fluorescence. Science 96: 157-158. 1942.

21. De Ment, J. The third law of fluorescence. Mineralogist 11: 115. 1943.

22. Dumont multiplier phototubes. Clifton, New Jersey, Fairchild Camera and Instrument Corp., Dumont Electron Tube Div., 750 Bloomfield Ave. 1965.

23. Eagle, H. Amino acid metabolism in mammalian cell cultures. Science 130: 432-437. 1959.

24. EMI photomultiplier tubes. Plainview, L.I., N.Y., Whittaker Corp., Gencom Div., 80 Express St. 1967.

25. Engstrom, R. W. Multiplier photo-tube characteristics: application to low light levels. Journal of the Optical Society of America 37: 420-431. 1947.

26. Falzone, J. A., Barrows, C. H., and Yiengst, M. J. Fractionation of rat liver nuclei into diploid and tetraploid DNA classes by continuous density gradient sedimentation. Experimental Cell Research 26: 552-561. 1962.

27. Foxon, G. E. H. Blood and respiration. In Moore, J. A. Physiology of the amphibia. Pp. 151-209. New York, N.Y., Academic Press, Inc. 1964.

28. Frommer, P. L. An automatic counter for blood cells. New York Academy of Sciences Annals 99(2): 233-241. 1962.

29. Frommer, P. L. An electronic blood-count meter. Electrical Engineering 74: 388-391. 1955.

30. Fulwyler, M. J. Electronic separation of biological cells by volume. Science 150: 910-911. 1965.

31. Fulwyler, M. J., Glascock, R. B., Hiebert, R. D., and Johnson, N. M. Device which separates minute particles according to electronically sensed volume. Review of Scientific Instruments 40(1): 42-48. 1969.

32. Garcia, A. M. The Feulgen-DNA content of human leucocytes. Acta Histochemica 17: 230-245. 1964.

33. Garcia, A. M. The Feulgen-DNA content of peripheral leucocytes, megakaryocytes, and other bone marrow cell types of the rabbit. Acta Histochemica 17: 246-258. 1964.

34. Goldman, S. Information theory. New York, N.Y., Prentice-Hall, Inc. 1953.

35. Greene, L. W. and Hesseltine, H. C. Use of ultraviolet light and fluorescent dyes in bacterial counting. Society for Experimental Biology and Medicine Proceedings 74: 171-173. 1950.

36. Happel, J. and Brenner, H. Low Reynolds number hydrodynamics. Englewood Cliffs, N.J., Prentice-Hall, Inc. 1965.

37. Harman, W. W. Principles of the statistical theory of communication. New York, N.Y., McGraw-Hill Book Co., Inc. 1963.

38. Hartman, F. A. and Lessler, M. A. Erythrocyte measurements in birds. Auk 80(4): 467-473. 1963.

39. Helstrom, C. W. Statistical theory of signal detection. New York, N.Y., Pergamon Press. 1960.

40. Hodkinson, J. R. and Greenleaves, I. Computations of light scattering and extinction by spheres according to diffraction and geometrical optics, and some comparisons with the Mie theory. Optical Society of America Journal 53(5): 577-588. 1963.

41. Hulett, H. R., Bonner, W. A., Barrett, J., and Herzenberg, L. A. Cell sorting: Automated separation of mammalian cells as a function of intracellular fluorescence. Science 166: 747-749. 1969.

42. Jackson, J. F. Supravital blood studies using acridine orange fluorescence. Blood: Journal of Hematology 17: 643-649. 1961.

43. Jenkins, F. A. and White, H. E. Fundamentals of optics. 3rd ed. New York, N.Y., McGraw-Hill Book Co., Inc. 1957.

44. Kamentsky, L. A. and Melamed, M. R. Spectrophotometric cell sorter. Science 156: 1364-1365. 1967.

45. Kamentsky, L. A., Melamed, M. R., and Derman, H. Spectrophotometer: New instrument for ultrarapid cell analysis. Science 150: 630-631. 1965.

46. Kasten, F. H. Cytochemical studies with acridine orange and the influence of dye contaminants in the staining of nucleic acids. In Bourne, G. H. and Danielli, J. F., eds. International review of cytology. Vol. 21. Pp. 141-202. New York, N.Y., Academic Press. 1967.

47. Katz, S. An introduction to proportional fluid control. In Fluid Amplification Symposium Proceedings. Vol. 1. Pp. 21-26. Washington, D.C., Harry Diamond Laboratories Oct. 1962.

48. Koller, L. R. Ultraviolet radiation. 2nd ed. New York, N.Y., John Wiley and Sons, Inc. 1965.

49. Kubitschek, H. E. Electronic counting and sizing of bacteria. Nature 182: 234-235. 1958.

50. Kurozumi, T. and Shibata, K. Anomalous diffraction spectra of biological cells. Biochimica et Biophysica Acta 88: 191-200. 1964.

51. Lagercrantz, C. Photo-electric counting of individual microscopic plant and animal cells. Nature 161: 25-26. 1948.

52. Loeser, C. N., West, S. S., and Schoenberg, M. D. Absorption and fluorescence studies on biological systems: Nucleic acid-dye complexes. Anatomical Record 138: 163-178. 1960.

53. Mansberg, H. P. and Kusnetz, J. Quantitative fluorescence microscopy: Fluorescent antibody automatic scanning techniques. Journal of Histochemistry and Cytochemistry 14: 260-273. 1966.

54. Mariano, A. and Iorio, R. Error in two-wavelength cytophotometry. In Wied, G. L., ed. Introduction to quantitative cytochemistry. Pp. 215-237. New York, N.Y., Academic Press Inc. 1966.

55. Mellors, R. C., Glassman, A., and Papanicolaou, C. N. A microfluorometric scanning method for the detection of cancer cells in smears of exfoliated cells. Cancer 5: 458-468. 1952.

56. Mellors, R. C. and Silver, R. A microfluorometric scanner for the differential detection of cells: Application to exfoliative cytology. Science 114: 356-360. 1951.

57. Meyer-Arendt, J. R. Diffraction: Light, on microscope structures. In Glasser, O., ed. Medical physics. Vol. 3. Pp. 226-229. Chicago, Ill., The Year Book Publishers, Inc. 1960.

58. Meyer-Arendt, J. R., Leiby, G. M., and Miner, E. D. Size determination of leukemic cells by light diffraction. Journal of Histochemistry and Cytochemistry 8(6): 445-446. 1960.

59. Moldavan, A. Photo-electric technique for the counting of microscopical cells. Science 80: 188. 1934.

60. Montgomery, P., editor. Scanning techniques in medicine and biology. New York Academy of Sciences Annals 97(2): 329-526. 1962.

61. Morthland, F. W., De Bruyn, P. P. H., and Smith, N. H. Spectrophometric studies on the interaction of nucleic acids with amino acridines and other basic dyes. Experimental Cell Research 7: 201-214. 1954.

62. Mullaney, P. F., Van Dilla, M. A., Coulter, J. R., and Dean, P. N. Cell sizing: A light scattering photometer for rapid volume determination. The Review of Scientific Instruments 40(8): 1029-1032. 1969.

63. Mullaney, P. F., Van Dilla, M. A., and Dean, P. N. Light scattering by biological cells and its relation to cell size. Biophysical Journal Society Proceedings 8: A-115. 1968.

64. Needham, G. H. The practical use of the microscope. Springfield, Ill., Charles C. Thomas, Publisher. 1958.

65. Nurnberger, J. I. Ultraviolet microscopy and microspectroscopy. In Mellors, R. C., ed. Analytical cytology. Pp. 1-44. New York, N.Y., McGraw-Hill Book Co., Inc. 1955.

66. Orstein, L. New horizons in fluorescency microscopy. Journal of Mt. Sinai Hospital, New York, N.Y. 24(6): 1066-1078. 1957.

67. Oster, G. Light scattering. In Oster, G. and Pollister, A. W., eds. Physical techniques in biological research. Vol. 1. Pp. 51-71. New York, N.Y., Academic Press Inc. 1955.

68. Ponder, E. Diffraction method of measuring small objects. In Glasser, O., ed. Medical physics. Vol. 1. Pp. 301-308. Chicago, Ill., The Year Book Publishers, Inc. 1950.

69. Porro, T. J., Dadik, S. P., Green, M., and Morse, H. T. Fluorescence and absorption spectra of biological dyes. Stain Technology 38: 37-48. 1963.

70. Powell, A. Characteristics and control of free laminar jets. In Fluid Amplifier Symposium Proceedings. Vol. 1. Pp. 289-296. Washington, D.C., Harry Diamond Laboratories. Oct. 1962.

71. Price, G. R. and Schwartz, S. Fluorescence microscopy. In Oster, G. and Pollister, A. W. Physical techniques in biological research. Vol. 3. Pp. 91-148. New York, N.Y., Academic Press, Inc. 1956.

72. Richards, O. W. Fluorescence microscopy. In Mellors, R. C. Analytical cytology. Pp. 1-37. New York, N.Y., McGraw-Hill Book Co., Inc. 1955.

73. Rigler, R. Microfluorometric characterization of intracellular nucleic acids and nucleoproteins by acridine orange. Acta Physiologic Scandinavica 67, Supplementum 267. 1966.

74. Rothstein, N. Vital staining of blood parasites with acridine orange. Journal of Parasitology 44: 588-595. 1958.

75. Rothstein, N. and Diamond, L. S. Vital staining of parasitic protozoa for dark-field microscopy (abstract). Journal of Protozoology 6: 8. 1959.

76. Ruch, F. Determination of DNA content by microfluorometry. In Wied, G. L., ed. Introduction to quantitative cytochemistry. Pp. 281-294. New York, N.Y., Academic Press Inc. 1966.

77. Sani, G., Citti, U., and Caramazza, G. Fluorescence microscopy in the cytodiagnosis of cancer. Springfield, Ill., Charles C. Thomas, Publisher. 1964.

78. Schwartz, M. Information transmission, modulation, and noise. New York, N.Y., McGraw-Hill Book Co., Inc. 1959.

79. Schwartz, M., Bennett, W. R., and Stein, S. Communication systems and techniques. Inter-University Electronics Series, Vol. 4. New York, N.Y., McGraw-Hill Book Co., Inc. 1966.

80. Smith, C. G., Lewis, W. M., and Kaplan, H. M. A comparative morphologic and physiologic study of fish blood. Progressive Fish-Culturist 14(1): 169-172. 1952.

81. Smith, W. J. Modern optical engineering. New York, N.Y., McGraw-Hill Book Co. 1966.

82. Steinkamp, J. A. An apparatus for the detection of fluorescing cells. Unpublished M.S. thesis. Ames, Iowa, Library, Iowa State University. 1967.

83. Stokes, G. G. On the change of refrangibility of light. Royal Society of London Philosophical Transactions 143: 463-562. 1852.

84. Streeter, V. L. Fluid mechanics. 3rd ed. New York, N.Y., McGraw-Hill Book Co., Inc. 1962.

85. Sturkie, P. D. Avian physiology. 2nd ed. Ithaca, N.Y., Comstock Publishing Associates. 1965.

86. Thaer, A. A. Instrumentation for microfluorometry. In Wied, G. L., ed. Introduction to quantitative cytochemistry. Pp. 409-426. New York, N.Y., Academic Press. 1966.

87. Thompson, S. W. Selected histochemical and histopathological methods. Springfield, Ill., Charles C. Thomas, Publisher. 1966.

88. Tolles, W. E. Applications and methods of counting and sizing in medicine and biology. New York Academy of Sciences Annals 99(2): 231-334. 1962.

89. Trautmann, A. and Fiebiger, J. The histology of domestic animals. Ithaca, N.Y., Comstock Publishing Associates. 1957.

90. Trujillo, T. T. and Van Dilla, M. A. Modification of feulgen reaction for fluorescent staining of cells in liquid suspension. Submitted to Stain Technology ca. 1969.

91. Udenfriend, S. Fluorescence assay in biology and medicine. In Kaplan, N. O. and Scheraga, H. A., eds. Molecular Biology. Vol. 3. New York, N.Y., Academic Press. 1962.

92. Van de Hulst, H. C. Light scattering by small particles. New York, N.Y., John Wiley and Sons, Inc. 1957.

93. Van Dilla, M. A., Mullaney, P. F., and Coulter, J. R. A new spectrophotometer for rapid measurement of fluorochrome-stained cells. Biophysical Journal Society Proceedings 8: A-160. 1968.

94. Van Dilla, M. A., Trujillo, T. T., Mullaney, P. F., and Coulter, J. R. Cell microfluorometry: A method for rapid fluorescence measurement. Science 163: 1213-1214. 1969.

95. Van Tilburg, R. W. and Cochran, W. L. Development of a proportional fluid amplifier for multi-stage operation. In Fluid Amplifier Symposium Proceedings. Vol. 2. Pp. 313-333. Washington, D.C., Harry Diamond Laboratories. May 1964.

96. Vennard, J. K. Elementary fluid mechanics. 4th ed. New York, N.Y., John Wiley and Sons, Inc. 1961.

97. Watson, L. J., Shechmeister, I. L., and Jackson, L. L. The hematology of goldfish, Carassius auratus. Cytologia 28: 118-130. 1963.

98. Weinger, S. D. Effect of aspect ratio on noise in proportional fluid amplifiers. In Brown, F. T., ed. Advances in fluid mechanics. New York, N.Y., The American Society of Mechanical Engineers. 1967.

99. West, S. S. Fluorescence microspectroscopy of mouse leucocytes supravitally stained with acridine orange. Acta Histochemica, Supplementband VI: 127-153. 1965.

100. West, W. Fluorescence and phosphorescence. In Weissberger, A. Technique of organic chemistry. Vol. 9. Pp. 707-758. New York, N.Y., Interscience Publishers, Inc. 1956.

101. Wheeless, L. L., Bahr, G. F., Wied, G. L., and Patten, S. F. Multiparameter cyto-fluorometric research system. 21st Annual Conference on Engineering in Medicine and Biology Proceedings, Nov. 18-21, 1968, Houston, Texas. 1968.

ACKNOWLEDGEMENTS

I wish to acknowledge my sincere appreciation to the many people who gave their support and advice throughout this research program.

Special thanks go to my major professor, Dr. N. R. Cholvin, for his guidance during this study and to my research program coordinator, Dr. D. L. Carlson, for his encouragement and insight into the many problems that arose while conducting this research study.

To Drs. L. Y. Quinn and H. W. Brockman, appreciation and thanks for counselling and guidance.

I am especially grateful to Professor R. V. Bulkley, Mr. R. J. Moore, and Mr. D. L. Cameron for furnishing some of the various types of biological cells; Mr. T. G. Innes for mercury arc lamp information; and Mr. R. Baker for writing the computer programs used here.

Special gratitude is most gratefully extended to my wife for typing this dissertation and the many sacrifices during my graduate studies.

The National Aeronautics and Space Administration and National Science Foundation both contributed financially to my support for which I am especially grateful.

APPENDIX A

Fluorescence and Light Scatter

Both darkfield and fluorescence microscopy depend upon the interaction of radiant light energy with matter. In both instances a portion of this radiant energy is absorbed. In the case of darkfield microscopy, where the object appears self-luminous against a dark background, no direct light reaches the eye or photo detector, but only the unabsorbed incident radiant energy which the objects themselves diffract, refract, and reflect, i.e., scatter into the microscope objective. In fluorescence microscopy, on the other hand, radiant energy in the ultraviolet and blue-violet region of the spectrum must be employed. The unabsorbed portion of the spectrum is not utilized, rather the conversion of absorbed radiation by the fluorescent substance into visible radiation is the source of the light seen by the eye or measured by the photo detector. Generally, highly colored fluorescent materials (dyes) are employed to tag various cell components such as the nucleic acids, proteins, lipids, etc., in fluorescence process.

Fluorescence

Whenever matter (molecules) absorbs light energy, the energy must reappear again in some other form, i.e., conservation of energy. This could be in the form of heat, electrical,

chemical, or physical energy, or re-emitted in the form of light energy as luminescence or photoluminescence.

Luminescence is the most general term for the emission of light. When re-emission of light occurs within about 10^{-8} seconds following absorption it is called fluorescence. If this period of time is longer than 10^{-8} seconds it is called phosphorescence. Fluorescence represents the direct return of the energy, whereas in phosphorescence, the molecule passes to a metastable state of lower energy, which slowly reverts to the normal state.

There are several distinct states (bands) of higher energy within the molecular structure of matter. The absorption of light energy may lift a molecule into any one of them. In this process some of the electrons of the molecule are raised into higher energy levels. The remaining absorbed energy is utilized to set the structure into vibration and rotation. The molecular structure is now in an excited state of energy (20). If the molecules do not decompose as a result of their increase in energy, and if all the energy is not dissipated by collisions with other molecules, the electrons will return to their fundamental energy state with the emission of photons (fluorescence). However, once the molecule is lifted into a higher energy state, it does not return to the fundamental state by emitting light energy corresponding to the energy difference between the higher, excited state, and

its fundamental, non-excited, state. The molecule first "slides down" into its lowest energy level. This transition is radiationless. Once the molecule has arrived at its lowest energy level of excitation, the final plunge to the fundamental state occurs with the emission of fluorescence. It is due to this loss of energy that the fluorescent light has a longer wavelength, or lower energy, than the exciting light which was absorbed--Stokes law (83).

Since the emission of fluorescence (Stokes) always occurs from the lowest energy level of the molecule, the spectral distribution of the emitted fluorescent light is independent of the spectral distribution of the exciting source, as long as the exciting source has a shorter wavelength (greater energy). The fluorescence spectrum shows near mirror symmetry to that of the absorption band of the fluorescing molecule (6). Spectrophotometry has made it possible to observe and compare quantitatively the absorption and emission spectrum of various biological (organic) dyes in the free or bound form (52, 61, 69).

Basically there are two types of fluorescence, primary and secondary. Primary fluorescence (autofluorescence) occurs when a compound possesses a particular molecular structure, which upon the absorption of ultraviolet light fluoresces (77). Secondary fluorescence is the property whereby non-fluorescent substances are impregnated with fluorescent dyes

called fluorochromes, thus rendering them fluorescent. Generally, fluorochromes are fluorescent at extremely low concentrations. As a consequence of fluorochroming, the original fluorescence spectrum of the dye changes in both wavelength and intensity (61). Fluorochromes can be classified according to their relative pH, as basic, neutral, or acidic. Complete listings of fluorochromes, along with recommended concentrations, colors, biological uses, and suppliers are given in Richards (72) and Sani et al. (77).

In the process of fluorescence the various molecular processes compete for the dissipation of the absorbed energy, which strongly affects the amount of fluorescence and thus brightness of the fluorescing object. Thus, they affect the quantum efficiency (yield), which is defined as the ratio of the emitted quanta to absorbed quanta (91):

$$\Phi = \frac{\text{number of quanta emitted}}{\text{number of quanta absorbed}}$$

Quantum yield is a measure of the amount of absorbed energy which can be re-emitted a fluorescence. In the absence of perturbations the emitted fluorescence is equal to the absorbed radiation ($\Phi = 1$). Quantum efficiencies range from 0.99 to near zero (91).

Quantum efficiencies of fluorescing compounds depend strongly upon their molecular structure and the physiochemical conditions of the medium in which they are contained. The majority of organic molecules capable of fluorescence contain

conjugated chains which are made up alternating double and single nonsaturated bonds in a cyclic pattern. In general, closed-ring structures of aromatic compounds have the fluorescence property and thus a high quantum efficiency. Open structures, which do not fluoresce, or fluoresce weakly, tend to convert excitatory light energy into vibration and rotation. Certain substitutes in the aromatic ring, such as -OH group, $-OCH_3$ group, and the $=CH_2$, $-NH_2$, and $-N(CH_3)_2$ groups increase the quantum efficiency, whereas others, such as, -CO, -COOH, -CN, $-NO_2$, and -CH=CH- decrease it (6, 72, 77).

Since fluorescence is an intermolecular phenomenon, the medium in which the fluorescent material is suspended should be considered. The principle elements capable of influencing the medium and thus altering the overall quantum yield are temperature, chemical composition of the solvent, viscosity, pH of the solution, and the concentration of the fluorochrome (77). An increase in temperature reduces the fluorescence yield, which is due to increased vibration and rotation of the molecular structure. Some solvents decrease fluorescence, thus lowering the fluorescence yield. Viscosity is important in that it alters the molecular mobility. An increase in viscosity thus increases the fluorescence yield. The pH of the solution affects both the intensity and coloration of fluorescence in that the hydrogen ion concentration modifies the coefficient of absorption and thus the emission spectrum.

If buffers are used to control pH, they are used at low concentrations, as the presence of ions in solution lowers the quantum yield of the fluorochromes. The intensity of fluorescence increases linearly as a function of concentration up to an optimal concentration (saturation), and then gradually decreases to self-extinction.

Light Scattering

Normally light energy is not completely absorbed, but is partially reflected, refracted, or diffracted (scattered) when it comes in contact with matter. No energy transfer occurs, but only an alteration in the original direction of the light path.

Light scattering by small particles is a complex phenomenon and analysis is difficult and lengthy. Rayleigh scattering (67) is applicable for small particles (near the wavelength of the incident light) when the difference in refractive index between the particle and medium is small, whereas, the treatment of Mie (92) is applicable to scattering from spherical particles of arbitrary size of any refractive index. The theory of Mie requires the solution of Maxwell's equations with appropriate boundary conditions. Although the treatment of the light scattering phenomena by Mie is rigorous, it is difficult to use and presents certain computational difficulties (92).

Recently, Hodkinson and Greenleaves (40) have developed a mathematical model for light scattering by spherical particles larger than a few wavelengths (>4) of light which greatly reduces the computational difficulties of Mie.

When particles are larger than a few wavelengths of light, their combined light scattering, and consequently their extinction, may be treated approximately as a combination of classical diffraction and geometrical refraction and reflection. Large particles require a way of looking at scattering problems that is quite different from treating small particles. The fundamental difference is that the incident light, which forms a plane wavefront of infinite extent, can be thought of as separate rays of light which pursue their own path. Rays hitting a particle surface are partially reflected and partially refracted. Refracted light may emerge after another refraction, or after several internal reflections. The light so emerging and the directly reflected light from the outer surface both contribute to the total scattering by the particle. The remaining energy which does not emerge is lost by absorption inside the particle. The amounts of light energy absorbed or scattered, along with the angular distribution and polarization, depend upon the form and composition of the particle and on its surface condition. The intensity distribution coefficients of the reflected ($I_1(\theta)$) and refracted ($I_2(\theta)$) light as given by Hodkinson and Greenleaves

(40) are

$$I_1(\theta) = \frac{1}{8\pi}\left\{\frac{\sin(\theta/2) - [m^2-1+\sin^2(\theta/2)]^{1/2}}{\sin(\theta/2) + [m^2-1+\sin^2(\theta/2)]^{1/2}}\right\}^2 + \frac{1}{8\pi}\left\{\frac{m^2\sin(\theta/2) - [m^2-1+\sin^2(\theta/2)]^{1/2}}{m^2\sin(\theta/2) + [m^2-1+\sin^2(\theta/2)]^{1/2}}\right\}^2 \tag{19}$$

and $$I_2(\theta) = \frac{2}{\pi}\left(\frac{m}{m^2-1}\right)^4 \frac{(m\cos\theta/2-1)^3(m-\cos\theta/2)^3}{\cos\theta/2(m^2+1-2m\cos\theta/2)^2} \times (1+\sec^4\theta/2), \tag{20}$$

where m is the relative refractive index and θ the scattering angle. These coefficients have a wide angular extent, but appear to predominate from 5 to 25° (63). The rays passing along the particle form a wavefront from which a part, in the form and size of the geometrical shadow, is missing. This incomplete wavefront gives rise by Huygen's principle to the Frauhofer diffraction pattern (10). The intensity distribution coefficient $I_o(\theta,d)$ of the diffracted light is given as

$$I_o(\theta,d) = \frac{1}{2}(1+\cos^2\theta)\,\frac{J_1^2(\frac{\pi d}{\lambda}\sin\theta)}{\pi\sin^2\theta}, \tag{21}$$

where d is the particle diameter and λ is the wavelength of the incident light. The intensity distribution of the diffraction pattern, which is limited to small angles near zero (40),

depends upon the form and size of the particle, but is independent of its composition (refractive index) and the nature of its surface (reflectively). Diffracted light also has the same state of polarization as the incident light. Therefore, the overall light scattering intensity coefficient is a sum of the individual scattering coefficients:

$$I(\theta,d) = I_o(\theta,d) + I_1(\theta) + I_2(\theta). \qquad (22)$$

APPENDIX B

Signal Detection Theory

Formulation of cell identification schemes from either the fluorescence and darkfield peak signal amplitude or relative ratio distributions is important in determining the type and number of cells in a mixture, i.e., differential cell counts.

As individual cells flow through the measurement system a maximum of two electronic signal pulses (fluorescence and darkfield) are produced. Individual peak signal amplitude and ratio distributions can be determined automatically (pulse height analyze or digital computer). The signal distributions of the various cells in the population tested may or may not overlap. Once these distributions are known, signal detection or decision theory offers a technique for cellular differentiation.

In order to formulate the decision process, it may first be advantageous to look at the general formulation of the decision situation.

Let the symbol x (signal input) represent the true state, i.e., the peak signal amplitude for a specific type of cell. If there is more than one type of cell within a mixture (group), the situation can be represented as x_1, x_2, ... x_n. Each of these possible states is assumed to occur with some

a priori probability $P(x_i)$. For example, in the case of goldfish blood: P(erythrocyte) = 99/100 and P(leucocyte) = 1/100. In a similar manner let y represent the measured observation (peak signal output). For a particular x_i, there is some probability $P_{ij} = P(y_j/x_i)$ that the measured observation will be y_j. This information can be presented in the form of a matrix, as shown below.

	y_1	y_2	.....	y_m
x_1	P_{11}	P_{12}	.....	P_{1m}
x_2	P_{21}	P_{22}	.....	P_{2m}
⋮	⋮	⋮		⋮
x_n	P_{n1}	P_{n2}	.....	P_{nm}

The final part of the decision process relates the error costs. Let a_k represent the decision that x_k is the true state of affairs, when in actuality the true state may be x_i, indicating an error. Now, let C_{ik} be a number indicating the relative cost of deciding x_k is the true state of affairs when in reality it is x_i, as shown below in the cost matrix.

	a_1	a_2	.....	a_n
x_1	C_{11}	C_{12}	.....	C_{1n}
x_2	C_{21}	C_{22}	.....	C_{2n}
⋮	⋮	⋮		⋮
x_n	C_{n1}	C_{n2}	.....	C_{nn}

The complete description of the decision situation is given by these three groups of data. If the description of the decision situation is known, then the problem is to determine a rule by which the decision a_k (based on the measurement of y_j) is to be made which minimizes the average cost associated with the process. The best decision rule, which minimizes the risk involved in making it, is termed a Bayes decision rule (37, 39).

When the number of possible input states (x_i) equals two, the decision situation is called hypothesis testing (signal detection). The problem then is to test the two hypotheses that the signal present is x_1 or x_2, and to make the decision that will result in the lowest average cost. For a particular measured output signal y_j, the risk or average cost can be formulated for either of the two decisions

$$r(a_1) = C_{11}P(x_1/y_j) + C_{21}P(x_2/y_j) \tag{23}$$

and

$$r(a_2) = C_{12}P(x_1/y_j) + C_{22}P(x_2/y_j) \tag{24}$$

where $r(a_1)$ is the average cost in making the a_1 decision (x_1 present at the output) and $r(a_2)$ is the average cost in making the a_2 decision (x_2 present at the output).

Bayes theorem, as shown below, can be used to determine the conditional probabilities $P(x_i/y_j)$, in terms of the a priori probabilities $P(x_i)$ and conditional probabilities $P(y_j/x_i)$

$$P(x_i/y_j) = \frac{P(y_j/x_i)\ P(x_i)}{\sum_x P(x)\ P(y_j/x)} \qquad (25)$$

The average cost functions $r(a_1)$ and $r(a_2)$ can now be rewritten in terms of the a priori probabilities $P(x_i)$, the conditional probabilities $P(y_j/x_i)$ and the costs.

Assuming that y_j has been received, then the decision a_1 (x_1 present) should be made if $r(a_1)$ is less than $r(a_2)$. A slight amount of algebraic manipulation yields

$$\Lambda \triangleq \frac{P_{1j}}{P_{2j}} > \frac{P(x_2)}{P(x_1)} \frac{C_{21} - C_{22}}{C_{12} - C_{11}} \triangleq \beta \qquad (26)$$

which is equivalent to choosing decision a_1. Here Λ is a ratio of conditional probabilities and is termed the likelihood ratio. The decision rule is then to choose hypothesis a_1 (x_1 present) if Λ is greater than β and hypothesis a_2 (x_2 present) if it is not.

On the basis of the decision rule, the average cost of errors when the signal is actually present is

$$r_1 = C_{12}P(a_2/x_1) + C_{22}P(a_2/x_2) \qquad (27)$$

whereas, the average cost when the signal is not present is

$$r_2 = C_{11}P(a_1/x_1) + C_{21}P(a_1/x_2) \qquad (28)$$

Equations 27 and 28 are termed the conditional risks (37). The average risk is thus $R = P(x_1)r_1 + P(x_2)r_2$ (29)

In some measurement situations the a priori probabilities $P(x_i)$, which enter into the determination of β, may not be known in advance. The conditional probabilities $P(y_j/x_i)$ and the error cost are assumed to be known. No matter what the unknown values of $P(x_i)$ are, the average risk will never be more than the larger of the two conditional risks r_1 and r_2. A conservative decision in this situation is to choose β such that the maximum conditional risk is minimized; this is termed a minimax decision rule. This condition is met when the two conditional risks are equal ($r_1 = r_2$). The a priori probabilities can be determined which satisfies this condition; and the threshold found using the Bayes decision procedure. Another approach to this problem is to plot the average risk as a function of the a priori probability $P(x_i)$ using Bayes strategy (39). The maximum Bayes risk corresponds to the minimax risk. The decision threshold can then be determined using Bayes procedure using the β that yielded a maximum Bayes risk, i.e., a minimax risk.

When there are more than two possible choices in the decision process, i.e., multiple hypothesis testing, Bayes rule can still be used in choosing the decision corresponding to the smallest risk. If such a problem lacks symmetry and the number of hypotheses to be tested is large, it can become very complicated to solve.

Consider now a typical measurement situation in which a voltage signal is known to be either $\bar{a}$ or $\bar{b}$ volts (mean peak

value), each having Gaussian distribution with a standard deviation of σ_a and σ_b, respectively. The a priori probabilities are known to be P(a) and P(b). In this measurement situation, the observed output signal voltage can take on any number of values. The cost of a correct decision in either case is taken to be zero. The cost of deciding signal a is present when signal b actually is present, is C_a, whereas, the cost of deciding signal b is present when signal a is actually present, is C_b. The cost of a correct decision is zero. In this measurement situation the conditional probability density functions p(y/a) and p(y/b) are continuous rather than discrete and are given below as:

$$p(y/a) = \frac{1}{\sqrt{2\pi}\,\sigma_a} \; e^{-\frac{(y-\bar{a})^2}{2\sigma_a^2}} \tag{30}$$

and

$$p(y/b) = \frac{1}{\sqrt{2\pi}\,\sigma_b} \; e^{-\frac{(y-\bar{b})^2}{2\sigma_b^2}} \tag{31}$$

The average error cost if y is received and hypothesis a_1 (signal a present) is chosen is:

$$r(a_1) = 0 \cdot P(a/y) + C_a P(b/y) \tag{32}$$

Similarly, the average error cost for hypothesis a_2 (signal b present) is

$$r(a_2) = C_b P(a/y) + 0 \cdot P(b/y) \tag{33}$$

Since the variable y is not discrete, but continuous, Bayes rule can be rewritten as

$$P(x_i/y) = \frac{P(x_i)\ p(y/x_i)dy}{\sum_x P(x_i)\ p(y/x_i)dy} \tag{34}$$

Algebraic manipulation yields $r(a_1) < r(a_2)$ (hence choose signal a) when

$$\Lambda(y) \triangleq \frac{p(y/a)}{p(y/b)} > \frac{P(b)}{P(a)} \frac{C_a}{C_b} \triangleq \beta \tag{35}$$

The likelihood ratio $\Lambda(y)$ for this example is

$$\Lambda(y) = \frac{\sigma_b}{\sigma_a} e^{-\frac{(y-\bar{a})^2}{2\sigma_a^2} + \frac{(y-\bar{b})^2}{2\sigma_b^2}} \tag{36}$$

Hypothesis a_1 should then be chosen when $\Lambda(y) > \beta$. After considerable algebraic manipulation this is equivalent to choosing hypothesis a_1 when

$$y > \frac{\bar{b}\sigma_a^2 - \bar{a}\sigma_b^2 + \sigma_a\sigma_b \sqrt{(\bar{a}-\bar{b}) + 2(\sigma_a^2-\sigma_b^2) \ln(\frac{\sigma_a}{\sigma_b}\beta)}}{\sigma_a^2 - \sigma_b^2} \tag{37}$$

for $\sigma_a^2 \neq \sigma_b^2$

If $\sigma_a^2 = \sigma_b^2 = \sigma^2$, then the above expression of Equation 37 simplifies to

$$y > \frac{\bar{a}^2 - \bar{b}^2 + 2\sigma^2 \ln \beta}{2(\bar{a} - \bar{b})}, \tag{38}$$

or

$$y > \frac{\bar{a} + \bar{b}}{2} + \frac{\sigma^2 \ln \beta}{\bar{a} - \bar{b}}$$

The conditional risks (37) can be computed, if desired, from the following expressions:

$$r_1 = C_b \int_{-\infty}^{y} p(y/a)dy, \tag{39}$$

and

$$r_2 = C_a \int_{y}^{\infty} p(y/b)dy. \tag{40}$$

The average risk is thus

$$R = P(a)r_1 + P(b)r_2. \tag{41}$$